PHENOTYPING APPLICATIONS FOR THE GENETIC ANALYSIS OF ROOT SYSTEM ARCHITECTURE IN CROP PLANTS

A Dissertation

Presented to the Faculty of the Graduate School

of Cornell University

In Partial Fulfillment of the Requirements for the Degree of

Doctor of Philosophy

by

Randy Todd Clark

August 2013

PHENOTYPING APPLICATIONS FOR THE GENETIC ANALYSIS OF ROOT SYSTEM ARCHITECTURE IN CROP PLANTS

Randy Todd Clark, Ph. D.

Cornell University 2013

Plant root systems and associated symbiotic organisms act as critical links between the growing shoot and the rhizosphere, providing both vital nutrients and water to sustain growth. Many tools have been developed to study plant root systems; however, the efficient quantification of root traits remains a key bottleneck to effectively utilizing expanding collections of genomic and germplasm resources during the study of root system development and function.

This dissertation presents results from root system phenotyping research where root phenotyping platforms were developed and used to investigate the genetic components of root system architecture and development in crop plants. It begins with a review chapter that discusses the importance of root system architecture (RSA) during resource acquisition and provides an overview of established root growth and measurement techniques while highlighting modern root phenotyping approaches that have been developed for genetic mapping studies. Subsequently, two distinct and complementary phenotyping platforms are described that were designed to improve the flexibility and throughput for root system phenotyping using digital imaging and software analysis tools to quantify root systems in 2-dimensions (2D) and 3-dimensions (3D).

The use of the 3D phenotyping platform is then discussed where global root system traits were captured and quantitative trait loci (QTL) and genome wide association (GWA) mapping studies were performed in order to investigate the genetic components of RSA development in rice (*Oryza sativa*). Finally, future research directions are outlined and include additional phenotyping platform development as well as new strategies to mine the RSA mapping results to identify candidate genes involved in root development and verify the functional relevance of the measured root traits and detected loci for nutrient and water acquisition.

BIOGRAPHICAL SKETCH

Randy Todd Clark was born on December 26, 1980 to Robert William Clark and Matilda Hsiang Clark in Cortland NY. He spent many carefree childhood days playing with friends and roaming the streets and backyards of Homer NY. He graduated from Homer Central High School in the spring of 1999 and immediately moved to Cornell University where he began his undergraduate study in the Biological and Environmental Engineering Department. During his undergraduate days he worked as a part-time student assistant in the lab of Dr. Leon V. Kochian at the UDSA at Cornell University where he received practical training and mentorship in the plant sciences. Upon graduating with a Bachelors of Science degree in spring of 2004, he continued working in Dr. Kochian's lab as a full-time research technician. After two years of applying his engineering background to plant research, he was convinced of a career path in the applied sciences and enrolled in the MS/PhD program in the Biological and Environmental Engineering Department at Cornell University under the mentorship of Professor Daniel J. Aneshansley. He continued work in Dr. Kochian's lab for nearly 7 more years as he worked to complete his doctoral research and degree.

ACKNOWLEDGMENTS

The completion of this work could not have been possible without the continuous support, reinforcement and opportunities provided by many people around me as I was growing up and continuing on with my doctoral degree. I first thank my parents for providing the solid foundation that allowed me to freely pursue my interest and for way too many other things along the way. I thank my sister for many warm meals and providing a comfortable vacation home for my cats. I thank my brother for continually looking out for my future and keeping me honest about getting my miles in. I thank Dan our weekly meetings and his support and Susan for her inspirational discussions. Lastly, I thank the members of the Kochian Lab, especially Leon for providing endless opportunities and being a kind and trusting mentor, Jon for teaching me to do things right, Jura and John for spotting me in a thicket of undergrads, Eric for our conversations over cooling tea water, and Adam, Matt, Janelle and Michael for being good friends and colleagues.

Dedicated in memory of I-Chun.

TABLE OF CONTENTS

CHAPTER I

ROOT SYSTEM MEASUREMENT AND ANALYSIS TECHNIQUES FOR THE STUDY OF PLANT RESOURCE ACQUISITION

ABSTRACT

Numerous methods have been developed to grow plants in systems that enable researchers to, capture, measure, and evaluate their root system characteristics. These techniques have been used to study root systems in settings ranging from natural field environments to contrived laboratory arrangements. With such a wide variety of experimental options, it is important review both established designs and consider new approaches and technologies. This chapter is intended to give an overview of the tools and techniques that are now available for studying the root system morphology and architecture of crop plants. Additionally, the importance of root systems and their relationship to plant growth and nutrition in suboptimal environments is discussed.

BIOLOGY OF ROOT SYSTEMS

Importance of roots systems and root system architecture

Plant root systems (and associated symbiotic organisms) act as critical links between the growing shoot and the rhizosphere, providing both vital nutrients and water to sustain growth. Additionally, roots anchor and stabilize the plant, enabling the growth of above-ground shoot and reproductive organs. Roots are an active part of the plant that respond and adapt to environmental conditions, signals and stresses.

Root system architecture (RSA) is one aspect of root systems that has been linked to the plant's ability to capture nutrient resources and water from the soil. Root system architecture is defined as the spatial configuration of the entire root system in the soil (Fitter, 1987; Lynch, 1995). The variation of RSA characteristics within and across species has been linked to improved resource acquisition and growth. Gaining a deeper understanding of RSA and its functional significance represents a promising area of study to improve the productivity and nutrient efficiency of crop plants (Berntson, 1994; Lynch, 2011).

It has been well documented that root systems have a vast ability to adapt to rhizosphere environments and respond to intrinsic and extrinsic stimuli from a variety of abiotic sources (Malamy, 2005). The status and supply of a number of essential mineral nutrients and water can have large impacts on root growth and development (Forde and Lorenzo, 2001). One essential nutrient that is a critical component for plant growth, function, and health is phosphorus (P). It is part of a number of structural compounds in the plant and plays important roles in many biochemical reactions (Marschner, 1995). Phosphorus, however, is a limiting nutrient for many agricultural system due to its low solubility, high-fixation and low mobility in the soil. Most agricultural systems require that additional P fertilizer be applied in order to maintain optimal plant growth and yield. Phosphorus is found in the bulk soil in both inorganic (Pi) and organic (Po) forms. Soluble forms of phosphorus (Pi) that can be absorbed from P-limited soils typically are found at concentrations in the bulk soil between 5 to 10μM (Shen et al., 2011). Thus plants have developed sophisticated strategies to acquire P from sparingly soluble Pi and Po soil sources to maintain a healthy P status.

These P acquisition strategies involve morphological and architectural adaptations of the plant root systems as well the regulation of physiological and biochemical processes aimed at “mining” P from the soil (Plaxton and Tran, 2011). Many plants species also exploit symbiotic associations with microorganisms (i.e. mycorrhiza and rhizobia) to enhance their ability to acquire P and other nutrients (primarily N) from the rhizosphere (Waisel et al., 1996). Even with highly effective mechanisms to solubilize P from fixed sources and absorb it from the soil, it is essential that the root system of the plant grow and develop in a way that reduces carbon expenditures while also maximizing the root systems access to the P reserves in the soil (Lynch et al., 2005).

RSA characteristics that are adapted to particular soil types and nutrient distributions enable the plants to grow optimally. One example of this is on acidic tropical soils where nearly all the P is found in the topsoil. In a study by Zhao et al (2004) on a collection of soybean varieties with diverse shoot and root architectures, those varieties that had a higher percentage of their root systems in the superficial zones of the soil performed and yielded better than those that tended to have more deeply distributed root systems. The improved performance of the varieties with shallow root systems was attributed to fact that the roots were better able to mine the topsoil for P while also avoiding the increasingly acidic and nutrient depleted environment of the subsoil. While RSA is only one component of a suite of traits that can improve crop production on marginal soils, new soybean varieties with beneficial root system characteristics have been released from soybean breeding programs to farmers and have significantly helped to increase agricultural productivity on the acidic soils of South China (Wang et al., 2010).

Root system components

Although roots on different plant species have similar functional roles in resource acquisition, the whole root system is comprised of different root classes and types that can vary both morphologically and functionally (Mattsson et al., 1993). Additionally, the anatomy and cellular structure of roots can be quite distinct between species (Hochholdinger et al., 2004). Some species also form specialized root structures that are induced only under certain environmental conditions, such as cluster or proteoid root formation by white lupin (*Lupinus albus*) to cope with phosphorus (P) deficient soils (Vance et al., 2003).

While there is no definitive classification system for root system types (Waisel et al., 1996), crop plant root systems can be broadly classified as either taproot systems or fibrous root systems. Taproot systems are characterized by having a prominent central taproot (or embryonic root) from which lateral roots emerge. This taproot maintains an important role throughout the entire lifecycle of the plant. Plants with taproot systems also have adventitious postembryonic roots that emerge from the base of the stem along tiers of nodular whorls that are referred to as basal or nodal roots (Weaver and Bruner, 1927). The number of nodular whorls and the distribution of basal roots have been hypothesized to play a role in and have been correlated with nutrient acquisition efficiency in taproot plants (Lynch and Brown, 2001; Lynch, 2011). Taproot systems are common to dicotyledonous legume crop species such as *Glycine max* (soybean). Fibrous root systems are composed of embryonic and postembryonic roots (Hochholdinger et al., 2004; Rebouillat et al., 2009), where the primordia of embryonic roots are formed when the embryos of the seeds develop on the parent plant. These

embryonic primary and seminal roots emerge upon germination and are involved in early seedling establishment and vigor, but serve less important roles as the plant matures (Hochholdinger and Tuberosa, 2009). In some species however, the seminal roots can continue to remain active throughout the life-span of the plant (Mattsson et al., 1993). The postembryonic roots form and develop throughout the life-span of the plant and consist of lateral roots, and adventitious shoot-borne crown and nodal roots. These postembryonic roots make up the bulk of the fibrous root system and have been implicated in the ability of a plant to survive and thrive under nutrient and resource limited environments (Zhu et al., 2005). Fibrous root systems are common to monocotyledonous cereal crop species such as maize (*Zea mays*), rice (*Oryza spp.*), and wheat (*Triticum spp.*).

Phenotyping of Root System Architecture (RSA) for Genetic Studies

The advancement of root growth and imaging methods has enabled detailed investigations into how root systems develop as well as how they adapt to abiotic and biotic stresses. For both linkage and association mapping studies of RSA, both manual and automated tools have been utilized to investigate the genetic components of root system growth and development. Manual methods have been used to elucidate several root-related genomic regions and genes (Johnson et al., 2000; Magalhaes et al., 2007; Krill et al., 2010) and digital imaging and analysis has further facilitated higher throughput and more precise mapping of root system development and tolerance to abiotic stress (Zheng et al., 2003; Zhu et al., 2005; Famoso et al., 2011).

Addtionally, the generation and study of root mutants with altered root system growth, morphology and/or development has been employed to further dissect the

genetic components of the root system. In reviews by Hocholdinger et al (2004) and Rebouillat et al (2009), analyses of several rice and maize root mutants are discussed. These mutant studies have led to the discovery of requisite genes involved in the development and emergence of crop root systems and have revealed that the various classes of root types are under distinct developmental control mediated by separate genetic networks.

In combination with more comprehensive whole plant phenotyping, the accurate and reliable imaging and measurement of root traits will continue to be utilized to unravel the genetic basis of root system development and the functional significance of variation in RSA during plant production, resource acquisition and stress adaptation. The further integration and advancement of root phenotyping and analysis tools will be needed as genotyping, mapping population and mutant resources continue to expand.

GROWTH, MEASUREMENT AND ANALYSIS OF ROOT SYSTEMS

Early methods for measuring root systems

Prior to the 1960's, root systems were mainly quantified using root weight and volume displacement measurements. In some cases, length and diameter were measured by hand on a small subsets of the roots in order estimate the surface area of the entire root system (Evans, 1938). As researchers began performing detailed investigations into the water and nutrient uptake capacity of root systems, reliable techniques to measure root system length and surface areas became necessary. Techniques that involve line-intersection methods were created to more directly assess root system lengths (Newman, 1966; Reicosky et al., 1970; Marsh, 1971; Tennant,

1975). The most highly accepted and utilized of these statistical approximation methods was described by Tennant (1975) and was based on line-intersect principles that were first developed by Newman (1966). To date, modern root measurement algorithms and root phenotyping systems still compare and validate their techniques using the Tennant method (Smit et al., 1994; Arsenault et al., 1995; Kimura et al., 1999).

Although the Tennant method was found to be quite robust for determining root system lengths, the reliance on the manual counting of root-grid intersections was quite time consuming, so automated procedures using electro-mechanical counters and the first digital root image analysis techniques were introduced (Kimura et al., 1999). Additionally, alternative methods to assess root system length and distribution in soil environments were also developed (Fusseder, 1983). As computer processing became more commonplace, many digital root image analysis techniques began to be introduced and validated (Bland, 1989; Tatsumi et al., 1989; Taylor et al., 1990; Zoon and Tienderen, 1990; Pan and Bolton, 1991; Smit et al., 1994; Dowdy et al., 1995). At that time digital flatbed scanners were more highly utilized than digital cameras, in part due to accessibility and cost, but also because high resolution images could be obtained with large capture areas. The number of pixels recorded across the width of the roots was later more rigorously tested and shown to be critical for the accurate and reliable assessment of root widths (Zobel, 2003; Genis et al., 2006). In the mid-1990's, the first commercial root analysis systems (Kirchhof and Pendar, 1993; Arsenault et al., 1995) as well as public domain software tools (Kaspar and Ewing, 1997) were released. The development and testing of measurement algorithms continued (Kimura et al.,

1999; Bouma et al., 2000; Costa et al., 2000; Kimura and Yamasaki, 2001, 2003; Himmelbauer et al., 2004; Genis et al., 2006), however, WinRHIZO analysis techniques (1995) became an excepted standard that is commonly used by researchers for many root system studies.

Modern root phenotyping systems

Much of modern root measurement for phenotyping purposes has been driven by the development of laboratory and greenhouse-based growth methodology along with the simultaneous expansion of imaging and analysis techniques and germplasm resources. To date, laboratory growth methods include hydroponics, agar plates, paper/cloth pouches, gel plates, box and cylinder growth systems, and aeroponic arrangements, while greenhouse growth methods typically include pots, cylinders, plates and troughs that are filled with soil, soil substitute, or sand mixtures. Rhizotron and minirhizotron growth methods have also been developed to complement coring and trenching techniques in field and greenhouse settings. Additionally, root system image capture techniques have been expanded. Digital flatbed scanner and camera systems are the most ubiquitous today, however methods using x-ray radiography, neutron radiography, laser scanning, laser sectioning, MRI, PET, CT, and μCT have also been demonstrated and refined to image crop root system in both two and three-dimensions.

Lab and greenhouse-based root growth methods

A wide range of lab and greenhouse-based techniques have been developed for growing plants to investigate and quantify root systems. Most take advantage of general purpose supplies, making them accessible to many research institutions. This section will briefly summarize the more common laboratory and greenhouse growth

systems, but will not comprehensively review all forms and combinations of growth techniques. These systems include hydroponic systems, paper/cloth pouch systems, gel-based systems and pot-based systems.

Hydroponic growth systems are widely used during root system experiments that require precise, reproducible, non-diffusion-limited control of the rhizosphere conditions, including nutrient, temperature and pH regimes (Gericke, 1945). In these systems, the shoots of the plants are suspended above a liquid nutrient solution using foam, mesh or cups, allowing the root systems to grow freely in the nutrient solution that fills the growth container. Hydroponic systems have been constructed with growth container sizes ranging from small magenta jars (Hoekenga et al., 2006) to large tubs and troughs. Some systems use recirculation and/or aeration to mix and homogenize the chemical environment, while others systems are left unaerated and/or unstirred.

Similar to hydroponic systems, aeroponic systems are nutrient solution-based systems that have been used to grow plants with controlled rhizosphere conditions, however, they have only recently been utilized during root system growth quantification experiments (Draye, 2012). In these systems, the root of the plants are allowed to grow freely in the open airspace of a closed container and are misted with nutrient solution on a fixed cycle (Zobel et al., 1976). Aeroponic systems have been adapted for studying plant nutrition and root-microbe interactions (Burgess et al., 1998; Kratsch et al., 2006) as well as for horticultural operations in order to manage and reduce nutrient and water usage.

Paper and fabric-based pouch and plate systems have also been used to quantify root systems. These systems constrain root growth to two dimensions by

forcing the root systems to grow inside plastic envelopes (Liao et al., 2001) or between two semi-rigid plastic or glass sheets (Chen et al., 2011). The inside surface(s) of the sheets are backed with paper or fabric so that root systems are in contact with absorbent material moistened with nutrient solution at all times. These systems preserve the 2D architecture of the root while also allowing temporal root system data to be collected. Multiple pouches are typically placed inside containers that are partially filled with nutrient solution. The pouches are placed in the container with their semi-open bottoms immersed in the solution in order to allow the solution to be drawn up and retained in the paper or fabric by capillary action. Other designs that have larger pouches or fabrics having insufficient capillary properties have also utilized controlled recirculation systems with drippers that water the pouches on a fixed cycle.

Gel-based agar, agarose and gellan gum systems have also been used for root system studies. Gel plates (such as petri plates) are commonly used during experiments involving smaller plants such as Arabidopsis (*Arabidopsis thaliana*), a model dicotyledonous species. In these plate systems, the seeds are planted on top of the gel media in the plates (Simmons et al., 1995). The plates are then oriented vertically and the plant root systems grow along the surface of the gel allowing the two dimensional growth of the root system to be observed and measured over time (Wells et al., 2012). Other types of gel-based techniques include gel box and cylinder systems. Similar to pouch systems, gel box systems constrain root growth to two dimensions with two closely spaced plates (usually one or both plates are clear) between which a gel layer poured (Bengough et al., 2004). This also allows the root systems to grow freely in two dimensions and preserve the 2D architecture of the root systems. Gel cylinder

systems are composed of clear plastic or glass cylinders ranging from 80mm to 300mm in diameter that are filled with clear, nutrient-replete gellan gum (Fang et al., 2009). The plant root systems are allowed to develop and grow in three dimensions within the confines of the cylinder. The 3D architectural characteristics of the root systems are preserved as the root system grows, allowing spatial data to be collected over time (Clark et al., 2011). For all gel-based techniques, the nutrient and pH conditions are typically set when the gel is prepared, however, pH buffers are commonly used in gel plate experiments.

Greenhouse growth systems typically use pots, cylinders and troughs that are filled with soil, soil-substitute or sand mixtures. For root system studies where the plant root systems are excavated, it is necessary to separate and clean the soil particles from the root surfaces. This process can be laborious and time consuming so a great deal of consideration is paid when designing and/or selecting a soil substrate to use during the study. Natural soils are often selected to reproduce the true rhizosphere conditions at specific field sites, however homogenous and heterogeneous mixtures of soil substitutes, potting mixes, and sand are also common. In most cases the growth containers are directly filled with the soil mixture, however some studies have also lined the inside of containers with an opaque plastic sheath that allows the root systems and soil to be removed for undisturbed viewing of root system distribution at harvest. Some experiments also subdivide the containers into vertical sections allowing the soil columns to be broken into distinct sections to record depth-related growth information (Hund et al., 2009). Additionally, other experiments use horizontally-oriented placed gridded material, such as mesh within the soil column, allowing the soil material to be

washed away and the roots to be collected, counted and imaged separately (Liao et al., 2001; Uga et al., 2011).

Rhizotron techniques are often used during greenhouse and field root system studies. Rhizotrons are soil filled containers, troughs and in-field trenches with a single or multiple clear surfaces in contact with the soil of the rhizosphere. The portions of the plant root systems that come in contact with the clear plastic or glass can be observed and measured over time. Rhizotrons come in many forms with some as small as plate designs similar to gel boxes, or as large as whole greenhouse units with basement galleries for viewing the roots and collecting samples (Huck, 1982). Recently, rhizotron techniques have also been integrated into automated public (Nagel et al., 2012) and commercial (LemnaTec GmbH, Wuerselen, Germany) greenhouse designs to capture and quantify both root and shoot characteristics simultaneously.

Minirhizotron techniques have also been developed and used during field and greenhouse experiments. Minirhizotrons are clear, hollow tubes that are installed in the soil underneath the plant before it is planted. The rhizotron tubes are inserted so that one end of the tube is accessible to a specialized camera that can be used to image the roots that come in contact with the outside surface of the tube (Aust, 1988).

Root image capture methods

Most modern root quantification methods involve some degree of image capture and software processing and analysis, however, it is still effective and common to collect root system weights or take manual measurements using rulers, protractors and calipers during many experimental situations (Trachsel et al., 2011). In addition to imaging via digital photography and scanning, many other techniques have been

introduced to capture root images. It should be noted that every technique has it's own specific advantages and each technique also has a unique set of constraints and limitations. Experimenters must first explore their options in order to balance tradeoffs between growth method(s), image capture technique(s) and analysis techniques for a particular root system study.

Root system image capture methods can be roughly broken into two categories, 2D imaging methods and 3D imaging methods. Additionally, some techniques can be used to cull 3D information from 2D data collection methods. These methods include specific growth and collection protocols such as minirhizotrons or soil column sectioning, or software-based techniques that statistically estimate 3D features from 2D image data (Arsenault et al., 1995).

Digital imaging via photography or scanning can be used to capture 2D images of root systems collected from almost any growth system. Depending on the application and desired measurements, it can more advantageous to use either camera-based systems or scanner-based systems. Digital cameras are useful during high-throughput applications and enable a range of hardware designs to be selected. In addition to rapid image capture rates, cameras can also collect multi-spectral data that can be useful during whole plant phenotyping under both biotic and abiotic stress. With digital cameras, however, tradeoffs exist between capture resolutions (pixels per mm) and capture areas because of the fixed density of their sensor arrays (Zobel, 2008). Scanners can capture very high resolution images at low costs and do not need to be aligned, focused and calibrated. Scanners are useful during root studies involving width classification of fine roots, but sometimes require the destructive staining of the root

system to improve contrast and accuracy. Based on the scanning area and desired image resolution, scanners can require much more time to capture images which reduces their throughput and applicability in large screening experiments.

In some 2D root imaging studies, the root systems are removed from their growth media and spread out in a clear, water-filled tray (Famoso et al., 2010; Clark et al., 2012). The roots are aligned in the focal plane of the camera or scanner and root system images are captured. This technique is further described as utilized in the research presented in Chapter II. Other types of 2D planar imaging protocols involve rhizotrons and gel plates, where images of the root systems are taken *in-situ*, however, the imaging principles are similar.

Other 2D imaging methods extract 2D images from 3D soil-based systems. One example is x-ray radiography, which has historically been used during medical diagnostics, but has also been applied to image roots. During x-ray imaging, x-ray radiation produces a 2D intensity image based on the attenuation of x-rays as they pass through objects in the imaging volume. During the process, the 3D structures in the volume are projected and flattened into two dimensions (Pierret et al., 2003). To complement x-ray imaging, neutron radiography produces similar intensity images using neutrons to capture images of root system growing *in-situ* (Willatt et al., 1978). Since neutrons are most strongly attenuated by hydrogen, neutron radiography is better at dealing with metal impurities and visualizing water saturation levels of the soil (Moradi et al., 2009). Similar to x-ray and neutron imaging, digital photography has also been used to image root systems growing in clear growth containers such as gel cylinders or hydroponic magenta jars (Hoekenga et al., 2006; Iyer-Pascuzzi et al., 2010). In these

cases, however, the growth substrate must be transparent and depth of the focal field must be adjusted to capture all the roots with clarity.

3D image capture methods can be broken into two categories, surface reconstruction methods and volumetric reconstruction methods. Since crop roots are small structures, during whole root system imaging studies all 3D imaging modalities capture the roots at resolutions that cannot resolve the cellular structure of the roots. Therefore, during the subsequent root extraction and analysis it is more common to represent the root systems as solid objects known as surface models. These surface models are sometimes also referred to as 2.5D representations of the root systems.

Volumetric imaging techniques are mainly used during medical diagnostics and have also been used to image root systems. X-ray computed tomography (CT) and microcomputed tomography (μCT) are techniques that use x-ray beams to non-destructively capture cross-sectional slices of root systems that are growing in soil substrates (Smit, 2000). The x-rays are emitted and captured from rotational positions around the imaging volume allowing the root objects to be reconstructed and extracted from the surrounding substrate. Similar to CT, magnetic resonance imaging (MRI) and positron emission tomography (PET) are other volumetric techniques that were developed for the medical community and have been applied to the imaging of root systems. MRI uses principles of nuclear magnetic resonance (NMR), where ^{1}H nuclei (or other nuclei) of the roots are oriented in a strong static magnetic field and an external electromagnetic radiation is applied at an optimal resonance frequency in a direction that is orthogonal to the static field (Antonsen et al., 1999). This radiation is absorbed then reemitted by the ^{1}H nuclei in the volume and can be recorded and

analyzed in order to reconstruct 3D images. PET imaging uses gamma rays that are generated by decaying positrons from ^{11}C atoms and interact with labeled tracers that have been assimilated by the root systems. These gamma rays are captured and recorded to generate 3D images of the root system (Jahnke et al., 2009). Even though CT, MRI and PET are typically used for medical imaging, several studies have been conducted to improve this methodology for root system imaging, including the optimization of the growth substrates, acquisition procedures and processing methods (Flavel et al., 2012; Mairhofer et al., 2012). While much improvement has been made since the initial demonstration of these techniques, many limitations still remain. These shortcomings include limited accessibility to imaging facilities, high cost, small capture volumes and/or low resolution, poor root extraction ability, and long image acquisition times.

Surface reconstruction techniques involving digital imaging or laser scanners are optical tomography approaches that require the growth substrate be optically clear or that the root systems be removed from the growth substrate prior to imaging. Image-based 3D reconstruction techniques initially stem from the computer vision discipline (Chien and Aggarwal, 1986), and were adapted for root system imaging by Zhu et al (2006) and Fang et al (2009) at South China Agricultural University. In these initial studies the root systems of soybean plants were grown in cylinders containing sand with a fixed number of mesh layers. After the experimental growth period, the cylinders were dried and the sand and mesh was removed allowing the dry, rigid root systems to be imaged and reconstructed. Later, a commercial laser scanner system was adapted by the same lab to non-destructively image living root systems that were growing in clear

growth cylinders filled with a gellan gum substrate. This allowed whole root systems to be imaged and measured in 3D over time. Both of these studies have demonstrated the practicality of using digital imaging and the gellan gum growth methods to investigate the 3D characteristics of root systems over time and have provided the foundation for a substantial part of this dissertation (Chapters III and IV).

Root quantification software and measurement types

With the variety of growth and imaging techniques available to capture root system images for quantification, many general purpose and custom software tools have been developed to process and analyze roots system images. A list of currently available root analysis software systems with general usage information is summarized in Table 1.1. Further information about these software tools can be found at the following website dedicated to root imaging analysis software: www.root-image-analysis.org/.

Many of these analysis tools were designed for specific types of root imaging experiments and share overlapping features with other software packages. This redundancy is unavoidable and increases their possible utility during other root studies. The types of measurements that are generally focused on during the root system quantification studies are summarized in a review on root architecture and plant productivity (Lynch, 1995). Root architecture is commonly used as a catch-all phrase to describe many aspects of root system quantification; however, four main classes of root system measurements (including root architecture) are outlined in the review.

Root architecture can be distinguished from three other root system features: root morphology, root topology and root distribution. Root morphology looks at the

features along a single root or root axis. These features include patterning of root hairs and daughter roots, root surface characteristics and undulations, and root diameters. Root topology describes how the roots within a root system are connected through branching. This contextualizes the whole root system in a network framework and subsequently allows established mathematical and computation principles from the fields of topology and graph theory to be applied. Root distribution describes the position where roots of the entire root system or a subset of the root system are present in the root volume. This positional distribution of the root system is comprised of root properties including root type, root length, root volume and root surface area. The focus of this research, root architecture, is defined as the geometric and spatial configuration of the entire root system and supersedes both root distribution and topology. Root morphology and root hair characteristics are not usually included in architecture quantification; however measurements of root architecture can also be used to describe root distribution and topology.

While the different types of root measurement can described and classified, a clear and defined ontological system has not been establish due to the extensive variation in plant root system architecture and formation. This complexity is further exacerbated by the numerous growth, imaging and analysis methods that are under continuous development for the study of root systems under specific conditions. Establishing a more unified and defined classification system would possibly reduce some the complexity and ambiguity of describing root systems and further direct how they are measured and studied.

Table 1.1: Currently available root analysis software tools and information about their applications.

Software	Availability	Website	Corresponding Growth System	Range of Measurements	General Description
DART	Freeware	http://www4.paca.inra.fr/psh/Outils/Dart	H	SR, TRS	Semi-automated software for studying inter-root branching of root networks. Relies on manual user interaction to identify roots across time series images. (Le Bot et al., 2010)
Delta-T-Scan	Commercial	http://www.delta-t.co.uk/default.asp	NS	TRS	Automated software to measure root characteristics from 2D root image scans.
EZ-Rhizo	Freeware	http://www.psrg.org.uk/ez-rhizo.htm	GP	TRS	Semi-automatic software to detect and measure several 2D root system architecture (RSA) traits. (Armengaud et al., 2009)
GiA Roots	Freeware	http://www.rootnet.biology.gatech.edu/giaroots/download/signup.php	NS	TRS	Automated software to facilitate the large-scale analysis of root system architecture and root structures. (Galkovskyi et al., 2012)
GROWMAP-root	Freeware (*unavailable*)	http://www.fz-juelich.de/ibg/ibg-2/EN/methods_jppc/GROWMAP-root/_node.html	GP	SR	Automated software system to monitor and determine velocity vectors of root tip growth. (Walter et al., 2002)
GROWSCREEN-Root	Freeware (*unavailable*)	http://www.fz-juelich.de/ibg/ibg-2/EN/methods_jppc/GROWSCREEN_root/_node.html	GP	SR, TRS	Automated software to analyze root architecture from whole root system grown on agar plates. (Nagel et al., 2009)
Growth Explorer	Freeware	http://home.iitk.ac.in/~apal/growthexplorer.html	PP	SR	Software tool and methodology to analyze the spatio-temporal emergence and growth of individual roots in a root system. (Basu and Pal, 2012)
ImageJ	Freeware	http://rsbweb.nih.gov/ij/	NS	SR	General purpose image processing program that is typically used to pre-process root images and assist of in the manual measurement of roots. The program can be extended using custom plugins. (Rasband, 1997-2012)
KineRoot	Freeware	http://roots.psu.edu/node/782	H	SR	Software tool to measure spatio-temporal growth patterns and curvature of roots by tracking small particles on the root surfaces. (Basu et al., 2007)

Corresponding Growth System: Hydroponics (H), Paper pouch (PP), Gel plate (GP), Gel cylinder (GC), Rhizotron (R), Minirhizotron (MR), Soil (S), Soil substitute (SS), Not specialized (NS); Range of Measurements: Single root (SR); Total root system (TRS)

Table 1.1 (continued)

Software	Availability	Website	Corresponding Growth System	Range of Measurements	General Description
MR-RIPL	Freeware	http://rootimage.msu.edu/MR-RIPL/index.html	R, MR	TRS	Automated software to detect and measure roots from rhizotron and minirhizotron root images.
Root Image Analyzer	Freeware	http://rootimage.msu.edu/root_images/new	R, MR	TRS	Automated software to measure roots from rhizotron and minirhizotron root images.
ROOTEDGE	Freeware	http://www.ars.usda.gov/Services/docs.htm?docid=10784	NS	TRS	Automatic software to measure geometric characteristics of binary objects. (Kaspar and Ewing, 1997)
RootFlowRT	Freeware	http://www.bio.umass.edu/biology/baskin/RootflowRT_html/About.htm	GP, H	SR	Software to measure the expansion profile of growing roots. (van der Weele et al., 2003)
RootFly	Freeware	http://www.ces.clemson.edu/~stb/rootfly/	R, MR	SR	Software to measure root traits from rhizotron and minirhizotron images. Uses color information analyze root birth and death rates. (Zeng et al., 2010)
RootLM	Freeware	http://digital.cs.usu.edu/~xqi/RootLM/	GP	SR	Automated software to measure root growth from manually drawn growth tracks on petri dish surfaces. (Qi et al., 2007)
RootReader2D	Freeware	http://www.plantmineralnutrition.net/rootreader.htm	NS	SR, TRS	Semi-automated software for measuring root lengths from 2D root system images. (Clark et al., 2013)
RootReader3D	Freeware (*unavailable*)	http://www.plantmineralnutrition.net/rootreader.htm	GC	SR, TRS	Semi-automated software to reconstruction and quantify 3D root traits from 2D rotational image sequences. (Clark et al., 2011)
RootScan	Freeware	http://roots.psu.edu./en/rootscan	NS	SR	Automated software to measure anatomical traits from microscope images of root cross-sections. (Burton et al., 2012)
RootSnap	Commercial	http://www.cid-inc.com/ci-690.php	R, MR	SR	Interactive software to measure roots from rhizotron and minirhizotron images.

Corresponding Growth System: Hydroponics (H), Paper pouch (PP), Gel plate (GP), Gel cylinder (GC), Rhizotron (R), Minirhizotron (MR), Soil (S), Soil substitute (SS), Not specialized (NS); Range of Measurements: Single root (SR); Total root system (TRS).

Table 1.1 (continued)

Software	Availability	Website	Corresponding Growth System	Range of Measurements	General Description
MR-RIPL	Freeware	http://rootimage.msu.edu/MR-RIPL/index.html	R, MR	TRS	Automated software to detect and measure roots from rhizotron and minirhizotron root images.
RootTrace	Freeware	http://www.cpib.ac.uk/tools-resources/roottrace/	GP	SR	Semi-automatic software to measure root length and curvature characteristics from root system images. (French et al., 2009)
RootTrak	Freeware	http://www.cpib.ac.uk/tools-resources/rootrak/	S, SS	TRS	Software to extract root systems form x-ray micro CT images. (Mairhofer et al., 2012)
RootVisFS	Commercial	http://www.phenotypescreening.com/	SS	TRS	Software to analyze root systems from x-ray images.
SAW Roots	Commercial	http://www.lemnatec.com/	MR	TRS	Software to analysis root images from minirhizotron cylinders.
SkyeRoot	Commercial	http://www.skyeinstruments.com/	NS	TRS	Automated software to measure and analyze root system images.
SmartRoot	Freeware	http://www.uclouvain.be/smartroot	GP	SR, TRS	Semi-automatic ImageJ software toolkit used to measure root growth and architecture from 2D root system images. (Lobet et al., 2011)
TIPTRACKER	Freeware *(unavailable)*	http://www.cpib.ac.uk/tools-resources/	H, GP	SR	Automated software for tracking the orientation of a growing root tip from high resolution microscopy images. (Wells et al., 2012)
WinRhizo	Commercial	http://www.regentinstruments.com/	NS	SR, TRS	Automated software to measure root characteristics based on diameter classes from 2D root images. (Arsenault et al., 1995)
WinRhizo Tron	Commercial	http://www.regentinstruments.com/	R, MR	SR	Semi-automated software to assist in the measurement and analysis of rhizotron and minirhizotron images.
WR-RIPL	Freeware	http://rootimage.msu.edu/WR-RIPL/index.html	NS	TRS	Automated software to measure root length and volume from scanned 2D root images.

Corresponding Growth System: Hydroponics (H), Paper pouch (PP), Gel plate (GP), Gel cylinder (GC), Rhizotron (R), Minirhizotron (MR), Soil (S), Soil substitute (SS), Not specialized (NS); Range of Measurements: Single root (SR); Total root system (TRS).

CONCLUSION

This chapter provides a general overview of the biological importance of root systems and the tools and techniques that have been established to study them. Many of the concepts that were discussed touch on a wide range of disciplines including root biology, engineering and computation. The application and integration of these and other interdisciplinary approaches will be necessary to continue to advance research in root biology as well as in other related disciplines.

REFERENCES

Antonsen F, Johnsson A, Futsaether C, Krane J (1999) Nuclear magnetic resonance imaging in studies of gravitropism in soil mixtures. New Phytologist 142: 59-66

Armengaud P, Zambaux K, Hills A, Sulpice R, Pattison RJ, Blatt MR, Amtmann A (2009) EZ-Rhizo: integrated software for the fast and accurate measurement of root system architecture. The Plant Journal 57: 945-956

Arsenault JL, Poulcur S, Messier C, Guay R (1995) WinRHIZO, a root-measuring system with a unique over-lap correction method. HortScience 30: 906

Aust H (1988) Minirhizotron observation tubes: Methods and applications for measuring rhizosphere dynamics, Vol 1

Basu P, Pal A (2012) A new tool for analysis of root growth in the spatio-temporal continuum. New Phytologist 195: 264-274

Basu P, Pal A, Lynch JP, Brown KM (2007) A Novel Image-Analysis Technique for Kinematic Study of Growth and Curvature. Plant Physiology 145: 305-316

Bengough AG, Gordon DC, Al-Menaie H, Ellis RP, Allan D, Keith R, Thomas WTB,

Forster BP (2004) Gel observation chamber for rapid screening of root traits in cereal seedlings. Plant and Soil 262: 63-70

Berntson GM (1994) Modelling Root Architecture: Are There Tradeoffs between Efficiency and Potential of Resource Acquisition? New Phytologist 127: 483-493

Bland WL (1989) Estimating Root Length Density by the Core-Break Method. Soil Sci. Soc. Am. J. 53: 1595-1597

Bouma T, Nielsen K, Koutstaal B (2000) Sample preparation and scanning protocol for computerised analysis of root length and diameter. Plant and Soil 218: 185-196

Burgess T, McComb J, Hardy G (1998) Influence of Low Oxygen Levels in Aeroponics Chambers on Eucalypt Roots Infected with Phytophthora cinnamomi. Plant Disease 82: 368-373

Burton AL, Williams M, Lynch JP, Brown KM (2012) RootScan: Software for high-throughput analysis of root anatomical traits. Plant and Soil: 1-15

Chen YL, Dunbabin VM, Diggle AJ, Siddique KHM, Rengel Z (2011) Development of a novel semi-hydroponic phenotyping system for studying root architecture. Functional Plant Biology 38: 355-363

Chien CH, Aggarwal JK (1986) Identification of 3D objects from multiple silhouettes using quadtrees/octrees. Computer Vision, Graphics, and Image Processing 36: 256-273

Clark RT, Famoso AN, Zhao K, Shaff JE, Craft EJ, Bustamante CD, McCouch SR, Aneshansley DJ, Kochian LV (2013) High-throughput two-dimensional root system phenotyping platform facilitates genetic analysis of root growth and development. Plant, Cell & Environment 36: 454-466

Clark RT, MacCurdy RB, Jung JK, Shaff JE, McCouch SR, Aneshansley DJ, Kochian LV (2011) Three-Dimensional Root Phenotyping with a Novel Imaging and Software Platform. Plant Physiology 156: 455-465

Costa C, Dwyer LM, Hamilton RI, Hamel C, Nantais L, Smith DL (2000) A Sampling Method for Measurement of Large Root Systems with Scanner-Based Image Analysis. Agronomy Journal 92: 621-627

Dowdy RH, Nater EA, Dolan MS (1995) Quantification of the length and diameter of root segments with public domain software. Communications in Soil Science and Plant Analysis 26: 459-468

Draye X (2012) Personal Communication. *In*,

Evans H (1938) Studies on the Absorbing Surface of Sugar-cane Root Systems. Annals of Botany 2: 159-182

Famoso AN, Clark RT, Shaff JE, Craft E, McCouch SR, Kochian LV (2010) Development of a Novel Aluminum Tolerance Phenotyping Platform Used for Comparisons of Cereal Aluminum Tolerance and Investigations into Rice Aluminum Tolerance Mechanisms. Plant Physiology 153: 1678-1691

Famoso AN, Zhao K, Clark RT, Tung C-W, Wright MH, Bustamante C, Kochian LV, McCouch SR (2011) Genetic Architecture of Aluminum Tolerance in Rice (Oryza sativa) Determined through Genome-Wide Association Analysis and QTL Mapping. PLoS Genetics 7: e1002221

Fang S, Yan X, Liao H (2009) 3D reconstruction and dynamic modeling of root architecture in situ and its application to crop phosphorus research. The Plant Journal 60: 1096-1108

Fitter AH (1987) An Architectural Approach to the Comparative Ecology of Plant Root Systems. New Phytologist 106: 61-77

Flavel RJ, Guppy CN, Tighe M, Watt M, McNeill A, Young IM (2012) Non-destructive quantification of cereal roots in soil using high-resolution X-ray tomography. Journal of Experimental Botany

Forde B, Lorenzo H (2001) The nutritional control of root development. Plant and Soil 232: 51-68

French A, Ubeda-Tomás S, Holman TJ, Bennett MJ, Pridmore T (2009) High-Throughput Quantification of Root Growth Using a Novel Image-Analysis Tool. Plant Physiology 150: 1784-1795

Fusseder A (1983) A method for measuring length, spatial distribution and distances of living roots *in situ*. Plant and Soil 73: 441-445

Galkovskyi T, Mileyko Y, Bucksch A, Moore B, Symonova O, Price CA, Topp CN, Iyer-Pascuzzi AS, Zurek PR, Fang S, Harer J, Benfey PN, Weitz JS (2012) GiA Roots: Software for the High Throughput Analysis of Plant Root System Architecture. BMC Plant Biology

Genis A, Blumberg DG, Ben-Asher J (2006) Optimizing application of image analysis tools to determine physical characteristics of fine roots. Environment Control in Biology 44: 11-20

Gericke WF (1945) The Meaning of Hydroponics. Science 101: 142-143

Himmelbauer ML, Loiskandl W, Kastanek F (2004) Estimating length, average diameter and surface area of roots using two different Image analyses systems. Plant and Soil 260: 111-120

Hochholdinger F, Park WJ, Sauer M, Woll K (2004) From weeds to crops: genetic analysis of root development in cereals. Trends in Plant Science 9: 42-48

Hochholdinger F, Tuberosa R (2009) Genetic and genomic dissection of maize root development and architecture. Current Opinion in Plant Biology 12: 172-177

Hoekenga OA, Maron LG, Piñeros MA, Cançado GMA, Shaff J, Kobayashi Y, Ryan PR, Dong B, Delhaize E, Sasaki T, Matsumoto H, Yamamoto Y, Koyama H, Kochian LV (2006) AtALMT1, which encodes a malate transporter, is identified as one of several genes critical for aluminum tolerance in Arabidopsis. Proceedings of the National Academy of Sciences 103: 9738-9743

Huck MG (1982) The rhizotron as a tool for root research. Advances in agronomy 35: 1

Hund A, Ruta N, Liedgens M (2009) Rooting depth and water use efficiency of tropical maize inbred lines, differing in drought tolerance. Plant and Soil 318: 311-325

Iyer-Pascuzzi AS, Symonova O, Mileyko Y, Hao Y, Belcher H, Harer J, Weitz JS, Benfey PN (2010) Imaging and Analysis Platform for Automatic Phenotyping and Trait Ranking of Plant Root Systems. Plant Physiology 152: 1148-1157

Jahnke S, Menzel MI, Van Dusschoten D, Roeb GW, Bühler J, Minwuyelet S, Blümler P, Temperton VM, Hombach T, Streun M, Beer S, Khodaverdi M, Ziemons K, Coenen HH, Schurr U (2009) Combined MRI–PET dissects dynamic changes in plant structures and functions. The Plant Journal 59: 634-644

Johnson WC, Jackson LE, Ochoa O, van Wijk R, Peleman J, St. Clair DA, Michelmore RW (2000) Lettuce, a shallow-rooted crop, and Lactuca serriola, its wild progenitor, differ at QTL determining root architecture and deep soil water exploitation. Theoretical and Applied Genetics 101: 1066-1073

Kaspar TC, Ewing RP (1997) ROOTEDGE: Software for Measuring Root Length from Desktop Scanner Images. Agron. J. 89: 932-940

Kimura K, Kikuchi S, Yamasaki S-i (1999) Accurate root length measurement by image analysis. Plant and Soil 216: 117-127

Kimura K, Yamasaki S (2001) Root length and diameter measurement using NIH Image: application of the line-intercept principle for diameter estimation. Plant and Soil 234: 37-46

Kimura K, Yamasaki S (2003) Accurate root length and diameter measurement using NIH Image: use of Pythagorean distance for diameter estimation. Plant and Soil 254: 305-315

Kirchhof G, Pendar K (1993) Delta-T Scan User Manual. Delta-T Devices Ltd, Cambridge, England

Kratsch HA, Graves WR, Gladon RJ (2006) Aeroponic system for control of root-zone atmosphere. Environmental and Experimental Botany 55: 70-76

Krill AM, Kirst M, Kochian LV, Buckler ES, Hoekenga OA (2010) Association and Linkage Analysis of Aluminum Tolerance Genes in Maize. PLoS ONE 5: e9958

Le Bot J, Serra V, Fabre J, Draye X, Adamowicz S, Pagès L (2010) DART: a software to analyse root system architecture and development from captured images. Plant and Soil 326: 261-273

Liao H, Rubio G, Yan X, Cao A, Brown KM, Lynch JP (2001) Effect of phosphorus availability on basal root shallowness in common bean. Plant and Soil 232: 69-79

Lobet G, Pagès L, Draye X (2011) A Novel Image-Analysis Toolbox Enabling Quantitative Analysis of Root System Architecture. Plant Physiology 157: 29-39

Lynch J (1995) Root Architecture and Plant Productivity. Plant Physiology 109: 7-13

Lynch J, Ho M, phosphorus L (2005) Rhizoeconomics: Carbon costs of phosphorus acquisition. Plant and Soil 269: 45-56

Lynch JP (2011) Root Phenes for Enhanced Soil Exploration and Phosphorus Acquisition: Tools for Future Crops. Plant Physiology 156: 1041-1049

Lynch JP, Brown KM (2001) Topsoil foraging – an architectural adaptation of plants to low phosphorus availability. Plant and Soil 237: 225-237

Magalhaes JV, Liu J, Guimaraes CT, Lana UGP, Alves VMC, Wang Y-H, Schaffert RE, Hoekenga OA, Pineros MA, Shaff JE, Klein PE, Carneiro NP, Coelho CM, Trick HN, Kochian LV (2007) A gene in the multidrug and toxic compound extrusion (MATE) family confers aluminum tolerance in sorghum. Nature Genetics 39: 1156-1161

Mairhofer S, Zappala S, Tracy SR, Sturrock C, Bennett M, Mooney SJ, Pridmore T (2012) RooTrak: Automated Recovery of Three-Dimensional Plant Root Architecture in Soil from X-Ray Microcomputed Tomography Images Using Visual Tracking. Plant Physiology 158: 561-569

Malamy JE (2005) Intrinsic and environmental response pathways that regulate root system architecture. Plant, Cell & Environment 28: 67-77

Marschner H (1995) Mineral nutrition of higher plants. Academic Press, London; San Diego

Marsh BAB (1971) Measurement of Length in Random Arrangements of Lines. Journal of Applied Ecology 8: 265-267

Mattsson M, Lundborg T, Larsson CM (1993) Growth and development of seminal and

crown root systems in N-limited barley, and their contributions to nitrate acquisition during vegetative and generative growth. Plant and Soil 151: 239-247

Moradi A, Conesa H, Robinson B, Lehmann E, Kuehne G, Kaestner A, Oswald S, Schulin R (2009) Neutron radiography as a tool for revealing root development in soil: capabilities and limitations. Plant and Soil 318: 243-255

Nagel KA, Kastenholz B, Jahnke S, van Dusschoten D, Aach T, Mühlich M, Truhn D, Scharr H, Terjung S, Walter A, Schurr U (2009) Temperature responses of roots: impact on growth, root system architecture and implications for phenotyping. Functional Plant Biology 36: 947-959

Nagel KA, Putz A, Gilmer F, Heinz K, Fischbach A, Pfeifer J, Faget M, Blossfeld S, Ernst M, Dimaki C, Kastenholz B, Kleinert A-K, Galinski A, Scharr H, Fiorani F, Schurr U (2012) GROWSCREEN-Rhizo is a novel phenotyping robot enabling simultaneous measurements of root and shoot growth for plants grown in soil-filled rhizotrons. Functional Plant Biology

Newman EI (1966) A Method of Estimating the Total Length of Root in a Sample. Journal of Applied Ecology 3: 139-145

Pan WL, Bolton RP (1991) Root Quantification by Edge Discrimination Using a Desktop Scanner. Agron. J. 83: 1047-1052

Pierret A, Kirby M, Moran C (2003) Simultaneous X-ray imaging of plant root growth and water uptake in thin-slab systems. Plant and Soil 255: 361-373

Plaxton WC, Tran HT (2011) Metabolic Adaptations of Phosphate-Starved Plants. Plant Physiology 156: 1006-1015

Qi X, Qi J, Wu Y (2007) RootLM: a simple color image analysis program for length

measurement of primary roots in Arabidopsis. Plant Root 1: 10-16

Rasband WS (1997-2012) ImageJ. *In*. U.S. National Institute of Health, Bethesda, Maryland, USA, http://imagej.nih.gov/ij/

Rebouillat J, Dievart A, Verdeil J, Escoute J, Giese G, Breitler J, Gantet P, Espeout S, Guiderdoni E, Périn C (2009) Molecular Genetics of Rice Root Development. Rice 2: 15-34

Reicosky DC, Millington RJ, Peters DB (1970) A Comparison of Three Methods for Estimating Root Length. Agron. J. 62: 451-453

Shen J, Yuan L, Zhang J, Li H, Bai Z, Chen X, Zhang W, Zhang F (2011) Phosphorus Dynamics: From Soil to Plant. Plant Physiology 156: 997-1005

Simmons C, Söll D, Migliaccio F (1995) Circumnutation and gravitropism cause root waving in Arabidopsis thaliana. Journal of Experimental Botany 46: 143-150

Smit A, Sprangers J, Sablik P, Groenwold J (1994) Automated measurement of root length with a three-dimensional high-resolution scanner and image analysis. Plant and Soil 158: 145-149

Smit AL (2000) Root methods : a handbook. Springer, Berlin; New York

Tatsumi J, Yamauchi A, Kono Y (1989) Fractal Analysis of Plant Root Systems. Annals of Botany 64: 499-503

Taylor HM, Upchurch DR, McMichael BL (1990) Applications and limitations of rhizotrons and minirhizotrons for root studies. Plant and Soil 129: 29-35

Tennant D (1975) A Test of a Modified Line Intersect Method of Estimating Root Length. Journal of Ecology 63: 995-1001

Trachsel S, Kaeppler S, Brown K, Lynch J (2011) Shovelomics: high throughput

phenotyping of maize (Zea mays L.) root architecture in the field. Plant and Soil 341: 75-87

Uga Y, Okuno K, Yano M (2011) Dro1, a major QTL involved in deep rooting of rice under upland field conditions. Journal of Experimental Botany 62: 2485-2494

van der Weele CM, Jiang HS, Palaniappan KK, Ivanov VB, Palaniappan K, Baskin TI (2003) A New Algorithm for Computational Image Analysis of Deformable Motion at High Spatial and Temporal Resolution Applied to Root Growth. Roughly Uniform Elongation in the Meristem and Also, after an Abrupt Acceleration, in the Elongation Zone. Plant Physiology 132: 1138-1148

Vance CP, Uhde-Stone C, Allan DL (2003) Phosphorus acquisition and use: critical adaptations by plants for securing a nonrenewable resource. New Phytologist 157: 423-447

Waisel Y, Eshel A, Kafkafi U (1996) Plant roots : the hidden half. Marcel Dekker, New York

Walter A, Spies H, Terjung S, Küsters R, Kirchgeßner N, Schurr U (2002) Spatio-temporal dynamics of expansion growth in roots: automatic quantification of diurnal course and temperature response by digital image sequence processing. Journal of Experimental Botany 53: 689-698

Wang X, Yan X, Liao H (2010) Genetic improvement for phosphorus efficiency in soybean: a radical approach. Annals of Botany 106: 215-222

Weaver JE, Bruner WE (1927) Root Development of Vegetable Crops. McGraw-Hill Book Company, Inc., New York

Wells DM, French AP, Naeem A, Ishaq O, Traini R, Hijazi H, Bennett MJ, Pridmore TP

(2012) Recovering the dynamics of root growth and development using novel image acquisition and analysis methods. Philosophical Transactions of the Royal Society B: Biological Sciences 367: 1517-1524

Willatt ST, Struss RG, Taylor HM (1978) In situ Root Studies Using Neutron Radiography. Agron. J. 70: 581-586

Zeng G, Birchfield S, Wells C (2010) Rapid automated detection of roots in minirhizotron images. Machine Vision and Applications 21: 309-317

Zhao J, Fu J, Liao H, He Y, Nian H, Hu Y, Qiu L, Dong Y, Yan X (2004) Characterization of root architecture in an applied core collection for phosphorus efficiency of soybean germplasm. Chinese Science Bulletin 49: 1611-1620

Zheng BS, Yang L, Zhang WP, Mao CZ, Wu YR, Yi KK, Liu FY, Wu P (2003) Mapping QTLs and candidate genes for rice root traits under different water-supply conditions and comparative analysis across three populations. Theoretical and Applied Genetics 107: 1505-1515

Zhu J, Kaeppler SM, Lynch JP (2005) Topsoil foraging and phosphorus acquisition efficiency in maize (Zea mays). Functional Plant Biology 32: 749-762

Zhu T, Fang S, Li Z, Liu Y, Liao H, Yan X (2006) Quantitative analysis of 3-dimensional root architecture based on image reconstruction and its application to research on phosphorus uptake in soybean. Chinese Science Bulletin 51: 2351-2361

Zobel RW (2003) Sensitivity Analysis of Computer-Based Diameter Measurement from Digital Images. Crop Sci. 43: 583-591

Zobel RW (2008) Hardware and software efficacy in assessment of fine root diameter distributions. Computers and Electronics in Agriculture 60: 178-189

Zobel RW, Del Tredici P, Torrey JG (1976) Method for Growing Plants Aeroponically. Plant Physiology 57: 344-346

Zoon FC, Tienderen PH (1990) A rapid quantitative measurement of root length and root branching by microcomputer image analysis. Plant and Soil 126: 301-308

CHAPTER II

HIGH-THROUGHPUT TWO-DIMENSIONAL ROOT PHENOTYPING PLATFORM TO ANALYZE ROOT GROWTH AND DEVELOPMENT

ABSTRACT

High-throughput phenotyping of root systems requires a combination of specialized techniques and adaptable plant growth, root imaging and software tools. A custom phenotyping platform was designed to capture images of whole root systems, and novel software tools were developed to process and analyze these images. The platform and its components are adaptable to a wide range root phenotyping studies using diverse growth systems (hydroponics, paper pouches, gel and soil) involving several plant species, including, but not limited to rice, maize, sorghum, tomato and Arabidopsis. The RootReader2D software tool is free and publicly available and was designed with both user-guided and automated features that increase flexibility and enhance efficiency when measuring root growth traits from specific roots or entire root systems during large-scale phenotyping studies. To demonstrate the unique capabilities and high-throughput capacity of this phenotyping platform for studying root systems, genome-wide association studies on rice (*Oryza sativa*) and maize (*Zea mays*) root growth were performed and root traits related to aluminum (Al) tolerance were analyzed on the parents of the maize nested association mapping (NAM) population.

INTRODUCTION

Digital imagery and automated analysis provide new opportunities for plant researchers to study a wide range of physiological and developmental plant processes with greater efficiency (Brewer et al., 2006; Chavarría-Krauser et al., 2008; Wang et al., 2009). With the development of both general purpose and custom root analysis systems, many unique quantitative studies of root system growth are now possible (Zeng et al., 2008; Le Bot et al., 2010). In recent years, root analysis system designs have focused on combining imaging methods with automated algorithms that enable root system features to be measured or tracked (Armengaud et al., 2009; French et al., 2009; Basu and Pal, 2012; Galkovskyi et al., 2012).

To date, notable progress has been made investigating plants grown on agar plate systems (Miller et al., 2007; Qi et al., 2007; Nagel et al., 2009; Yazdanbakhsh and Fisahn, 2009); however, due to the high specificity of these designs, many researchers still depend on manual methods involving tracing or hand measurement of roots. Manual techniques remain reliable for small experiments involving simple root system structures and measurements, however there is continued interest in exploring new techniques to capture and extract phenotypes from a wider variety of root systems with greater throughput and reduced subjectivity (French et al., 2009). Furthermore, as researchers work to unravel the genetic, molecular and developmental networks that underlie the subtle growth characteristics and responses of root systems, the development of high-throughput, multi-functional platforms becomes essential (Malamy, 2005; de Dorlodot et al., 2007; Gregory et al., 2009; Hochholdinger and Tuberosa, 2009).

The design of phenotyping systems requires the integration of image capture techniques combined with complementary processing and analysis tools. Off-the-shelf imaging systems have been incorporated successfully into many phenotyping systems to generate high quality root images and software analysis tools have been developed to complement these techniques (Miller et al., 2007; French et al., 2009; Lobet et al., 2011). The potential for automated analysis of crop root systems during genetic mapping studies and the importance of including user-guided processes to assist with the analysis of root-specific characteristics have been highlighted by several recent studies from our lab as well as other labs (Iyer-Pascuzzi et al., 2010; Le Bot et al., 2010; Clark et al., 2011; Lobet et al., 2011; Nagel et al., 2012).

For the research detailed here, a platform was developed to acquire intact root system images in order to quantify root growth responses both from whole root systems and specific roots of interest. Using standard photography equipment, a digital imaging system was designed to efficiently capture high resolution root images with high contrast, precision and accuracy. Using the Java programing language, a semi-automated analysis software was developed to process and measure root system traits. Here, the RootReader2D software is introduced as a general tool designed for the 2D analysis of root system images from a broad range of phenotyping studies. Working with a hydroponic growth system, two whole genome screens of rice and maize diversity panels were performed to demonstrate the high-throughput capabilities during large-scale mapping studies. Additionally, to highlight the flexibility of the platform for measuring unique, root type-based traits were also evaluated on the parents of the maize (*Zea mays*) nested association mapping (NAM) population.

RESULTS AND DISCUSSION

The following sections summarize key aspects of the 2D root phenotyping platform and present results from studies with rice and maize to demonstrate the utility of this approach during both large-scale mapping and unique root system investigations.

The RootReader2D software tool is free and publicly available as a Java Web Start (Sun Microsystems, Santa Clara, CA, USA) application and can be used in a wide range of root system studies. Its graphical interface contains several viewing, processing and measurement options combined with batch processing and user-guided features (Fig. 2.1). For more information on the RootReader2D software tool, visit http://www.plantmineralnutrition.net/rootreader.htm for software documentation or to access and launch the software.

RootReader2D processing and analysis

During the analysis of a single root system image (Fig. 2.2A), the color or grayscale image is first opened with the RootReader2D software and thresholded to generate a binary image where the root system appears blue against the background (Fig. 2.2B). The binary root image is then skeletonized (Hilditch, 1969) to generate a unit width curve representation of the root system composed of skeleton points (Fig. 2.2C). The root system skeleton points are then classified as either endpoints or connector points based on their adjacency, defined as “valence”, to neighboring skeleton points within local 3 x 3 pixel regions of the image. Each skeleton point can have a valence value of 0 to 8, where endpoints have valances of either 1 or 3 to 8 and

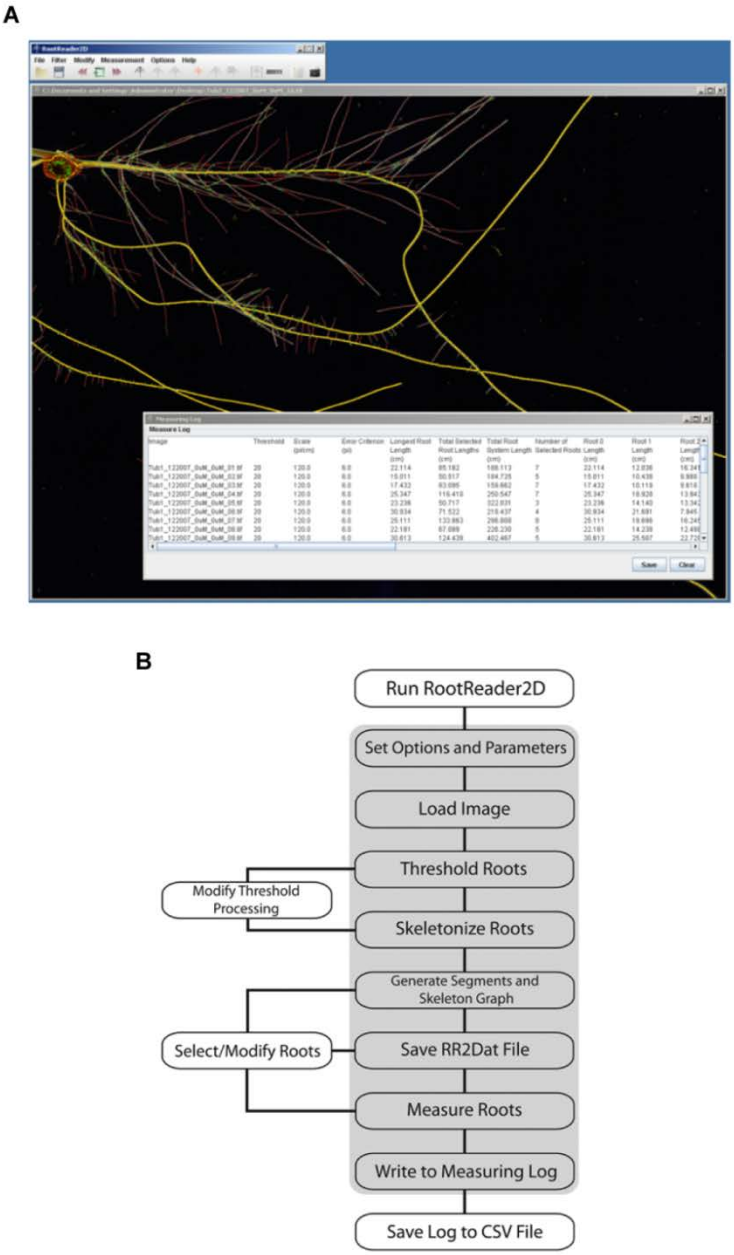

Figure 2.1: A) RootReader2D software screenshot with measuring log and image of analyzed maize root system where primary, seminal and total root lengths have been measured. B) Diagram of processing steps for root analysis with the RootReader2D software. The steps shaded in gray are performed automatically during batch processing routines.

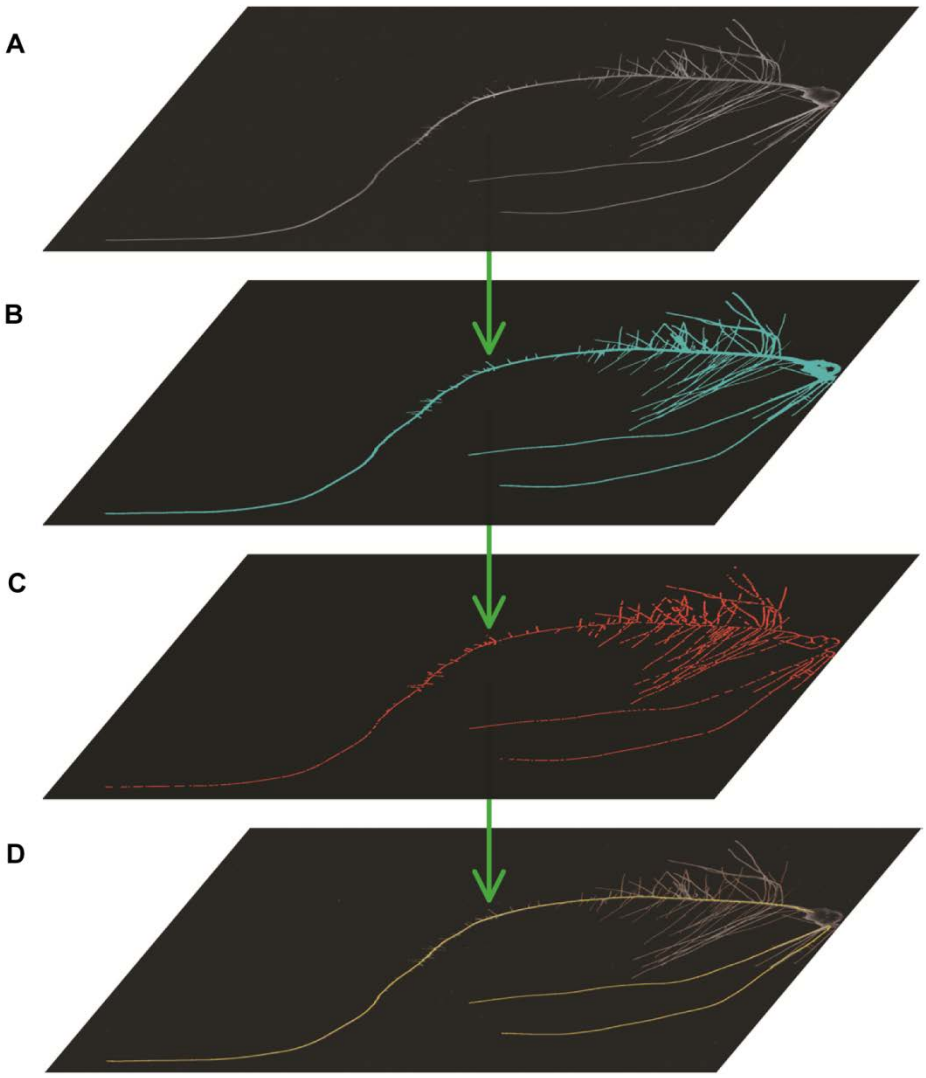

Figure 2.2: Depiction of processing and analysis steps with RootReader2D software. A) Original maize root image. B) Threshold points (blue). C) Skeleton points (red). D) Processed root image with primary and two seminal roots selected (yellow).

connector points have valances of 2. Isolated points that have valences of 0 are removed from further processing and groups of clustered endpoints are reduced into single, representative endpoints using a “valence driven spatial median” technique described by Wang and Cheng (2008). The classified skeleton points are then separated into distinct segments that contain two endpoints joined by zero or more connector points. The lengths of the generated segments are then found using an automated polyline estimation technique. A polyline is a continuous line consisting of one or more line segments and is commonly used during the estimation of curve lengths (Shirley and Ashikhmin, 2005). A graph-based data structure (or network) is then created where the skeleton endpoints represent nodes and connector points represent edges (Weiss, 2002). Dijkstra’s algorithm (Dijkstra, 1959) is then applied to find the shortest connected path through the skeleton network from each endpoint to every other endpoint where the individual segment lengths are used as weight criteria. These paths are stored in computer memory for use during root selection and further analysis.

During the segment length calculation, the total length of the whole root system is automatically found by summing the total length of skeleton segments in the image. If specific roots need to be measured, the start (usually the seed) and end (root tip) of any root of interest can be selected via interactive mouse commands. During the root selection process, the RootReader2D software uses the interactively selected root endpoints and stored shortest path information to display the selected root path in real-time (Fig. 2.2D). If any portion of the generated root path through the skeleton network is incorrect, the user can modify and correct the generated path using mouse and keyboard commands. For each selected root, estimates of lateral root branching counts

are automatically generated by summing the root skeleton intersections along the selected root path, excluding the start and end endpoints. The processing information and measurement data for the image can then be saved to an xml-formatted rr2dat data file.

High-throughput root phenotyping and general applications

The growth, imaging and RootReader2D software tools (Fig. 2.1A and Fig. 2.3) were designed to facilitate the efficient measurement of root lengths from crop root systems during large-scale phenotyping experiments. Building off previous hydroponic techniques developed in our lab (Magalhaes et al., 2004), a floating foam system was designed to support the plants and allow unimpeded access of all roots to the nutrient solution during growth, while also reducing plant handling and improving efficiency during photography. Utilizing this foam support system in conjunction with the stationary imaging setup allows intact seedling root systems of rice and maize (less than 7 days old) to be spread out, imaged (with one imaging system) and replaced by two people at an optimal rate of 12 seconds per plant during multi-tub experiments.

The RootReader2D software was developed with batch processing capability to minimize user interaction, allowing repetitive image processing and measurement tasks such as thresholding, skeletonization, and graph generation to be performed automatically on large image sets using fixed parameters (Fig. 2.1B). During batch processing routines, all of the generated processing data are stored in rr2dat data files and thresholded root system images can be saved for analysis with other software

Figure 2.3: A) Illustration of the imaging system with close-ups of small components (C – camera; CS – copy stand; LB – light box; ST – specimen tray). B) Image of the hydroponic growth system with floating foam strips. This system has been used for growing maize (*Zea mays*), wheat (*Triticum aestivum*), rice (*Oryza sativa*) and sorghum (*Sorghum bicolor*).

A

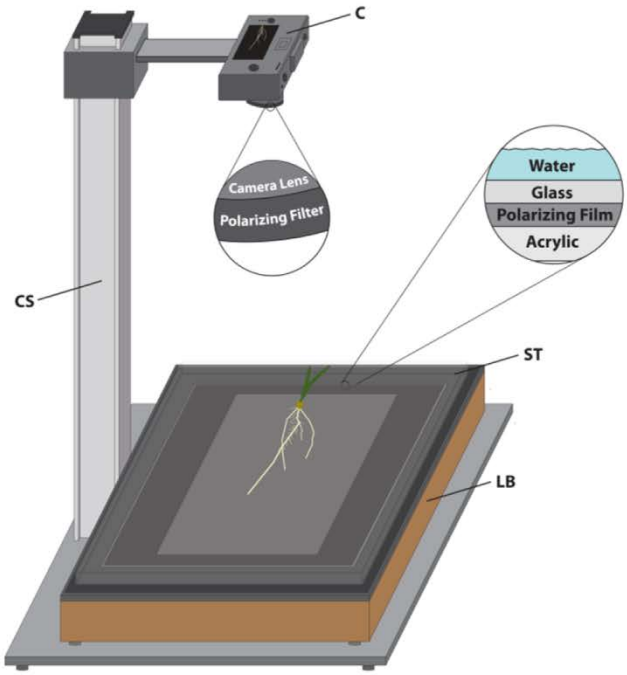
C
Camera Lens
Polarizing Filter
Water
Glass
Polarizing Film
Acrylic
CS
ST
LB

B

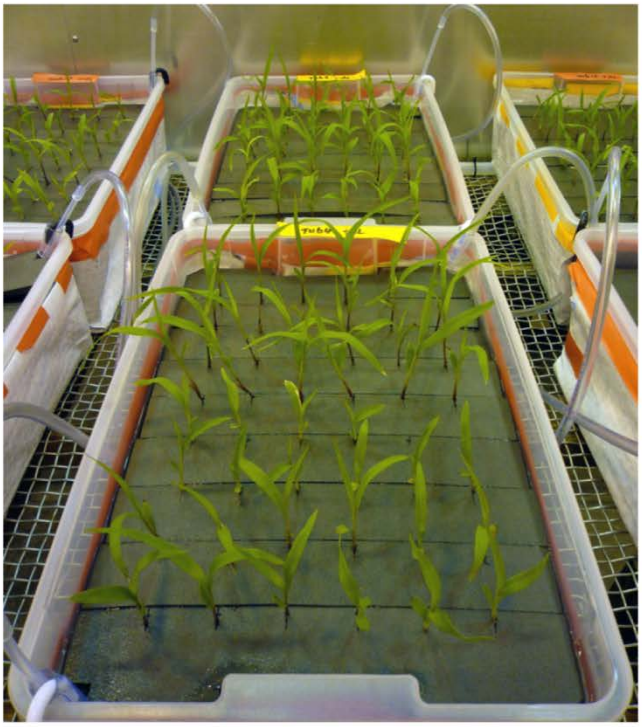

(de Sousa et al., 2012). The individual rr2dat and corresponding image files can be opened at any time with the RootReader2D software, displaying the processing data on the image for further inspection, commenting, root selection, modification and measurement. In cases where only whole root system measurements are needed, batch analysis is performed and root phenotypes for thousands of plants can be obtained overnight (Famoso et al., 2010; Famoso et al., 2011). Although the rate of batch processing is a function of the selected thresholding filter, the complexity of the root systems in the images, and the computer's hardware specifications, 4 day old maize seedling images (similar to those shown in Fig. 2.2 and Fig. 2.11A) are automatically processed at an average rate of less than 60 seconds per image on a modern personal computer. When analyzing older, intact plants (more than 7 days old) with complex root systems, large increases in the number of skeleton endpoints can result in slower performance and longer processing times during the shortest path routine during graph generation. Additionally, older root system images require larger processing (random access memory) and storage (hard drive) capacities to generate and store the rr2dat data files. The data files generated for very complex root systems can sometime be larger than 200MB per image and require thoughtful data management and storage strategies, however, for young seeding root systems (less than 7 days old), the data file sizes are typically less than 30MB per image. After processing the images, all of the root system measurements can be individually or batch written to a measurement log for viewing and can be exported to comma-separated value (CSV) files.

The integration of user-guided root selection features into the RootReader2D

software increases the power and flexibility to analyze specific root components of whole root systems, but consequently reduces the throughput of the complete image analysis process. To improve efficiency during root selection, RootReader2D software was designed with a simple graphical user interface (GUI) that takes advantage of both keyboard shortcuts and mouse section and navigation commands. Depending on the complexity and prevalence of root overlaps in the image, roots can sometimes be selected with one mouse click/selection (for example, primary roots can be selected by clicking on the seed only), however in most cases it is more efficient to select both the start and end of the desired roots. Individual roots from older or more highly overlapped root systems (similar to the root system in Fig. 2.1A) can also be selected and measured using built-in path modification techniques. For 4 day old maize images, the semi-automatic selection of the primary and seminal roots typically takes less than 40 seconds per image by an experienced user.

Although the imaging platform and RootReader2D software has mainly been used to quantify roots of hydroponically grown plants, these tools have also been used by our lab to phenotype a variety of plant species that were grown in other growth systems with little or no changes. Recent applications have included the phenotyping of micronutrient toxicity/deficiency in Arabidopsis (*Arabidopsis thaliana*) ecotypes grown on agarose plates with multiple plants (Fig. 2.4A) (Milner et al., 2012) and root architecture and trait evaluation of sorghum (*Sorghum bicolor*), maize and rice plants grown in paper pouch, gellan gum and sand culture systems (Fig. 2.4B) (Clark et al., 2011; de Sousa et al., 2012). Additionally, non-root phenotypes such as shoot, awn and seed characteristics have also been measured (Fig. 2.4C).

Figure 2.4: Examples of other types of images processed and analyzed with RootReader2D (RR2D). See http://www.plantmineralnutrition.net/rootreader.htm for details on lighting arrangements and thresholding techniques. A) RR2D analyzed image of agar plate grown Arabidopsis root systems. Image captured using oblique lighting and thresholded with an adaptive thresholding technique. B) RR2D analyzed sand culture grown rice root system. Image captured using backlighting and thresholded with a double adaptive blur thresholding technique. C) RR2D analyzed rice shoots. Image captured using backlighting and thresholded with a fixed thresholding technique.

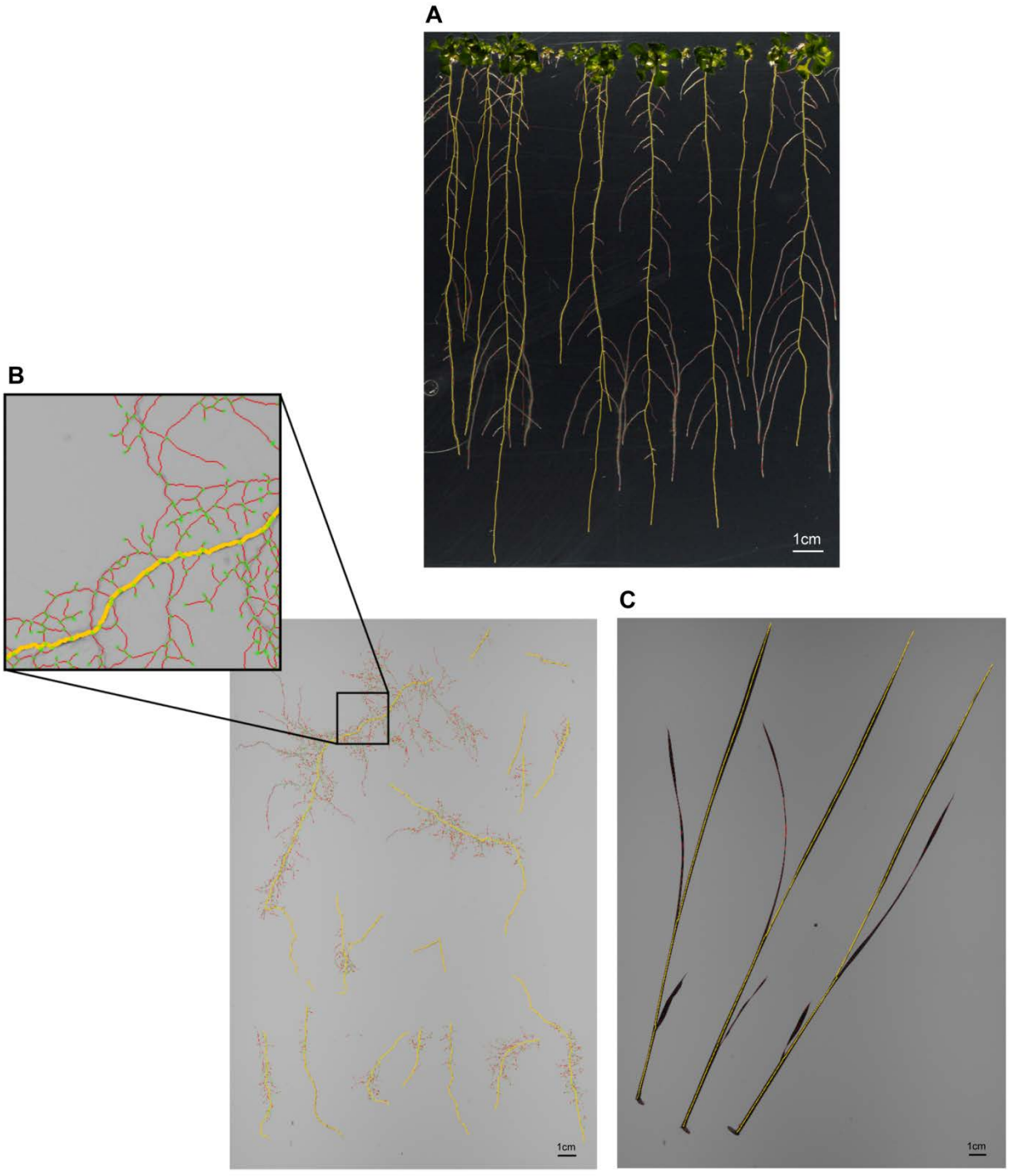
A
1cm
B
1cm
C
1cm

Other root phenotyping tools

Due to the varying nature of plant growth experiments, a wide variety of phenotyping systems and software analysis tools have been developed to investigate root systems. Most root image analysis tools are designed to maximize utility during specific applications and have complementary overlap with other tools. In many cases, different phenotyping platforms and their respective analysis tools can be adapted after thoughtful consideration and refinement of experimental methods, however the comprehensive analysis of root systems often requires the use of several phenotyping strategies and tools.

Two root phenotyping platforms that have been developed and used in our lab to investigate root systems are the 3D imaging system that was introduced by Clark *et al* (2011) and the 2D imaging system that is presented here (Clark et al., 2012). The 3D imaging system and the RootReader3D analysis tool were created to capture and measure 3D root system architecture (RSA) characteristics over time from plants grown in 3D gellan gum systems, but have modest throughput (~100 plants per week). The 2D imaging system and RootReader2D analysis tool described here were designed for measuring 2D root length and growth characteristics of the whole root systems or selected roots of interest during large scale (>1000 plants per week), semi-automated hydroponic studies. Although these two systems serve different niches, they both have been used to measure root lengths (Famoso et al., 2010; Clark et al., 2011; Famoso et al., 2011; Milner et al., 2012) and contain novel algorithms and features that enable both whole root system (global) or specific root or root type (local) characteristics to be quantified.

In addition to the two imaging platforms utilized by our lab, many other platforms and software tools have been developed to analyze roots growing in setups ranging from soil (field and greenhouses) to hydroponics and gel (greenhouses and laboratories). These tools have complementary features to RootReader2D and RootReader3D, but also fill unique and varying experimental niches. General details about these software tools and their applications can be found in Chapter I and Table 1.1 or at www.root-image-analysis.org, a website dedicated to root image analysis that was created by the developer of the SmartRoot software toolkit (Lobet et al., 2011).

Example 1: High-Throughput evaluation of primary and total root system growth of rice and maize diversity panels

The genotyping of linkage and association mapping populations with next generation sequencing technology has greatly expanded the genomic information available to plant researchers. In combination with higher throughput phenotyping techniques, these resources provide powerful tools for genetic mapping studies. Two mapping populations with publicly available germplasm and genotypic information are the rice diversity panel (http://ricediversity.org/) and the maize association panel (http://maizecoop.cropsci.uiuc.edu/). To demonstrate how the high-throughput capacity of our phenotyping platform can be used to take advantage of these kinds of genomic resources during root system studies, we have phenotyped both mapping populations for basic root traits and performed genome-wide association (GWA) analysis on the rice root phenotypes.

Based on genetic variability within the panels, 233 rice accessions and 273

maize lines were selected from the rice diversity panel and maize association panel, respectively. In order to capture the root traits with a high degree of statistical confidence, ten or more biological replicates were analyzed for each line. Whole root system images were captured one and four days after transplanting and primary and total root system lengths were measured using RootReader2D. For each line, average primary and total root growth was determined over the three days. As depicted in the frequency distribution plots in Figure 2.5, the primary and total root growth phenotypes for the rice (Fig. 2.5A,B) and maize (Fig. 2.5C,D) association panels are normally distributed. The broad-sense heritability estimates (H2) for the measured phenotypes were 0.57 and 0.46 for rice primary and total root growth, and 0.72 and 0.65 for maize primary and total root growth.

Genome-wide association mapping was then performed with the rice root phenotypes using the public genotypic dataset consisting of 36,901 high quality SNPs (Zhao et al., 2011). Efficient mixed-model analysis (EMMA) was performed across all 233 accessions from the diversity panel and also within the *aus, indica, temperate japonica* and *tropical japonica* rice subpopulations. For each of the respective analyses (all 233 accessions, *aus, indica, temperate japonica, tropical japonica*), 2, 2, 0, 3, 1 genomic region(s) were found to be correlated with primary root growth and 4, 2, 4, 0, 2 regions were found to be correlated with total root growth (Fig. 2.6). These regions were defined by having one or more SNPs with significance levels greater than 4 ($-\log_{10}(P) > 4$) that grouped within linkage disequilibrium (LD) decay blocks, where LD decay was estimated to be between 50kb and 500kb for rice (Mather et al., 2007).

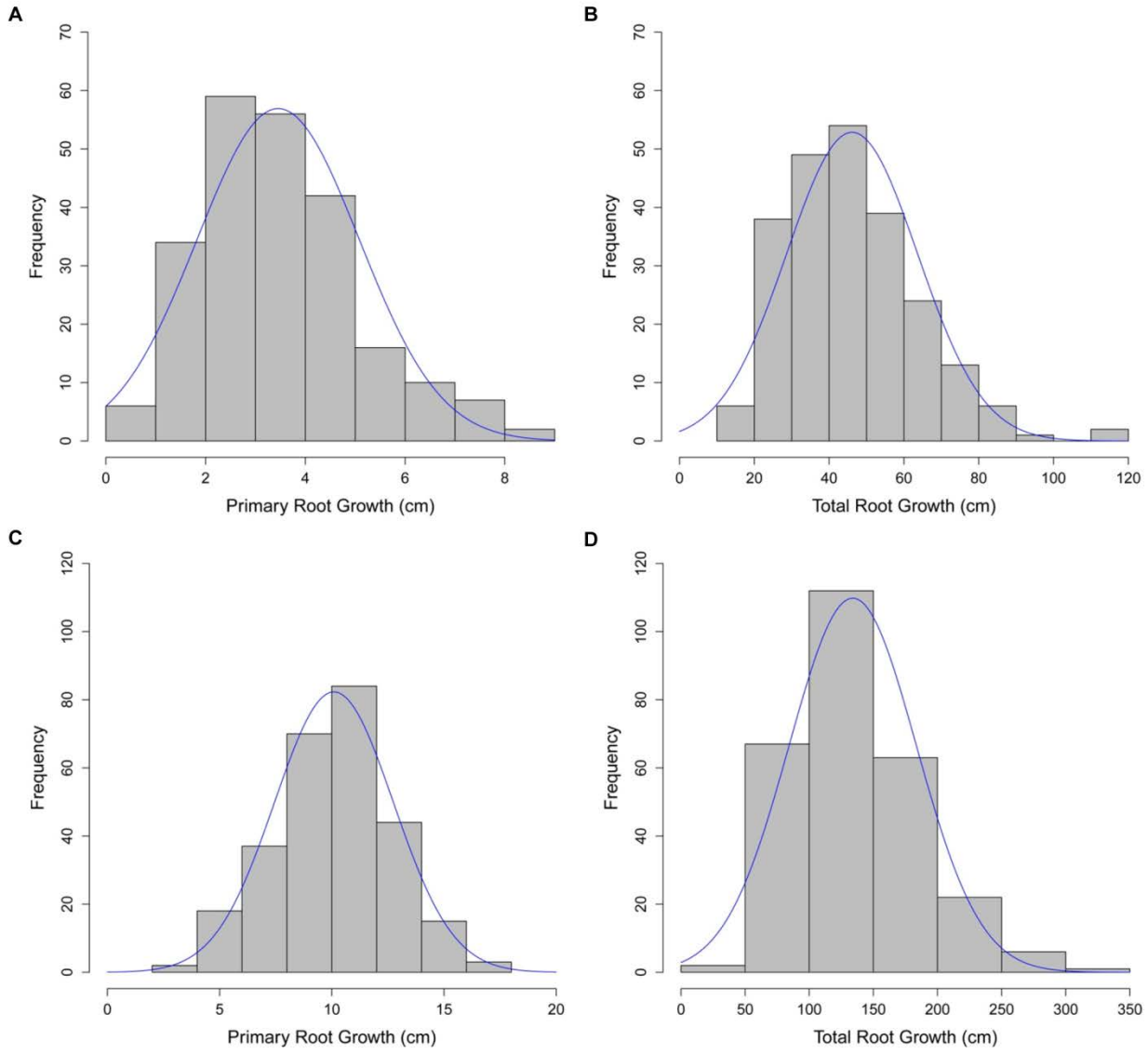

Figure 2.5: Frequency distribution plots of rice and maize root growth for the rice diversity and maize association panels grown over a 3 day period. A,B) Plots of primary and total root system growth frequency distributions with fitted normal curves for the 233 rice accessions. C,D) Plots of primary and total root system growth frequency distributions with fitted normal curves for the 273 maize lines.

Figure 2.6: GWA analysis of primary and total root growth across all 233 rice diversity accessions and within rice subpopulations. The rice subpopulations are denoted as AUS (*aus*), IND (*indica*), TEJ (*temperate japonica*), and TRJ (*tropical japonica*). The shaded bands indicate the positions of 72 bi-parental root length-related QTL from previous reports. SNPs with significance levels greater than 4 ($-\log_{10}(P) > 4$) that were co-localized with *a-priori* QTL are surrounded by red ovals.

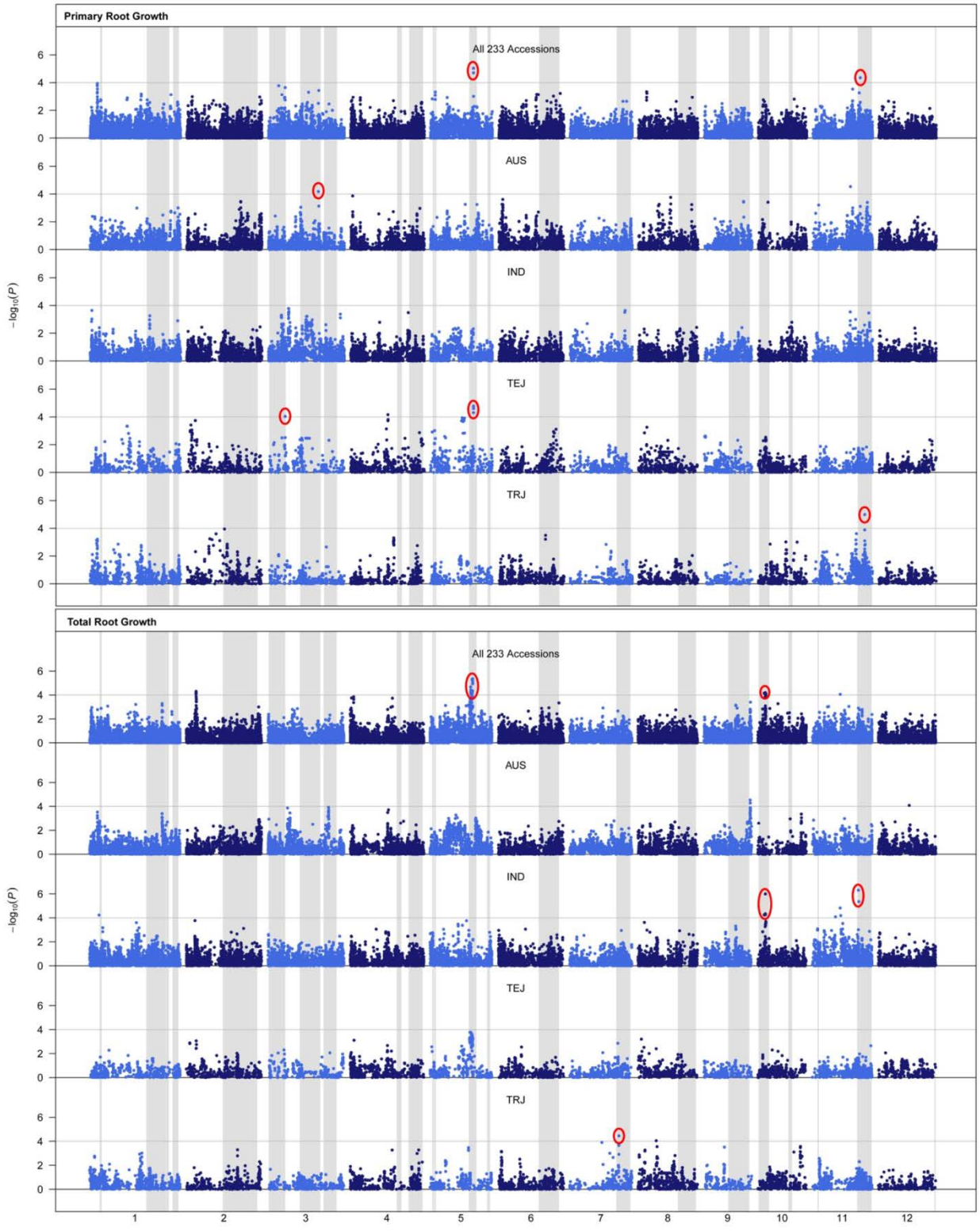
Primary Root Growth
All 233 Accessions
AUS
IND
TEJ
TRJ
Total Root Growth
All 233 Accessions
AUS
IND
TEJ
TRJ
−log10(P)
0
2
4
6
1
2
3
4
5
6
7
8
9
10
11
12

When further analyzing the results for the primary and total root growth, 4 regions for primary root growth and 4 regions for total root growth co-localized with previously identified rice root length-related QTL from bi-parental mapping studies curated by Gamene.org. Although there were no significant SNPs detected for both traits simultaneously (Fig. 2.7), several SNPs from primary and total root growth fall within estimated LD regions of one another. These results are the starting point for more detailed genetic analyses of root traits and provide further evidence that root system components (primary, lateral, embryonic and postembryonic crown roots) are controlled by independent genetic and developmental networks as discovered through mutant analysis studies reviewed by Hochholdinger *et al* (2004) and Rebouillat *et al* (2009). It should also be noted that although phenotypic data was collected for root traits from the maize association panel, due to the low degree of linkage disequilibrium in maize, GWA analysis of maize root traits await significant increases in marker density that are currently being generated in the Buckler lab using genotyping by sequencing and imputation techniques.

Example 2: Assessing the aluminum tolerance and other root characteristics of the maize founder lines

Evaluating root types as distinct classes has been shown to improve investigations into the aluminum (Al) tolerance of maize (Bushamuka and Zobel, 1998), but further work in this area has been limited due to the challenges of acquiring

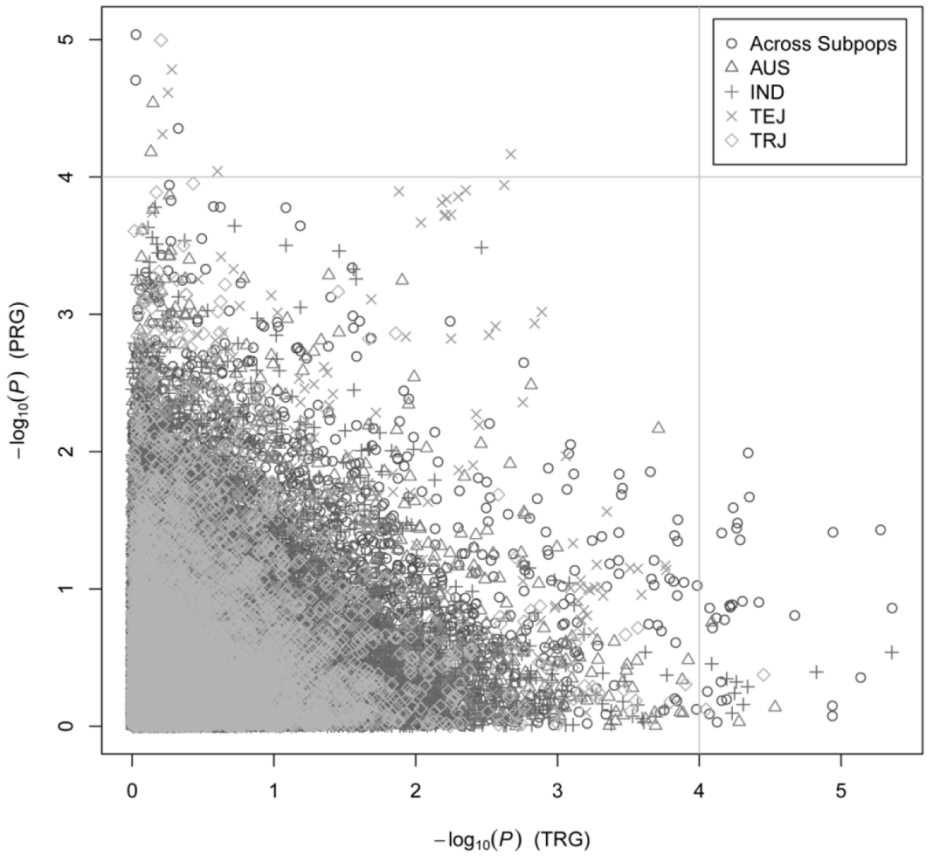

Figure 2.7: Scatterplot of significance levels from GWA analysis of rice primary root growth (PRG) and total root growth (TRG) for all 36,901 SNPs. The rice subpopulations are denoted as IND (*indica*), AUS (*aus*), TEJ (*temperate japonica*) and TRJ (*tropical japonica).* The horizontal and vertical lines on the plot at $-\log_{10}(P)$ values of 4 indicate the significance threshold based on previous reports of GWA analysis in rice (Famoso *et al.* 2011 and Zhao *et al.* 2011).

measurements from specific root types. Using the current root phenotyping platform, we were able to use the RootReader2D software to non-destructively quantify growth of the different root types from whole root system images and thus evaluate the Al tolerance of the primary, seminal and lateral root types of the 25 founder lines of the maize nested association mapping (NAM) population (Yu et al., 2008). Primary, seminal and lateral root types were identified using the criteria reviewed by Hochholdinger and Tuberosa (2009).

The most common measure of plant Al tolerance is relative root growth (RRG) of the primary root, where primary root RRG is calculated by dividing the primary root growth of a set of seedlings under Al exposure by the primary root growth of a second set of the same seedlings grown under control (-Al) conditions (Piñeros et al., 2002). When evaluating the 26 lines for Al tolerance, it was found that they exhibited a range of Al tolerances (Table 2.1), with primary root RRG (PR-RRG) ranging from very Al sensitive lines with RRG values as low as 0.20 to very Al tolerant lines that displayed stimulated growth under the same Al exposure (RRG as high as 1.19) (Note: line M162W could not be phenotyped due to poor germination). This range in PR-RRG captures the variation found in all individuals of the Goodman-Buckler maize association panel (unpublished data) and is similar to what is observed during Al tolerance screening studies of rice and other crop species (Famoso et al., 2010). Note however that the free Al^{3+} activity in the nutrient solution is typically chosen to maximize the spread of the RRG frequency distribution for the selected species or germplasm. When assessing the relationships between primary root RRG (PR-RRG) and seminal root RRG (SR-RRG), lateral root RRG (LatR-RRG), and total root system RRG (TRS-

RRG), the correlation coefficients (r^2) were 0.482 for PR-RRG vs. SR-RRG, 0.318 for PR-RRG vs. LatR-RRG, and 0.415 for PR-RRG vs. TRS-RRG (Fig. 2.8). Changes in Al tolerance rankings were also observed when comparing the different root type-based phenotypes (Table 2.1). These results suggest that seminal and lateral root phenotypes contain tolerance information that cannot be captured solely by analyzing PR-RRG. Additionally, these genotypes showed variation for other seedling root system characteristics that were measured using RootReader2D, including primary, seminal and lateral root growth rates, and root counts (Fig. 2.9).

As shown in Table 2.1 and Fig. 2.8, RRG of the various root types are partially correlated, however, the growth of different root types can have large impacts on crop performance under stress conditions (Waisel et al., 1996). Further analysis of Al tolerance based on the quantification of growth of different root types may help provide additional insight into root-specific responses to Al and related tolerance mechanisms. One approach to analyze the RRG data for different root types is to analyze each of the RRG phenotypes separately. However, the correlated information that is common to all of the RRG measures may hide some of the unique growth behaviors of the individual root types and possibly reduce the power to reveal Al tolerance components specific to the root types. Another complementary approach that can be used to help capture the most correlated information for phenotypes based on root types and separate it from the non-correlated information is principle component analysis (PCA). During PCA, the phenotypes are transformed so that the maximum variation in the combined phenotypes across the lines falls along the first principle axis (or first principle component, PC1).

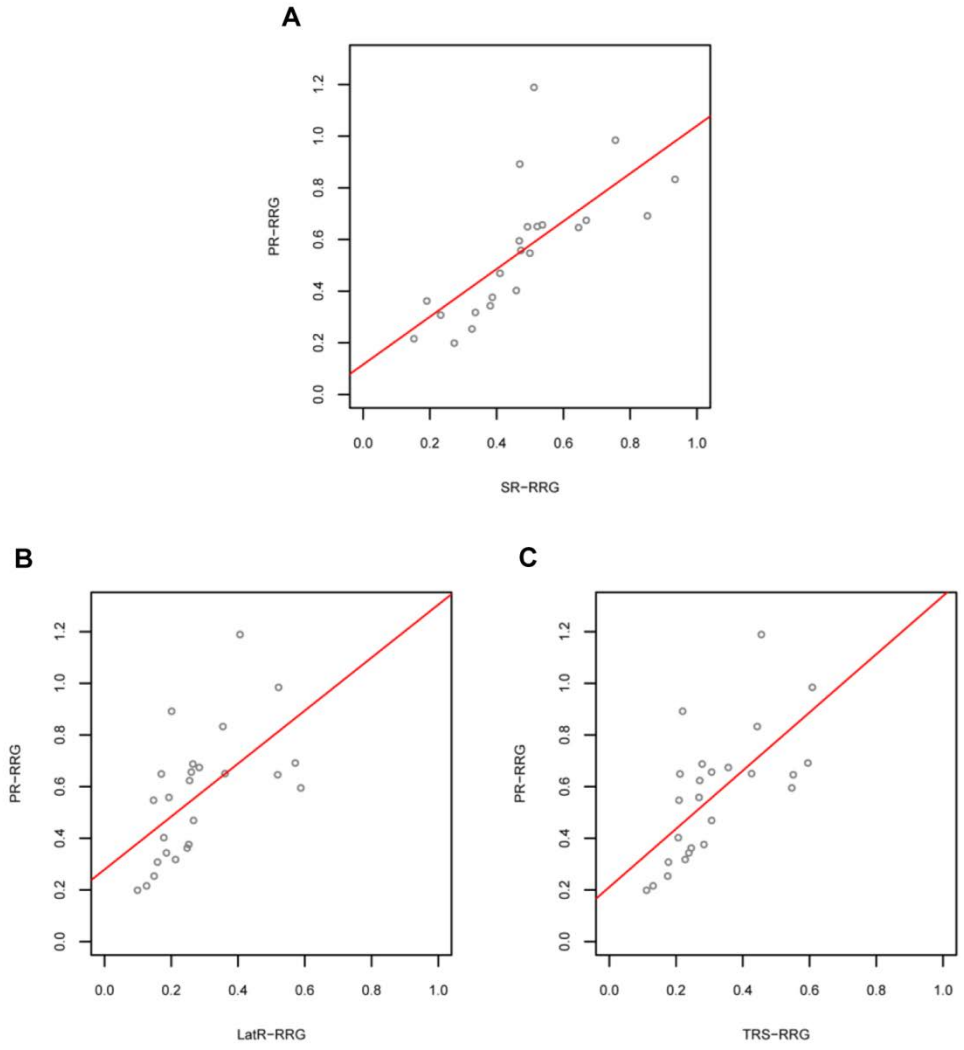

Figure 2.8: Comparison of relative root growth (RRG) indices for the 25 maize founder lines. Data points represent the mean RRG of the individual lines. A) Primary root RRG (PR-RRG) as a function of seminal root RRG (SR-RRG), $r^2 = 0.482$. B) Primary root RRG as a function of lateral root RRG (LatR-RRG), $r^2 = 0.318$. C) Primary root RRG as a function of total root system RRG (TRS-RRG), $r^2 = 0.415$.

Figure 2.9: Bar graph depicting untreated (-Al) root characteristics of the 25 founder lines (excluding line M162W) and the recurrent parent (B73) of the maize nested association mapping (NAM) population measured using the RootReader2D software. Each bar is comprised of three different types of root growth data - average primary root growth, average total seminal root growth and average total lateral root growth between days 1 and 4. The numbers in the seminal and lateral root sections of each bar represent the average number of seminal and lateral roots measured for each line on Day 4.

Lateral Roots
Seminal Roots
Primary Root
Average Root Growth (cm)
0
50
100
150
200
250
B73
B97
CML103
CML228
CML247
CML277
CML322
CML333
CML52
CML69
HP301
IL14H
K111
K13
KY21
M37W
MO18W
MS71
NC350
NC358
OH43
OH7B
P39
TX303
TZI8
131
2
142
1.4
170
3.7
174
3.3
176
1
119
2.8
158
3.6
242
2.7
112
3.4
187
3.4
131
1
140
1
193
3.1
125
4
231
2.2
148
1.9
165
1.6
154
3.7
177
4.3
88
1.8
184
2.8
261
2.7
171
1
169
2.4
122
2.4

Table 2.1: Relative root growth (root growth with Al / root growth without Al) and rankings as measures of Al tolerance for maize founder lines based on selected root types. Rankings for the lines are listed from 1 (most Al tolerant) to 25 (least Al tolerant).

Lines	Relative Root Growth (RRG) Based On				Rankings Based On			
	Primary Root (PR)	Seminal Roots (SR)	Lateral Roots (LatR)	Total Root System (TRS)	PR-RRG	SR-RRG	LatR-RRG	TRS-RRG
B73	0.55	0.50	0.15	0.21	15	9	23	20
B97	0.32	0.34	0.21	0.23	21	18	15	17
CML103	0.98	0.76	0.52	0.61	2	3	3	1
CML228	0.36	0.19	0.25	0.25	19	22	14	15
CML247	0.69	na	0.26	0.28	6	na	10	12
CML277	0.47	0.41	0.27	0.31	16	15	9	9
CML322	0.25	0.33	0.15	0.17	23	19	22	23
CML333	0.40	0.46	0.18	0.21	17	14	19	21
CML52	0.34	0.38	0.19	0.24	20	17	18	16
CML69	0.56	0.47	0.19	0.27	14	11	17	14
HP301	0.69	0.85	0.57	0.60	5	2	2	2
IL14H	0.62	na	0.25	0.27	12	na	12	13
KI11	0.66	0.54	0.26	0.31	8	6	11	10
KI3	0.59	0.47	0.59	0.55	13	13	1	4
KY21	0.67	0.67	0.28	0.36	7	4	8	8
M37W	0.65	0.49	0.17	0.21	10	10	20	19
MO18W	0.20	0.27	0.10	0.11	25	20	25	25
MS71	0.65	0.52	0.36	0.43	9	7	6	7
NC350	0.83	0.93	0.35	0.44	4	1	7	6
NC358	1.19	0.51	0.41	0.46	1	8	5	5
OH43	0.22	0.15	0.13	0.13	24	23	24	24
OH7B	0.31	0.23	0.16	0.18	22	21	21	22
P39	0.89	0.47	0.20	0.22	3	12	16	18
TX303	0.38	0.39	0.25	0.28	18	16	13	11
TZI8	0.65	0.65	0.52	0.55	11	5	4	3

When performing PCA on the three root type RRG phenotypes (PR-RRG, SR-RRG, and LatR-RRG), PC1 accounted for 76.2 percent of the variation in the RRG data indicating that a large amount of the RRG data is correlated and can be captured by PC1 (Fig. 2.10A). The non-correlated information in the phenotypes can then be extracted during a second round of PCA where each of the root type-based phenotypes is separately analyzed with respect to the prior PC1 results (Fig. 2.10B,C,D). The second principle component from each of the paired analyses is known as the contrast principle component and represents the non-correlated portion of the data that is unique to each of the root type phenotypes. Thus the PCA technique can help separate correlated information common to all the RRG phenotypes from non-correlated information that is specific to each of the root types, however further application of this technique to larger datasets is needed to determine how effectively it can further extract Al tolerance information during mapping studies.

Figure 2.10: Biplots derived for principle components analysis (PCA). The directional vectors (red) from the origins display the degree correlation between the RRG parameters and each principle component. A) Biplots derived from PCA of the primary, seminal and lateral root relative root growth (PR-RRG, SR-RRG, and LatR-RRG, respectively). B) Biplot derived from PCA of PC1 (above) and PR-RRG. C) Biplot derived from PCA of PC1 (above) and SR-RRG. D) Biplot derived from PCA of PC1 (above) and LatR-RRG.

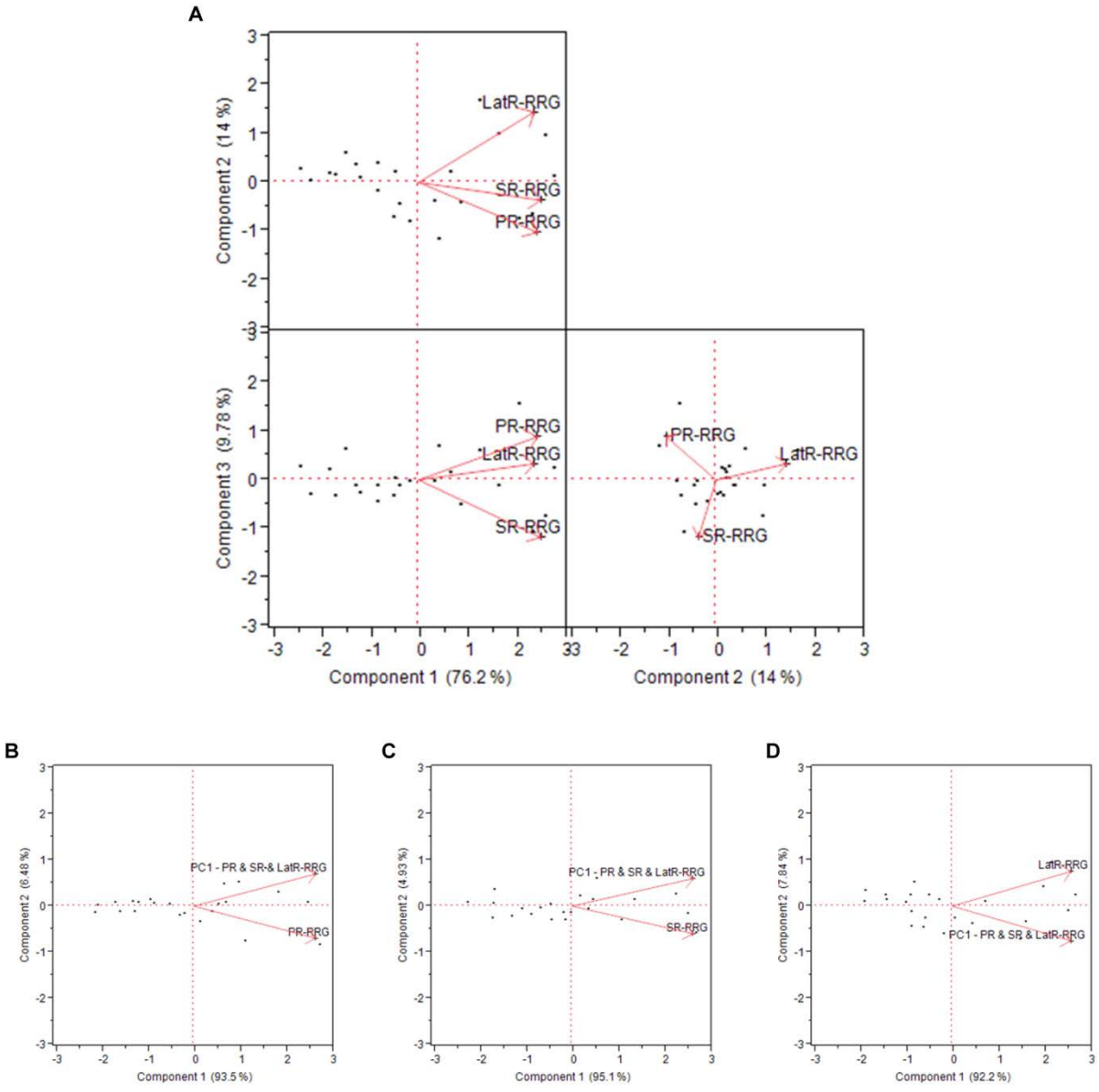
A
LatR-RRG
SR-RRG
PR-RRG
Component2 (14 %)
Component3 (9.78 %)
Component 1 (76.2 %)
Component 2 (14 %)
B
PC1 - PR & SR-& LatR-RRG
PR-RRG
Component2 (6.48 %)
Component 1 (93.5 %)
C
PC1 - PR & SR & LatR-RRG
SR-RRG
Component2 (4.93 %)
Component 1 (95.1 %)
D
LatR-RRG
PC1 - PR & SR & LatR-RRG
Component2 (7.84 %)
Component 1 (92.2 %)

MATERIALS AND METHODS

Imaging system

A Nikon D200 digital SLR camera with a Nikon 60mm macro lens (Nikon Inc., Melville, NY, USA) and circular polarizing filter (Heliopan, Germany) was mounted on a copy stand (Adorama, New York, NY, USA). The camera was set to have manual capture settings of 1/30 second shutter speed, 7mm aperture, and a sensor sensitivity of 1000 ISO. The optical axis of the camera was aligned to face a light box (Hall Productions, San Luis Obispo, CA, USA) that uniformly illuminated the root systems. A clear acrylic specimen tray with linear polarizing film (Techspec®, Edmund Optics, Barrington, NJ, USA) and a non-tempered glass plate was placed on top of the light box and was filled with a 2 to 3 mm layer of nutrient solution (Fig. 2.3A) to allow the root systems to be efficiently spread out with reduced parallel overlaps of main and lateral roots. Images of bright roots on a dark background were generated by placing the root systems between the two cross polarized filters to enhance the contrast of the root systems from the background and improve the image analysis properties (Fig. 2.11).

Camera alignment and image plane calibration

To assess the precision of the images that were captured and minimize potential measurement errors caused by varying root placement within the imaging plane, the digital camera was aligned and calibrated with a calibration grid (5 x 5 mm grid size). The grid was photographed and the average grid lengths from 3 x 3 grid regions at the four corners and center of the image were measured using the RootReader2D software

Figure 2.11: Depiction of high contrast imaging using polarized light. A) Typical maize root system image using the cross polarized light design. B) Diagram illustrating the cross polarized design used to generate high contrast root images. During the cross polarized alignment, the polarized light that is intercepted by root objects is scattered and depolarized as it is transmitted through the root tissue. The light that does not encounter any roots passes through the specimen tray unscattered and polarized. As the light passes the second polarizer, the unscattered, polarized light is blocked, allowing only the scattered, unpolarized light coming from the roots to be recorded by the CCD array in the camera.

A

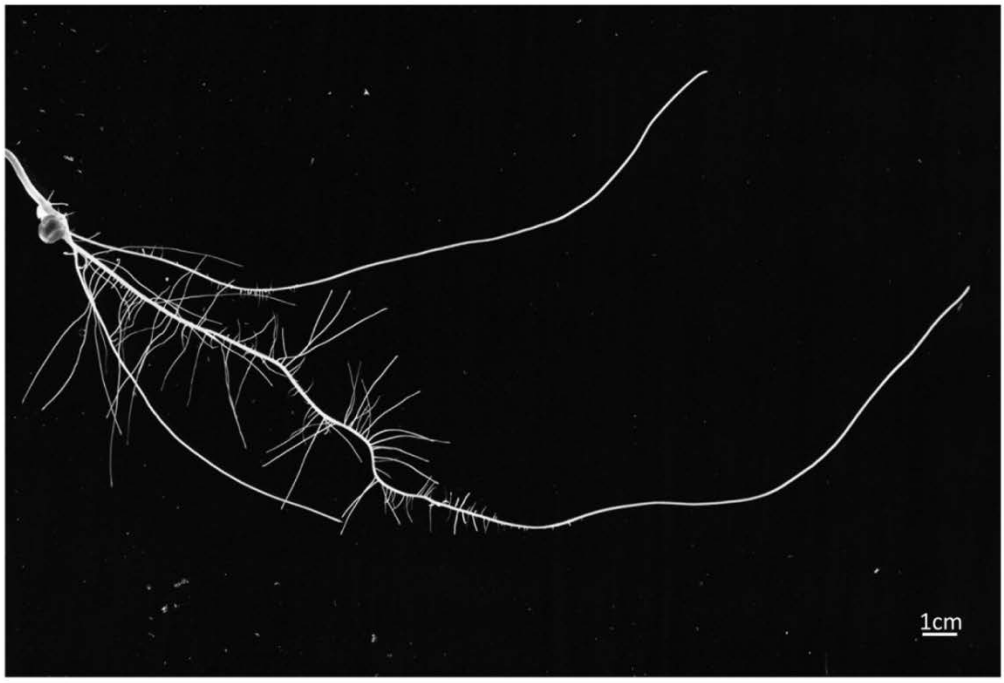
1cm

B

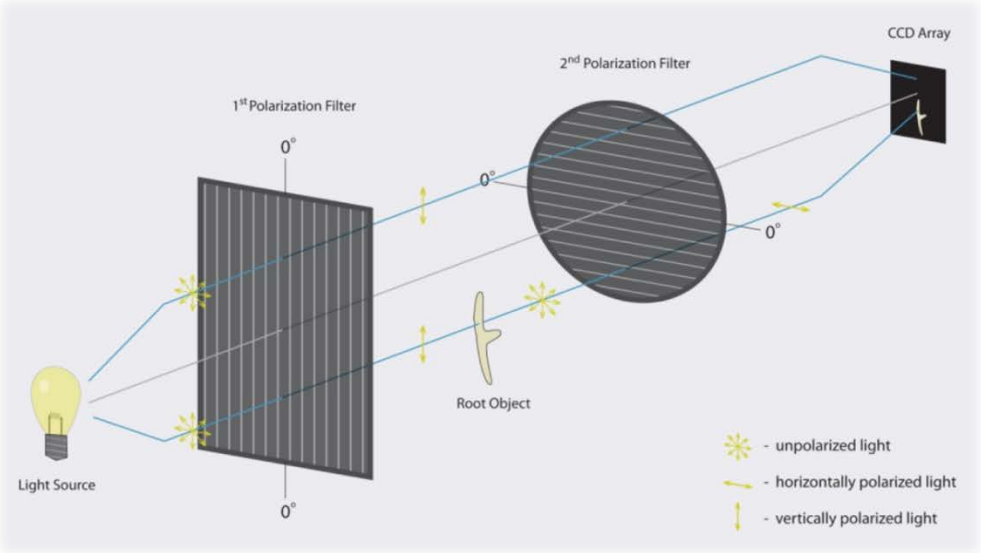
CCD Array
2nd Polarization Filter
1st Polarization Filter
0°
0°
0°
0°
Root Object
Light Source
- unpolarized light
- horizontally polarized light
- vertically polarized light

tool. The gaze of the camera was systematically adjusted until the average corner grid lengths fell within ±1.0 pixels of one another. Once the camera was aligned, the maximum difference in 5 mm grid lengths at any position of the image was automatically measured with RootReader2D and determined to be less than 4.0% or 0.2 mm. The average of the central grid length was found to be approximately 0.44% larger than the average of the corner grid lengths thus confirming that image corrections due to radial lens distortions were not necessary.

Image acquisition and analysis

The camera was interfaced to a personal computer (Dell Inspiron 6000, 1.6GHz, 2GB RAM) via a USB 2.0 port and digital images were captured, saved, and converted from a raw NEF format to a color TIF format using Nikon Camera Control Pro and Capture NX software. Root system images were captured by laying and spreading the roots of individual seedlings into nutrient solution in a specimen tray and photographing the roots. The images were captured with a focal plane pixel size of 87 ±1.8 x 87 ±1.8 µm corresponding to a field-of-view of 33.7 x 22.5 cm.

The color RGB images were batch processed using Adobe Photoshop (Adobe Systems Inc.) to crop and convert them to a grayscale format. The images were then batch processed and analyzed using the RootReader2D software.

Plant culture and growth experiments

The 233 rice (*Oryza sativa*) accessions used in this study were selected from the McCouch rice diversity panel (Zhao et al., 2011) and were germinated and grown under control (-Al) environmental conditions as described by Famoso *et al* (2011). The 273 maize (*Zea mays*) genotypes used during the growth studies belong to the Goodman-

Buckler maize association panel (Yu and Buckler, 2006) and the 26 genotypes selected for further root type studies are the parents of the maize nested association mapping (NAM) population (Yu et al., 2008). For the maize experiments, the seeds were surface treated with a fungicide cocktail containing Captan400, Trilex and Allegiance and germinated in moist germination paper rolls (Anchor Paper, St. Paul, MN, USA) for 4-5 days in the dark at 26ºC. Upon germination, 24 seedlings from each genotype with primary root lengths between 6 and 9 cm and shoot lengths between 2 and 4 cm were selected and transplanted into hydroponic growth vessels consisting of translucent plastic growth tubs (Rubbermaid, Winchester, VA, USA) with dimensions of 40.0 x 27.5 x 14.5 cm (L x W x H) that were wrapped with opaque plastic and filled with 9 liters of Magnavaca's nutrient solution, pH 4.0 (Magnavaca et al., 1987). The nutrient solution in each tub was covered with gray, closed-cell polyethylene foam strips (McMaster-Carr, Elmhurst, IL, USA) to prevented light penetration and support the seedlings during the experiment (Fig. 2.3B). Plants were grown under controlled conditions for the duration of the experiment (26°C day/23°C night, 12/12 h photoperiod, 550 µmol m^{-2} sec^{-1} photons).

For both rice and maize, the seedlings were photographed and measured using the RootReader2D software on days 1 and 4 after transplanting. For maize Al tolerance studies, following photography on day 1, Al treatment was initiated on half of the maize seedlings by replacing the control nutrient solution with an identical solution that contained either 0 or 178 µM AlK_2SO_4. The total lateral root lengths were calculated by subtracting primary and seminal root lengths from the total root system length.

Measurement validation

Four days after transplanting, the root systems of 188 maize seedlings were imaged and the primary roots were carefully measured by hand with a ruler. These manual measurements were compared to the measurements generated by RootReader2D and to tracing methods (Hoekenga et al., 2006) using ImageJ software (Rasband, 1997-2012). Polyline error criteria sensitivity studies were then performed on the primary root measurements and RootReader2D total root length measurements were compared to WinRHIZO total root length measurements. These studies revealed that error criterion parameter is important factor in the calibration of RootReader2D to other quantification methods (Fig. 2.12 and 2.13). The WinRHIZO software used is part of the WinRHIZO root analysis system (Regent Instruments Inc., Canada) which consists of both image acquisition hardware and root analysis software (Arsenault et al., 1995). During WinRHIZO analysis, the root images were imported into WinRHIZO and analyzed using a fixed threshold parameter of 40. The root images and threshold level corresponded to the same images and threshold level used during the RootReader2D processing and analysis of the maize root systems.

Genome-Wide Association Analysis

Using a rice genotypic dataset consisting of 36,901 SNPs (Zhao et al., 2011), genome-wide association (GWA) analysis was performed across and within *aus*, *indica*, *temperate japonica*, and *tropical japonica* subpopulations using primary and total root growth phenotypic data from the 233 rice accessions of the rice diversity panel. To account for different degrees of population structure and relatedness between the

Figure 2.12: Comparison of maize root system lengths quantified with RootReader2D (RR2D) to root lengths determined by other standard methods (manual with ruler, ImageJ tracing, and automated with WinRHIZO) at varying RR2D error criterions. The optimal error criterion was found to be 6.0 pixels when the image resolution was 115 pixels/cm. Data points (♦) represent means and error bars indicate the standard deviation, n=188. A) Difference in average measured primary root lengths, ruler minus RR2D. B) Difference in average measured primary root lengths, ImageJ traced minus RR2D. C) Difference in average measured total root system lengths, WinRHIZO minus RR2D.

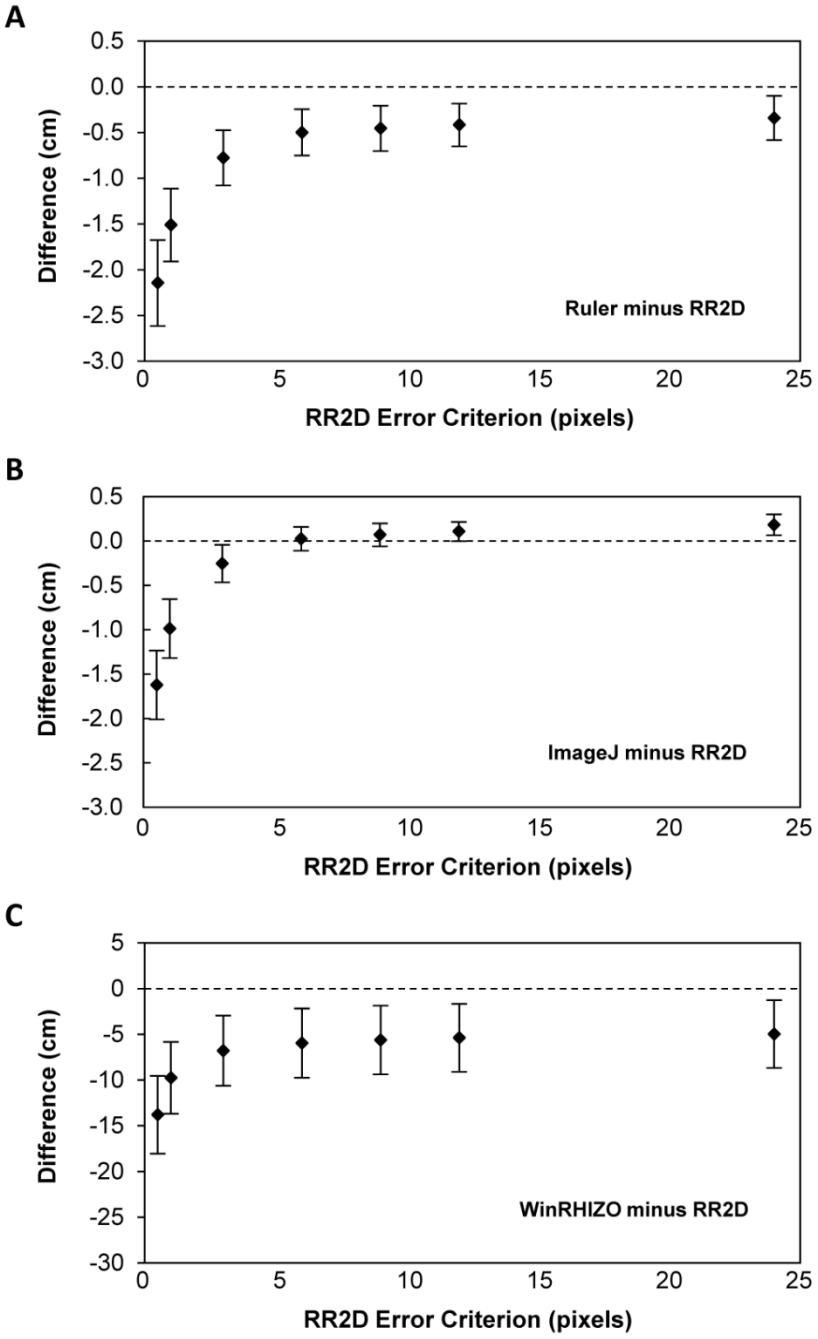
A
0.5
0.0
-0.5
-1.0
-1.5
-2.0
-2.5
-3.0
Difference (cm)
Ruler minus RR2D
0
5
10
15
20
25
RR2D Error Criterion (pixels)
B
0.5
0.0
-0.5
-1.0
-1.5
-2.0
-2.5
-3.0
Difference (cm)
ImageJ minus RR2D
0
5
10
15
20
25
RR2D Error Criterion (pixels)
C
5
0
-5
-10
-15
-20
-25
-30
Difference (cm)
WinRHIZO minus RR2D
0
5
10
15
20
25
RR2D Error Criterion (pixels)

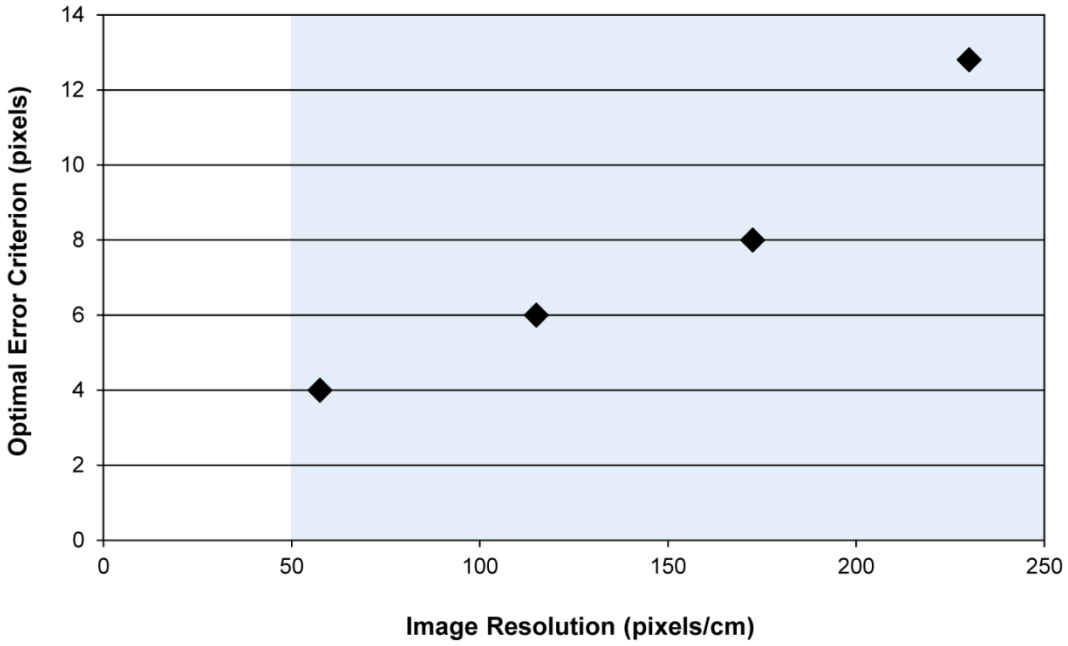

Figure 2.13: Optimal RootReader2D error criterion at varying image resolutions. The shaded area represents the range of probable resolutions during crop root system imaging. Data points (♦) were determined on sets of 94 maize images with primary roots of known length.

accessions, a linear mixed model approach was used (Yu et al., 2006; Zhao et al., 2007; Kang et al., 2008). The model can be written in matrix form as: $y = X\beta + C\gamma + Z\mu + e$ where β and X correspond to the SNP coefficient and SNP vectors, γ and C correspond to the subpopulation coefficient and subpopulation PC (principle component) vectors, μ corresponds to the random effects vector that accounts for population structures and relatedness, Z corresponds to the design matrices, and e is the random error term. SNPs having a minor allele frequency less than 5% (MAF<0.05) across and within subpopulations were excluded from the analysis.

Statistical Analysis

Statistical calculations were performed using JMP Pro version 9.0 (SAS Institute) and R (2011).

CONCLUSION

A novel phenotyping platform to grow, capture, process and measure root systems using digital imaging has been presented. This platform facilitates the high-throughput phenotyping of root systems while also allowing the non-destructive measurement of unique and challenging root phenotypes. The whole platform or parts of the imaging and analysis platform have been adapted and are generally applicable to a wide range of plant species, growth systems and root traits. The integration of both batch processing functionality and user-guided features into the RootReader2D software enhances utility when measuring root system characteristics while also ensuring flexibility for further trait extraction and development.

ACKNOWLEDGEMENTS

For the work presented in this chapter, I would like to thank Prof. Anthony P. Reeves for his discussions and lessons on image processing, automated analysis, and the importance of technique validation, Prof. Randy O. Wayne for his conversations on lighting and optics, Dr. Owen A. Hoekenga for his advice on using ImageJ software during the validation studies, Prof. Neil S. Mattson for providing access to the WinRHIZO software used during the validation studies, Dr. Anthony J. Greenburg for his insight into data analysis with PCA, the Weitz (Georgia Tech), Benfey (Duke University)

and Edelsbrunner (Duke University) Labs for their stimulating discussions on the mathematical and biological considerations of RSA quantification, and Xiaomin Jia, Zhifang Cheng, Sophia Ng, James Jones-Rounds and Joe Gage for providing valuable assistance during the phenotyping experiments. I would also like to thank Adam N. Famoso, Keyan Zhao, Jon E. Shaff, Eric J. Craft, Carlos D. Bustamante, Susan R. McCouch, Daniel J. Aneshansley and Leon V. Kochian who helped coauthor a publication with me on this work (Clark et al., 2012).

REFERENCES

Armengaud P, Zambaux K, Hills A, Sulpice R, Pattison RJ, Blatt MR, Amtmann A (2009) EZ-Rhizo: integrated software for the fast and accurate measurement of root system architecture. The Plant Journal 57: 945-956

Arsenault JL, Poulcur S, Messier C, Guay R (1995) WinRHIZO, a root-measuring system with a unique over-lap correction method. HortScience 30: 906

Basu P, Pal A (2012) A new tool for analysis of root growth in the spatio-temporal continuum. New Phytologist 195: 264-274

Brewer MT, Lang L, Fujimura K, Dujmovic N, Gray S, van der Knaap E (2006) Development of a Controlled Vocabulary and Software Application to Analyze Fruit Shape Variation in Tomato and Other Plant Species. Plant Physiology 141: 15-25

Bushamuka VN, Zobel RW (1998) Maize and Soybean Tap, Basal, and Lateral Root Responses to a Stratified Acid, Aluminum-Toxic Soil. Crop Science 38: 416-421

Chavarría-Krauser A, Nagel KA, Palme K, Schurr U, Walter A, Scharr H (2008) Spatio-

temporal quantification of differential growth processes in root growth zones based on a novel combination of image sequence processing and refined concepts describing curvature production. New Phytologist 177: 811-821

Clark RT, Famoso AN, Zhao K, Shaff JE, Craft EJ, Bustamante CD, McCouch SR, Aneshansley DJ, Kochian LV (2012) High-throughput two-dimensional root system phenotyping platform facilitates genetic analysis of root growth and development. Plant, Cell & Environment 36: 454-466

Clark RT, MacCurdy RB, Jung JK, Shaff JE, McCouch SR, Aneshansley DJ, Kochian LV (2011) Three-Dimensional Root Phenotyping with a Novel Imaging and Software Platform. Plant Physiology 156: 455-465

de Dorlodot S, Forster B, Pagès L, Price A, Tuberosa R, Draye X (2007) Root system architecture: opportunities and constraints for genetic improvement of crops. Trends in Plant Science 12: 474-481

de Sousa SM, Clark RT, Mendes FF, Carlos de Oliveira A, Vilaça de Vasconcelos MJ, Parentoni SN, Kochian LV, Guimarães CT, Magalhães JV (2012) A role for root morphology and related candidate genes in P acquisition efficiency in maize. Functional Plant Biology

Dijkstra EW (1959) A note on two problems in connexion with graphs. Numerische Mathematik 1: 269-271

Famoso AN, Clark RT, Shaff JE, Craft E, McCouch SR, Kochian LV (2010) Development of a Novel Aluminum Tolerance Phenotyping Platform Used for Comparisons of Cereal Aluminum Tolerance and Investigations into Rice Aluminum Tolerance Mechanisms. Plant Physiology 153: 1678-1691

Famoso AN, Zhao K, Clark RT, Tung C-W, Wright MH, Bustamante C, Kochian LV, McCouch SR (2011) Genetic Architecture of Aluminum Tolerance in Rice (Oryza sativa) Determined through Genome-Wide Association Analysis and QTL Mapping. PLoS Genetics 7: e1002221

French A, Ubeda-Tomás S, Holman TJ, Bennett MJ, Pridmore T (2009) High-Throughput Quantification of Root Growth Using a Novel Image-Analysis Tool. Plant Physiology 150: 1784-1795

Galkovskyi T, Mileyko Y, Bucksch A, Moore B, Symonova O, Price CA, Topp CN, Iyer-Pascuzzi AS, Zurek PR, Fang S, Harer J, Benfey PN, Weitz JS (2012) GiA Roots: Software for the High Throughput Analysis of Plant Root System Architecture. BMC Plant Biology

Gregory PJ, Bengough AG, Grinev D, Schmidt S, Thomas WTB, Wojciechowski T, Young IM (2009) Root phenomics of crops: opportunities and challenges. Functional Plant Biology 36: 922-929

Hilditch C (1969) Linear skeletons from square cupboards. *In* B Mertzer, D Michie, eds, Machine Intelligence IV, Edinburgh, Scotland, pp 403-420

Hochholdinger F, Tuberosa R (2009) Genetic and genomic dissection of maize root development and architecture. Current Opinion in Plant Biology 12: 172-177

Hochholdinger F, Woll K, Sauer M, Dembinsky D (2004) Genetic Dissection of Root Formation in Maize (Zea mays) Reveals Root-type Specific Developmental Programmes. Annals of Botany 93: 359-368

Hoekenga OA, Maron LG, Piñeros MA, Cançado GMA, Shaff J, Kobayashi Y, Ryan PR, Dong B, Delhaize E, Sasaki T, Matsumoto H, Yamamoto Y, Koyama H, Kochian

LV (2006) AtALMT1, which encodes a malate transporter, is identified as one of several genes critical for aluminum tolerance in Arabidopsis. Proceedings of the National Academy of Sciences 103: 9738-9743

Iyer-Pascuzzi AS, Symonova O, Mileyko Y, Hao Y, Belcher H, Harer J, Weitz JS, Benfey PN (2010) Imaging and Analysis Platform for Automatic Phenotyping and Trait Ranking of Plant Root Systems. Plant Physiology 152: 1148-1157

Kang HM, Zaitlen NA, Wade CM, Kirby A, Heckerman D, Daly MJ, Eskin E (2008) Efficient Control of Population Structure in Model Organism Association Mapping. Genetics 178: 1709-1723

Le Bot J, Serra V, Fabre J, Draye X, Adamowicz S, Pagès L (2010) DART: a software to analyse root system architecture and development from captured images. Plant and Soil 326: 261-273

Lobet G, Pagès L, Draye X (2011) A Novel Image-Analysis Toolbox Enabling Quantitative Analysis of Root System Architecture. Plant Physiology 157: 29-39

Magalhaes JV, Garvin DF, Wang Y, Sorrells ME, Klein PE, Schaffert RE, Li L, Kochian LV (2004) Comparative Mapping of a Major Aluminum Tolerance Gene in Sorghum and Other Species in the Poaceae. Genetics 167: 1905-1914

Magnavaca R, Gradner CD, Clark RB (1987) Evaluation of inbred maize lines for aluminum tolerance in nutrient solution. *In* HW Gabelman, BC Loughman, eds, Genetic Aspects of Plant Mineral Nutrition. Martinus Nijhoff Publishers, Dordrecht, Netherlands, pp 255-265

Malamy JE (2005) Intrinsic and environmental response pathways that regulate root system architecture. Plant, Cell & Environment 28: 67-77

Mather KA, Caicedo AL, Polato NR, Olsen KM, McCouch S, Purugganan MD (2007) The Extent of Linkage Disequilibrium in Rice (Oryza sativa L.). Genetics 177: 2223-2232

Miller ND, Parks BM, Spalding EP (2007) Computer-vision analysis of seedling responses to light and gravity. The Plant Journal 52: 374-381

Milner MJ, Craft E, Yamaji N, Koyama E, Ma JF, Kochian LV (2012) Characterization of the high affinity Zn transporter from Noccaea caerulescens, NcZNT1, and dissection of its promoter for its role in Zn uptake and hyperaccumulation. New Phytologist 195: 113-123

Nagel KA, Kastenholz B, Jahnke S, van Dusschoten D, Aach T, Mühlich M, Truhn D, Scharr H, Terjung S, Walter A, Schurr U (2009) Temperature responses of roots: impact on growth, root system architecture and implications for phenotyping. Functional Plant Biology 36: 947-959

Nagel KA, Putz A, Gilmer F, Heinz K, Fischbach A, Pfeifer J, Faget M, Blossfeld S, Ernst M, Dimaki C, Kastenholz B, Kleinert A-K, Galinski A, Scharr H, Fiorani F, Schurr U (2012) GROWSCREEN-Rhizo is a novel phenotyping robot enabling simultaneous measurements of root and shoot growth for plants grown in soil-filled rhizotrons. Functional Plant Biology

Piñeros MA, Magalhaes JV, Carvalho Alves VM, Kochian LV (2002) The Physiology and Biophysics of an Aluminum Tolerance Mechanism Based on Root Citrate Exudation in Maize. Plant Physiology 129: 1194-1206

Qi X, Qi J, Wu Y (2007) RootLM: a simple color image analysis program for length measurement of primary roots in Arabidopsis. Plant Root 1: 10-16

Rasband WS (1997-2012) ImageJ. *In*. U.S. National Institute of Health, Bethesda, Maryland, USA, http://imagej.nih.gov/ij/

RDCT (2011) R: A Language and Environment for Statistical Computing. *In*, Vienna, Austria, http://www.r-project.org/

Rebouillat J, Dievart A, Verdeil J, Escoute J, Giese G, Breitler J, Gantet P, Espeout S, Guiderdoni E, Périn C (2009) Molecular Genetics of Rice Root Development. Rice 2: 15-34

Shirley P, Ashikhmin M (2005) Fundamentals of computer graphics. AK Peters, Wellesley, Mass.

Waisel Y, Eshel A, Kafkafi U (1996) Plant roots : the hidden half. Marcel Dekker, New York

Wang L, Uilecan IV, Assadi AH, Kozmik CA, Spalding EP (2009) HYPOTrace: Image Analysis Software for Measuring Hypocotyl Growth and Shape Demonstrated on Arabidopsis Seedlings Undergoing Photomorphogenesis. Plant Physiology 149: 1632-1637

Wang T, Cheng I (2008) Generation of Unit-Width Curve Skeletons Based on Valence Driven Spatial Median (VDSM)

Advances in Visual Computing. *In* G Bebis, R Boyle, B Parvin, D Koracin, P Remagnino, F Porikli, J Peters, J Klosowski, L Arns, Y Chun, T-M Rhyne, L Monroe, eds, Vol 5358. Springer Berlin / Heidelberg, pp 1051-1060

Weiss MA (2002) Graphs and Paths. *In* SH Sullivan, ed, Data structures & problem solving using Java, Ed Second. Pearson/Addison-Wesley, Boston, MA, pp 447-511

Yazdanbakhsh N, Fisahn J (2009) High throughput phenotyping of root growth dynamics, lateral root formation, root architecture and root hair development enabled by PlaRoM. Functional Plant Biology 36: 938-946

Yu J, Buckler ES (2006) Genetic association mapping and genome organization of maize. Current Opinion in Biotechnology 17: 155-160

Yu J, Holland JB, McMullen MD, Buckler ES (2008) Genetic Design and Statistical Power of Nested Association Mapping in Maize. Genetics 178: 539-551

Yu J, Pressoir G, Briggs WH, Vroh Bi I, Yamasaki M, Doebley JF, McMullen MD, Gaut BS, Nielsen DM, Holland JB, Kresovich S, Buckler ES (2006) A unified mixed-model method for association mapping that accounts for multiple levels of relatedness. Nat. Genet. 38: 203-208

Zeng G, Birchfield ST, Wells CE (2008) Automatic discrimination of fine roots in minirhizotron images. New Phytologist 177: 549-557

Zhao K, Aranzana MJ, Kim S, Lister C, Shindo C, Tang C, Toomajian C, Zheng H, Dean C, Marjoram P, Nordborg M (2007) An arabidopsis example of association mapping in structured samples. PLoS Genet 3: e4

Zhao K, Tung C-W, Eizenga GC, Wright MH, Ali ML, Price AH, Norton GJ, Islam MR, Reynolds A, Mezey J, McClung AM, Bustamante CD, McCouch SR (2011) Genome-wide association mapping reveals a rich genetic architecture of complex traits in Oryza sativa. Nature Communications 2: 467

CHAPTER III

THREE-DIMENSIONAL ROOT PHENOTYPING WITH A NOVEL IMAGING AND SOFTWARE PLATFORM

ABSTRACT

A novel imaging and software platform was developed for the high-throughput phenotyping of 3-dimensional root traits during seedling development. To demonstrate the platform's capacity, plants of two rice (*Oryza sativa*) genotypes, Azucena and IR64, were grown in a transparent gellan gum system and imaged daily for 10 days. Rotational image sequences consisting of forty 2-dimensional images were captured using an optically corrected imaging system. Three-dimensional root reconstructions were generated and analyzed using a custom designed software, RootReader3D. Using the automated and interactive capabilities of RootReader3D, 5 rice root types were classified and 27 phenotypic root traits were measured to characterize these two genotypes. Where possible, measurements from the 3D platform were validated and were highly correlated with conventional 2-dimensional measurements. When comparing gellan gum grown plants to those grown under hydroponic and sand culture, significant differences were detected in morphological root traits ($p<0.05$). This highly flexible platform provides the capacity to measure root traits with a high degree of spatial and temporal resolution and will facilitate novel investigations into the development of the entire root systems, or selected components of the root systems. In combination with the extensive genetic resources that are now available, this platform

will be a powerful resource to further explore the molecular and genetic determinants of root system architecture.

INTRODUCTION

Root system architecture (RSA) and development has received an increased amount of attention due to advances in phenotyping capabilities and growing insight into the genetic control of root growth (Liu et al., 2005; Tuberosa and Salvi, 2006; de Dorlodot et al., 2007; Armengaud et al., 2009). Previous studies have shown that external factors can affect root morphology and architecture and that root systems have an innate ability to respond and adapt to their rooting environment (Malamy, 2005). Additionally, many reports indicate that certain root qualities in crop plants can help enhance productivity in resource-limited environments due to improved nutrient and water scavenging abilities (Liao et al., 2001; Zhu et al., 2005; Ribaut et al., 2009). Identifying, evaluating and selectively introducing both intrinsic and environmentally responsive root architectural characteristics into breeding programs may be a promising area for improving crop production on resource-limited agricultural systems (de Dorlodot et al., 2007).

Elucidating the genetic and developmental basis of RSA presents many challenges that must be addressed through a combination of field, greenhouse, and laboratory-based approaches. Field studies provide the “ground truth” about plant growth in a particular environment, but these types of root studies are hindered by intensive excavation processes that destructively sample root systems at a single point during development (Smit, 2000). Furthermore, heterogeneity within and along the soil

profile (Lynch, 1995), combined with physical and chemical interactions between various components of the rhizosphere can drastically impact RSA, even under presumably controlled situations (Ward et al., 2008; Shaff et al., 2009).

The overwhelming variety and complexity of field environments combined with the high responsiveness of root systems make it difficult to obtain precise information about the genetic components of RSA and developmental root traits under field conditions, and has subsequently led many researchers to pursue predictive practices (Hochholdinger and Tuberosa, 2009). Predictive techniques provide insight about root systems by extrapolating root information from soil cores and root crowns of field grown plants (Trachsel et al., 2011) or from plants grown in controlled growth systems including hydroponic, pouch, pot and plate systems. *In situ* methods involving rhizotron, magnetic resonance, and computed tomography techniques have also been developed to facilitate non-destructive spatial and temporal investigations into root systems grown in soil (Taylor et al., 1990; Gregory et al., 2003; Tracy et al., 2010), however, the current scale, resolution, throughput, and cost-efficiency of these techniques limits their utility. Additionally, simulation and modeling studies that integrate rhizosphere and growth data help form links between predictive techniques and field studies, allowing researchers to strategically predict, evaluate, and target beneficial root traits or genotypes for specific growth environments (Berntson, 1994; Ho et al., 2004; de Dorlodot et al., 2007).

As a complementary tool to other predictive techniques, gellan gum growth systems with superior optical clarity have been introduced to facilitate non-invasive 2-dimensional (2D) (Iyer-Pascuzzi et al., 2010) and 3-dimensional (3D) (Fang et al., 2009)

imaging and temporal studies of plant root systems while also allowing reproducible control of the rhizosphere . These recent studies demonstrate the use of gellan gum systems and discuss their enormous potential for high-throughput root phenotyping and novel trait discovery when working with 2-dimensional image sets, however efforts to expand investigations into 3D structure remain constrained by low-throughput that requires over an hour to acquire a single root system, small scanning volumes, and limited quantification capabilities.

In this paper we introduce a novel 3D imaging and software platform to investigate root system development and quantify RSA of plants grown in a gellan gum system (Fig. 3.1). This highly versatile phenotyping platform greatly improves throughput and reduces root system capture times to less than 5 minutes, while also advancing our phenotyping capacity beyond 2D whole root system traits into a range of 3D RSA and root type-specific traits.

RESULTS

RootReader3D reconstruction and analysis software

To process and analyze the images captured with the 3D imaging system (Figure 3.1A,C), custom software was written in the Java programming language (Sun Microsystems) that reconstructs 3D root system models from 2D image sequences and quantifies 3D root system traits. This software, RootReader3D, utilizes a silhouette-based back-projection algorithm (Mulayim et al., 2003; Zhu et al., 2006) combined with cross-sectional volume segmentation to generate 3D root models (Figure 3.2). It adopts a template matching technique (Kalman and Attila, 1999), followed by a valence driven

spatial median filter to generate unit-width skeleton representations of the root models (Wang and Cheng, 2008). Various viewing interfaces and mouse and keyboard commands were incorporated into the RootReader3D software to assist in visualizing and interacting with the 3D reconstructions and to facilitate both automated batch analysis of the entire root system and semi-automated modification, separation, selection, labeling and measurement of individual roots, root components and zones of interest within the root system (Figure 3.3).

Measured root traits

The 27 measured root traits calculated with the RootReader3D software can be separated into two categories: static and dynamic root traits. Static root traits are root characteristics that can be measured at a single point in time, whereas dynamic root traits relate to growth and spatial-temporal changes in root characteristics (de Dorlodot et al., 2007). Static and dynamic traits are not mutually exclusive, i.e. some dynamic traits that describe the growth and development of root systems can be derived from static traits, and both categories can be further sub-divided into global and local traits. Global traits are derived from the entire root system or large subsets of the whole system, whereas local traits are derived from individual roots, root classes, or topological zones of interest. The ability to explore a suite of static/dynamic and global/local traits allows for detailed analysis of traditional RSA traits as well as for novel traits that account for developmental changes such as root emergence time and growth characteristics of individual roots and root classes. A list of 3D traits that have been currently integrated into the RootReader3D software along with further descriptions, explanations and classifiers for each root trait is found in Table 3.1.

Figure 3.1: 3D Root Growth and Imaging System. A) Schematic of the 3D imaging system used for capturing image sequences consisting of forty 2D images every 9 degrees of rotation over a full 360° revolution. (L-lightbox ; OCT-optical correction tank; IT-internal turntable; ET-external turntable; MI-magnetic interface; GC-growth cylinder; C-camera; CC-computer controlling turntable and camera) B) Growth cylinder containing gellan gum and a 10 day old Azucena rice seedling. C) Representative single 2D root system image from an image sequence captured with the 3D imaging system.

A

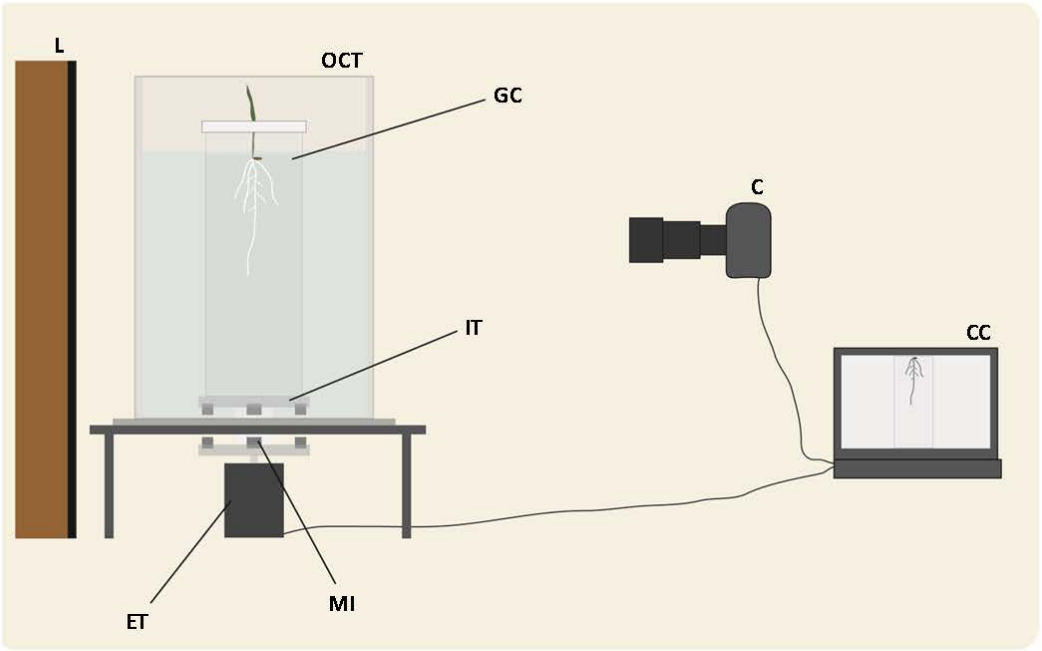

B

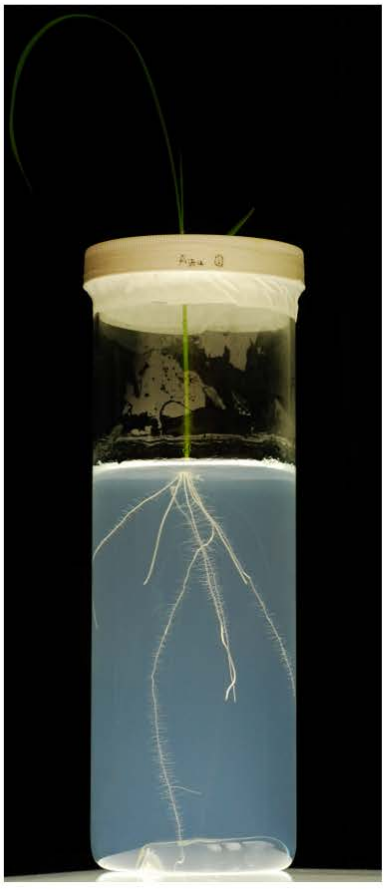

C

Figure 3.2: Depiction of silhouette-based back-projection and cross-sectional volume segmentation process used by RootReader3D during the generation of 3D root models.

Thresholded Rotational Image Sequence Consisting of 40 2D Images

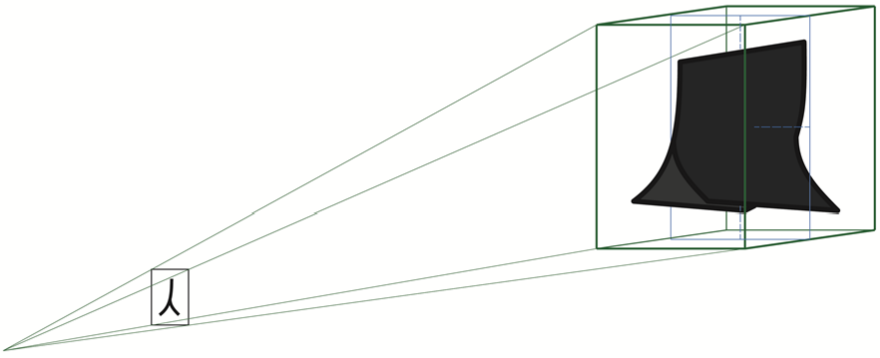

Perspective Back Projection of 2D Root Points from Each 2D Image
into a Temporary 3D Voxel Volume

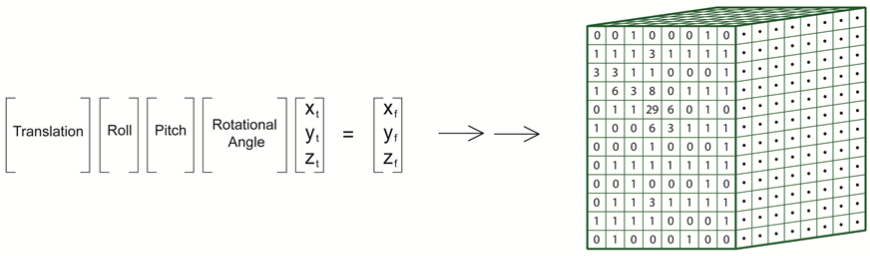

Transformation of Each Temporary Voxel into a Final Voxel Volume

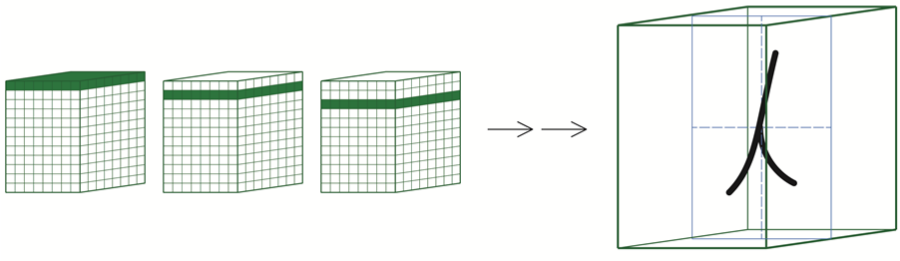

Adaptive Thesholding of Each Horizontal Cross-Section Through
the Final Voxel Volume to Generate a 3D Root Model

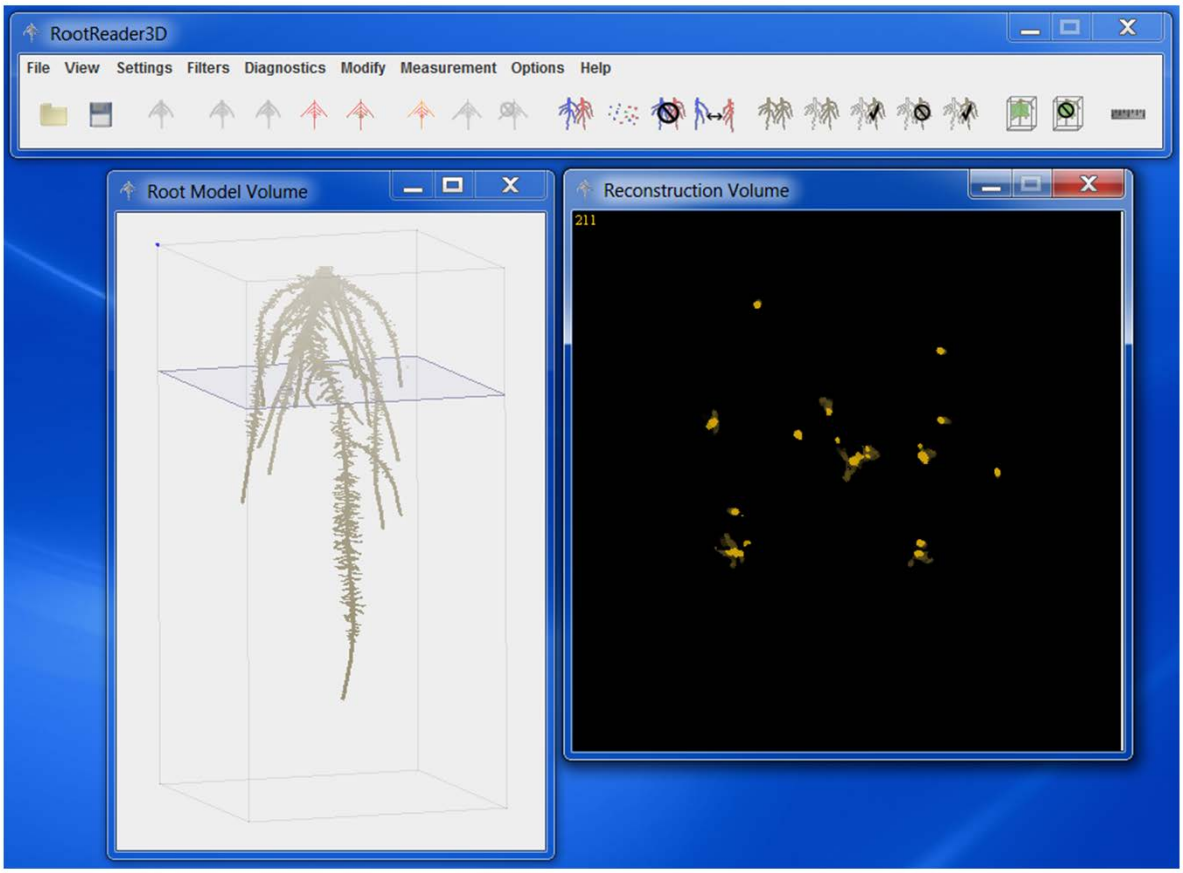

Figure 3.3: RootReader3D screenshot. RootReader3D software generates high resolution 3D root system reconstructions from forty 2D images of root systems for plants grown in the gellan gum growth system and also provides the tools to perform both automated and semi-automated trait analysis. The screenshot shows the RootReader3D toolbar (top), the root model volume window (left) and the reconstruction volume window (right) used for visualizing and interacting with the generated 3D root system models. The shaded slice through the 3D root model (left) corresponds to the horizontal cross-section through the root system shown in the reconstruction volume window on the right.

Table 3.1: Table containing a list of root traits that can currently be measured using the RootReader3D software.

Trait	Root Types	Processing	Units	Description
Length (L)	trs, zoi, pr, ecr, pecr, llr, pr+, cr+	a, sa	cm	Length along the skeleton of the whole root system, root system component, or root using a polyline length estimation technique.
Max Width (MaxW)	trs, pr+, cr+	a, sa	cm	Maximum horizontal width of the whole roots system or root system component measured every 0.2 degrees of rotation.
Min Width (MinW)	trs, pr+, cr+	a, sa	cm	Minimum horizontal width of the whole roots system or root system component measured every 0.2 degrees of rotation.
Max Depth (MaxD)	trs, pr+, cr+	a, sa	cm	Maximum vertical depth of the whole root systems or root system component measured in relation to upper most slice containing a root system voxel.
MinW/MaxW Ratio	trs, pr+, cr+	a, sa	cm/cm	Ratio of minimum width to maximum width.
MaxW/MaxD Ratio	trs, pr+, cr+	a, sa	cm/cm	Ratio of maximum width to maximum depth.
Centroid	trs, pr+, cr+	a, sa	cm	Vertical position of the center of mass of the whole root system or root system component.
Exploitation Volume	trs, zoi, pr+, cr+	a, sa	cm^3	Volume surrounding the root system or root system component at specified radius minus the root system or root components volume. Adapted from Berntson, 1994.
Exploitation Index	trs, zoi, pr+, cr+	a, sa	cm^3/cm	Ratio of the exploitation volume to the root system to root system length. Adapted from Berntson, 1994.
Median Number of Roots (MedR)	trs, zoi, pr+, cr+	a, sa	#	Median number of roots from root counts taken from all horizontal cross-sectional slice through the entire root system or root system component. Adapted from Iyer-Pascuzzi, et al, 2010.
Maximum Number of Roots (MaxR)	trs, zoi, pr+, cr+	a, sa	#	Number of roots at the 84th percentile of a sorted list (smallest to largest) of root counts from all horizontal cross-sections through the entire root system or root system component. Adapted from Iyer-Pascuzzi, et al, 2010.
MaxR/MedR Ratio (Bushiness)	trs, zoi, pr+, cr+	a, sa	#/#	Ratio maximum number of roots to median number of roots. Adapted from Iyer-Pascuzzi, et al, 2010.
Surface Area (SA)	trs, zoi, pr+, cr+	a, sa	cm^2	Summed surface area of the whole root system or root system component voxels that are 6-connected with a background voxel.
SA/V Ratio	trs, zoi, pr+, cr+	a, sa	cm^2/cm^3	Ratio of surface area to volume.
SA/L Ratio	trs, zoi, pr+, cr+	a, sa	cm^2/cm	Ratio of surface area to length.
Volume Distribution	trs	a	cm^3/cm^3	Ratio of the volume of root system contained above one third depth of the root system to the volume of root system contained below one third depth of the root system.

Total root system (trs), Zone of interest (zoi), Primary root (pr), Embryonic crown roots (ecr), Postembryonic crown roots (pecr), Large lateral roots (llr), Primary root plus connected lateral roots (pr+), Crown roots plus connected lateral roots (cr+), Automated (a), Semi-automated (sa)

Table 3.1 (continued)

Trait	Root Types	Processing	Units	Description
Convex Hull Volume (CHV)	trs	a	cm^3	Volume of the convex hull that encompasses the whole root system. The convex hull is found by summing the convex hulls of all horizontal cross-sectional slices through the root system, where the convex hull is the smallest convex set of voxels that contains all other root voxels in the slice. Adapted from Iyer-Pascuzzi, et al, 2010.
V/CHV (Solidity)	trs	a	cm^3/cm^3	Ratio of volume to convex hull volume. Adapted from Iyer-Pascuzzi, et al, 2010.
Emergence Time	pr, ecr, pecr, llr	sa	days	Average root emergence time for a given root type in relation to the planting date.
Initiation Angle	pr, ecr, pecr, llr	sa	degrees	Average horizontal root initiation angle for a given root type. Measured in relation to gellan gum surface or horizontal.
Gravitropic Response	pr, ecr, pecr, llr	sa	degrees/cm	Difference in the horizontal root angle divided by the length of the root or root section.
Circumnutation	pr, ecr, pecr, llr	sa	degrees/cm	Difference in the root turn angle divided by the length of the root or root section.
Narrowness Index	trs, pr+, cr+	a, sa	cm/cm	Average ratio of minimum width to maximum width for each horizontal cross-sectional slice through the whole root system. Slices that only contain the primary root and its connected laterals are excluded.
Volume (V)	trs, zoi, pr+, cr+	a, sa	cm^3	Volume of the whole root system or root system component.
Count	pr, ecr, pecr, llr	sa	#	Number of roots of a particular type.
Tip Count	trs	a	#	Number of root tips in the whole root system. Measured from root system skeleton and is the number of skeleton voxels that have only one 26-connected neighbor voxel.
L/V (Specific Root Length, SRL)	trs, zoi, pr+, cr+	a, sa	cm/cm^3	Ratio of length to volume of the whole root system or root system component. Adapted from Eissenstat, 1991 and Iyer-Pascuzzi, et al, 2010.

Total root system (trs), Zone of interest (zoi), Primary root (pr), Embryonic crown roots (ecr), Postembryonic crown roots (pecr), Large lateral roots (llr), Primary root plus connected lateral roots (pr+), Crown roots plus connected lateral roots (cr+), Automated (a), Semi-automated (sa)

Root type classification

Taking advantage the phenotyping platform's ability to capture and measure both dynamic and local traits, five specific rice root types can be identified and separated from whole root system reconstructions based on emergence time and visual characteristics, as described in Rebouillat *et al.*, 2009 (Figure 3.4A). These five root types include the primary root, which develops from the radicle, the embryonic crown roots, the postembryonic crown roots, the large, indeterminate lateral roots, and the small, determinant lateral roots (Hochholdinger and Tuberosa, 2009). Utilizing the growth rates derived from the daily selection, labeling and measurement of individual crown root lengths, root emergence time was predicted and the crown roots were separated into embryonic and postembryonic crown roots classes, where embryonic and postembryonic crown roots emerged 2 and 6 days after the primary root, respectively (Figure 3.4B). The primary root and large lateral roots were identified using visual features such as root length and branching patterns. Once the root types of the entire root systems were classified, root type specific traits were measured including counts (number of roots), lengths, growth rates, circumnutation, initiation angle, and gravitropic response (Table 3.2). Additionally, to complement root type classification, the structurally complex and overlapping 10 day root systems can also be algorithmically separated, enabling clearer visualization and the finer analysis of global root system qualities. The crown roots can be digitally separated from the entire root system allowing further computational analysis of each root system component separately.

Figure 3.4: Rice root types. A) Depiction of the five root types which are the primary (pr), embryonic crown (ecr), postembryonic crown (pecr), large lateral (llr), and small lateral (slr) roots. As labeled on the 3D root model above, the primary, crown and large and small lateral roots can be visually distinguished from one another. Temporal imaging is performed to further separate the crown roots into embryonic and postembryonic crown root types based on emergence time. Roots that emerged from the crown between 1 and 5 days after planting were classified as embryonic crown roots, whereas roots that emerged later than 5 days after planting were classified as post-embryonic crown roots. B) Average root emergence time of primary and crown roots. Roots were individually selected and measured daily to determine emergence times based on average growth rates. Error bars represent standard errors for all roots of a particular genotype and type.

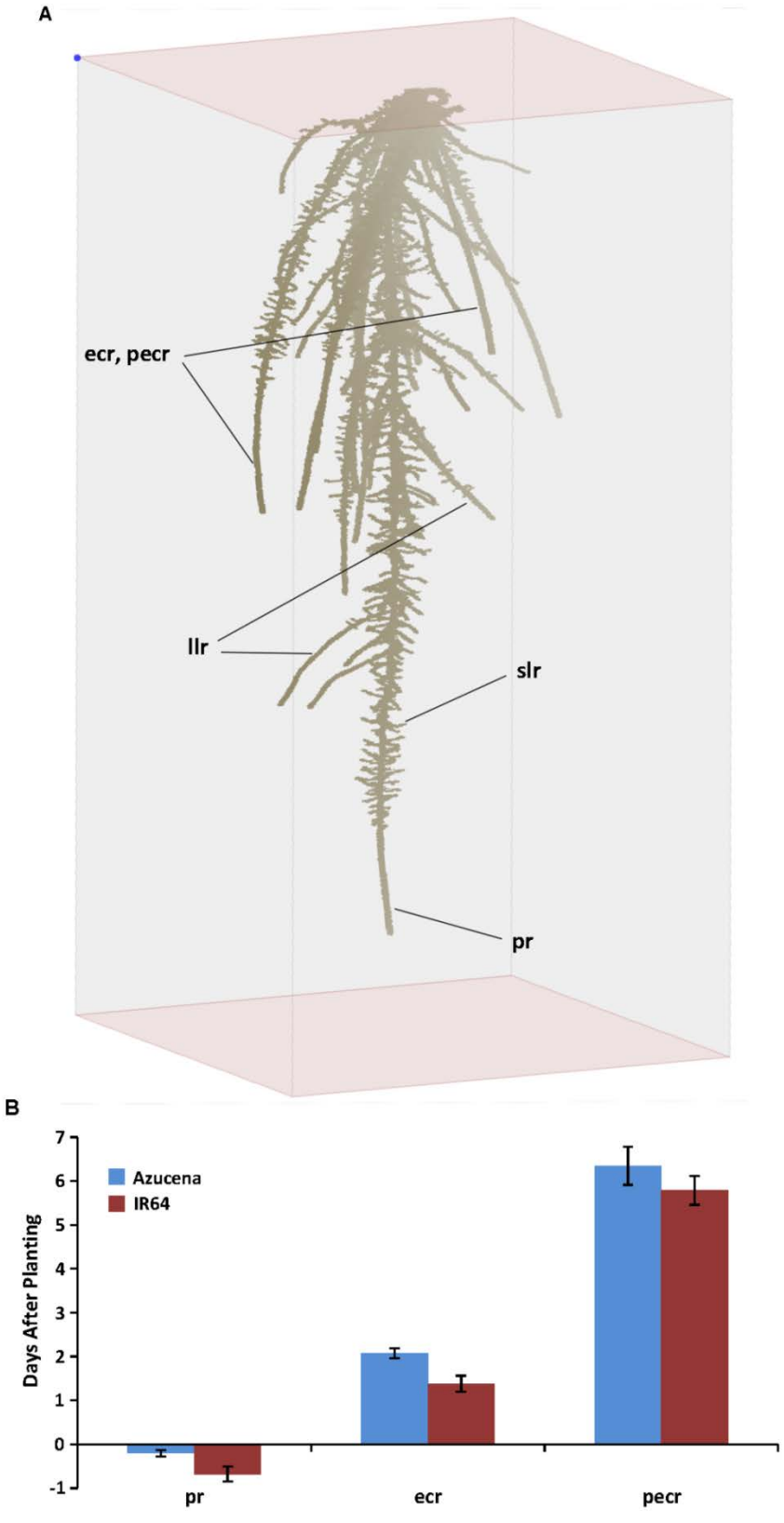
A
ecr, pecr
llr
slr
pr
B
Azucena
IR64
Days After Planting
7
6
5
4
3
2
1
0
-1
pr
ecr
pecr

Table 3.2: Table summarizing all of the calculated RSA traits for Azucena and IR64 plants used in the daily growth experiment.

			Azucena										IR64									
Trait	**Units**	**Root Type**	**D1**	**D2**	**D3**	**D4**	**D5**	**D6**	**D7**	**D8**	**D9**	**D10**	**D1**	**D2**	**D3**	**D4**	**D5**	**D6**	**D7**	**D8**	**D9**	**D10**
Length (L)	cm	trs	4.3	11.5	44.0	87.3	119.4	146.9	184.3	234.8	296.2	361.5	3.1	11.4	54.6	101.8	129.7	162.1	214.2	271.5	316.1	386.7
		pr	3.5	6.4	9.8	13.0	16.1	18.6	20.8	na	na	na	2.8	5.4	8.0	9.8	11.6	13.6	14.5	15.9	17.0	18.1
		ecr		1.0	5.0	12.1	17.6	24.7	31.5	40.4	49.9	60.8			5.0	11.3	18.8	24.5	34.1	45.5	57.9	72.7
		pecr						2.0	4.1	6.4	9.6	15.5						2.8	6.1	12.1	20.0	30.5
		lr	0.8	4.0	29.2	62.1	85.8	101.7	128.0	166.8	215.5	264.2	0.3	6.0	41.7	80.6	99.3	121.2	159.6	198.0	221.1	265.4
		pr+	nm	nm	nm	nm	nm	nm	nm	nm	nm	178.89	nm	nm	nm	nm	nm	nm	nm	nm	nm	212.64
		cr+	nm	nm	nm	nm	nm	nm	nm	nm	nm	202.34	nm	nm	nm	nm	nm	nm	nm	nm	nm	196.31
Max Width (MaxW)	cm	trs	1.1	1.8	3.1	4.5	5.5	6.3	6.6	6.8	6.9	7.2	0.8	1.3	2.6	3.8	4.6	5.2	5.6	5.8	6.0	6.3
Min Width (MinW)	cm	trs	0.5	0.9	1.8	2.6	3.1	3.4	3.7	3.9	4.2	4.6	0.4	0.9	2.0	2.8	3.2	3.6	3.9	4.2	4.5	4.8
Max Depth (MaxD)	cm	trs	3.6	6.5	9.2	12.0	14.5	16.8	18.3	na	na	na	2.9	5.5	7.5	9.2	10.6	11.9	13.1	14.1	14.9	15.6
MinW/MaxW Ratio	cm/cm	trs	0.453	0.518	0.584	0.582	0.571	0.551	0.552	0.567	0.611	0.643	0.493	0.695	0.777	0.743	0.691	0.689	0.706	0.733	0.761	0.762
MaxW/MaxD Ratio	cm/cm	trs	0.302	0.272	0.341	0.378	0.377	0.372	0.363	na	na	na	0.291	0.229	0.345	0.410	0.430	0.436	0.425	0.409	0.400	0.401
Centroid	cm	trs	1.5	2.1	2.4	3.1	4.1	5.0	5.6	6.3	6.9	7.1	1.2	1.7	1.8	2.2	2.8	3.4	3.6	4.0	4.2	4.4
Exploitation Volume	cm3	trs	1.51	2.99	7.97	15.19	21.02	26.48	32.12	39.26	47.01	54.66	1.14	2.57	7.82	15.06	20.11	25.73	32.91	40.32	47.11	55.48
Exploitation Index	cm3/cm	trs	0.35	0.26	0.18	0.17	0.18	0.18	0.17	0.17	0.16	0.15	0.37	0.23	0.14	0.15	0.16	0.16	0.15	0.15	0.15	0.14
Median Number of Roots (MedR)	#	trs	1.00	1.00	1.00	1.00	2.14	2.86	3.43	4.71	5.86	7.43	1.00	1.00	1.00	1.71	3.14	3.43	4,29	4.86	5.29	6.29
Maximum Number of Roots (MaxR)	#	trs	1.00	1.57	7.71	11.57	11.86	7.57	8.43	9.43	10.71	12.14	1.00	1.43	9.57	14.57	16.43	12.29	14.71	18.14	20.29	24.00
MaxR/MedR Ratio (aka Bushiness)	##	trs	1.00	1.57	7.71	11.57	6.17	2.74	2.48	2.01	1.85	1.66	1.00	1.49	9.57	9.86	5.78	3.83	3.53	3.87	3.92	3.85
Surface Area (SA)	cm2	trs	1.81	5.13	19.84	37.64	53.72	76.10	96.61	126.03	159.95	194.16	1.01	4.73	22.55	39.51	53.61	77.76	104.19	131.71	155.61	190.10
		pr+	nm	nm	nm	nm	nm	nm	nm	nm	nm	103.30	nm	nm	nm	nm	nm	nm	nm	nm	nm	96.20
		cr+	nm	nm	nm	nm	nm	nm	nm	nm	nm	89.91	nm	nm	nm	nm	nm	nm	nm	nm	nm	90.00
SA/V Ratio	cm2/cm3	trs	28.55	39.82	64.82	74.78	78.06	64.66	67.00	70.74	73.03	74.46	22.60	43.12	78.37	85.13	86.43	69.73	71.84	73.27	72.97	74.11
		pr+	nm	nm	nm	nm	nm	nm	nm	nm	nm	69.50	nm	nm	nm	nm	nm	nm	nm	nm	nm	79.28
		cr+	nm	nm	nm	nm	nm	nm	nm	nm	nm	78.97	nm	nm	nm	nm	nm	nm	nm	nm	nm	69.56
SA/L Ratio	cm2/cm	trs	0.42	0.43	0.45	0.43	0.45	0.52	0.52	0.54	0.54	0.54	0.31	0.40	0.41	0.39	0.41	0.48	0.49	0.49	0.49	0.49
		pr+	nm	nm	nm	nm	nm	nm	nm	nm	nm	0.51	nm	nm	nm	nm	nm	nm	nm	nm	nm	0.47
		cr+	nm	nm	nm	nm	nm	nm	nm	nm	nm	0.51	nm	nm	nm	nm	nm	nm	nm	nm	nm	0.48

Total root system (trs); Primary root (pr); Embryonic crown roots (ecr); Postembryonic crown roots (pecr); Lateral roots (lr); Large lateral roots (llr); Primary root plus connected lateral roots (pr+); crown roots plus connected lateral roots (cr+); Not applicable because the primary root had reached and was growing along the bottom of the growth cylinder (na); Not measured (nm); Day (D)

Table 3.2 (continued)

			Azucena										IR64									
Trait	**Units**	**Root Type**	**D1**	**D2**	**D3**	**D4**	**D5**	**D6**	**D7**	**D8**	**D9**	**D10**	**D1**	**D2**	**D3**	**D4**	**D5**	**D6**	**D7**	**D8**	**D9**	**D10**
Third/Two-Third Volume Distribution	cm3/cm3	trs	2.01	2.55	4.56	3.50	2.62	2.21	1.98	1.54	1.19	1.04	2.16	2.82	5.27	3.64	3.01	2.82	2.73	2.75	2.69	2.59
Convex Hull Volume (CHV)	cm3	trs	0.08	0.24	2.04	6.93	13.14	23.26	36.82	55.60	76.12	99.59	0.06	0.22	2.14	7.39	12.82	22.31	35.29	49.40	63.20	81.35
V/CHV (aka Solidity)	cm3/cm3	trs	0.766	0.551	0.159	0.076	0.055	0.056	0.045	0.038	0.033	0.030	0.795	0.532	0.138	0.066	0.050	0.052	0.042	0.037	0.034	0.032
Emergence Time	days	ecr										2.07										1.38
		pecr										6.35										5.79
Initiation Angle	degrees	ecr										54.3										52.6
		pecr										63.1										62.3
		llr										25.9										29.8
Gravitropic Response Rate	degrees/ cm	ecr										4.2										7.8
		pecr										3.3										3.1
		llr										10.1										19.5
Circumnutation Rate	degrees/ cm	pr										33.5										33.6
		ecr										26.7										26.6
		pecr										13.4										11.7
		llr										42.6										35.8
Narrowness Index	cm/cm	trs	nm	nm	nm	nm	nm	nm	nm	nm	nm	0.437	nm	nm	nm	nm	nm	nm	nm	nm	nm	0.584
Volume (V)	cm3	trs	0.06	0.13	0.30	0.50	0.69	1.18	1.44	1.78	2.19	2.60	0.04	0.11	0.29	0.46	0.62	1.12	1.45	1.80	2.14	2.56
		pr+	nm	nm	nm	nm	nm	nm	nm	nm	nm	1.17	nm	nm	nm	nm	nm	nm	nm	nm	nm	1.32
		cr+	nm	nm	nm	nm	nm	nm	nm	nm	nm	1.60	nm	nm	nm	nm	nm	nm	nm	nm	nm	1.36
Count	#	pr	1.00	1.00	1.00	1.00	1.00	1.00	1.00	1.00	1.00	1.00	1.00	1.00	1.00	1.00	1.00	1.00	1.00	1.00	1.00	1.00
		ecr	0.00	1.29	2.43	3.00	3.00	3.00	3.00	3.00	3.00	3.00	0.00	0.00	2.57	4.43	5.29	5.29	5.29	5.29	5.29	5.29
		pecr	0.00	0.00	0.00	0.00	0.00	0.43	0.43	0.86	1.29	1.86	0.00	0.00	0.00	0.00	0.00	0.57	1.71	3.14	4.00	4.71
Tip Count	#	trs	4.9	24.3	123.1	245.0	351.1	388.7	541.1	792.4	994.4	1231.4	3.9	26.7	162.1	306.9	373.1	468.1	692.6	951.0	1153.3	1500.4
L/V (aka Specific Root Length, SRL)	cm/cm3	trs										138.82										150.87
		pr+										153.49										160.65
		cr+										126.26										144.36

Total root system (trs); Primary root (pr); Embryonic crown roots (ecr); Postembryonic crown roots (pecr); Lateral roots (lr); Large lateral roots (llr); Primary root plus connected lateral roots (pr+); crown roots plus connected lateral roots (cr+); Not applicable because the primary root had reached and was growing along the bottom of the growth cylinder (na); Not measured (nm); Day (D)

Imaging time course

To further investigate a variety of static/dynamic and global/local RSA traits, Azucena and IR64 plants were grown and imaged daily for 10 days (Figure 3.5). The phenotyping platform enables us to precisely quantify and monitor a number of root growth and RSA traits in both genotypes daily over the 10 day period. As depicted in Figure 3.6 A and B, it is clear that there are significant differences in RSA when objectively viewing the 3D reconstructions of the Azucena and IR64 root systems. However, these differences were not detected when the average length of the different root types (primary root, lateral roots, embryonic crown roots, postembryonic crown roots) was quantified in individual Azucena and IR64 seedlings over the 10 day period (Figure 3.6C,D). When traits that describe different aspects of the total root system architecture were determined, the differences in RSA between Azucena and IR64 could be quantified. Three RSA traits that were significantly different between the two rice genotypes are centroid, volume distribution, and bushiness. Centroid is the vertical position of the center of mass for the entire root system in relation to the seed (see Table I). From the upper panel of Figure 3.6D, Azucena has a significantly larger value for its center of mass as early as day 3, indicating that the Azucena root system tends to grow deeper in the gellan gum profile and has less root volume and branching near the top of the root system. Volume distribution is the ratio of the volume occupied by the upper 1/3 of the root system divided by the volume occupied by the bottom 2/3 of the root system. From the middle panel of Figure 3.6D, IR64 has a considerably larger volume distribution over the last 4 days of the growth experiment, again indicating that its root system explores the upper gellan gum profile more broadly than Azucena.

Figure 3.5: 3D root system models generated from daily imaging of root systems over a ten day period using the RootReader3D software (Day 1 (D1) to Day 10 (D10)). The skeleton of the root systems are shown in red and the primary and crown roots are shown in yellow. The primary and crown roots were selected and labeled, allowing for dynamic tracking of root type specific growth features.

Azucena

(upland rice variety)

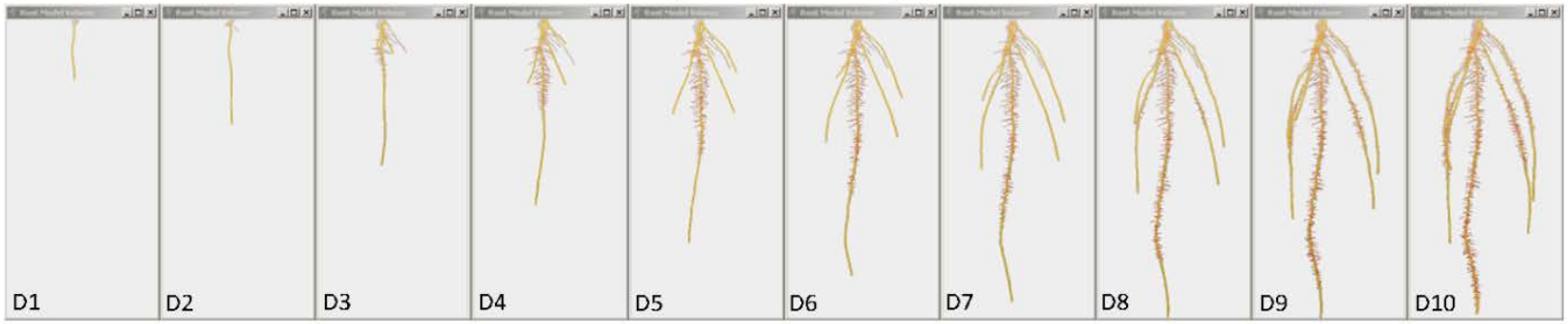

IR64

(lowland rice variety)

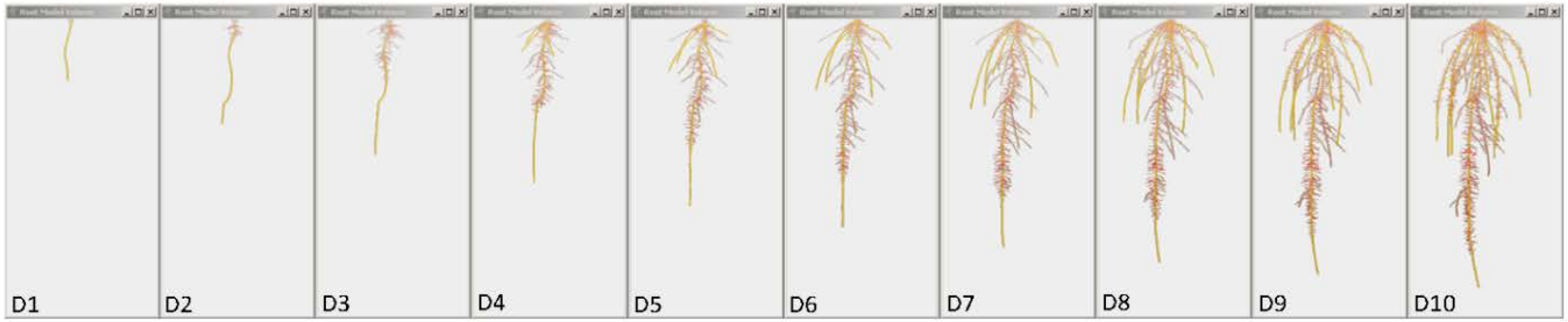

Figure 3.6: Quantitative description of Azucena and IR64 root system differences. A) Day 10 Azucena 3D root system reconstruction. B) Day 10 IR64 3D root system reconstruction. C) Average root length for different root types for Azucena (blue) and IR64 (red) plants, day 1 (D1) to day 10 (D10), n=7. D) A subset of quantified root system architecture traits, including vertical centroid position, volume distribution and bushiness, that quantitatively describe the differences between Azucena and IR64 root system architecture. Each data point represents a single measurement made on an individual Azucena (blue diamond) or IR64 (red triangle) plant on a given day. Asterisks indicate where significant differences were detected between Azucena and IR64 genotypes using a t-test ($p<0.05$). Volume distribution and bushiness traits were adapted to 3D from 2D methods described in Iyer-Pascuzzi et al (2010).

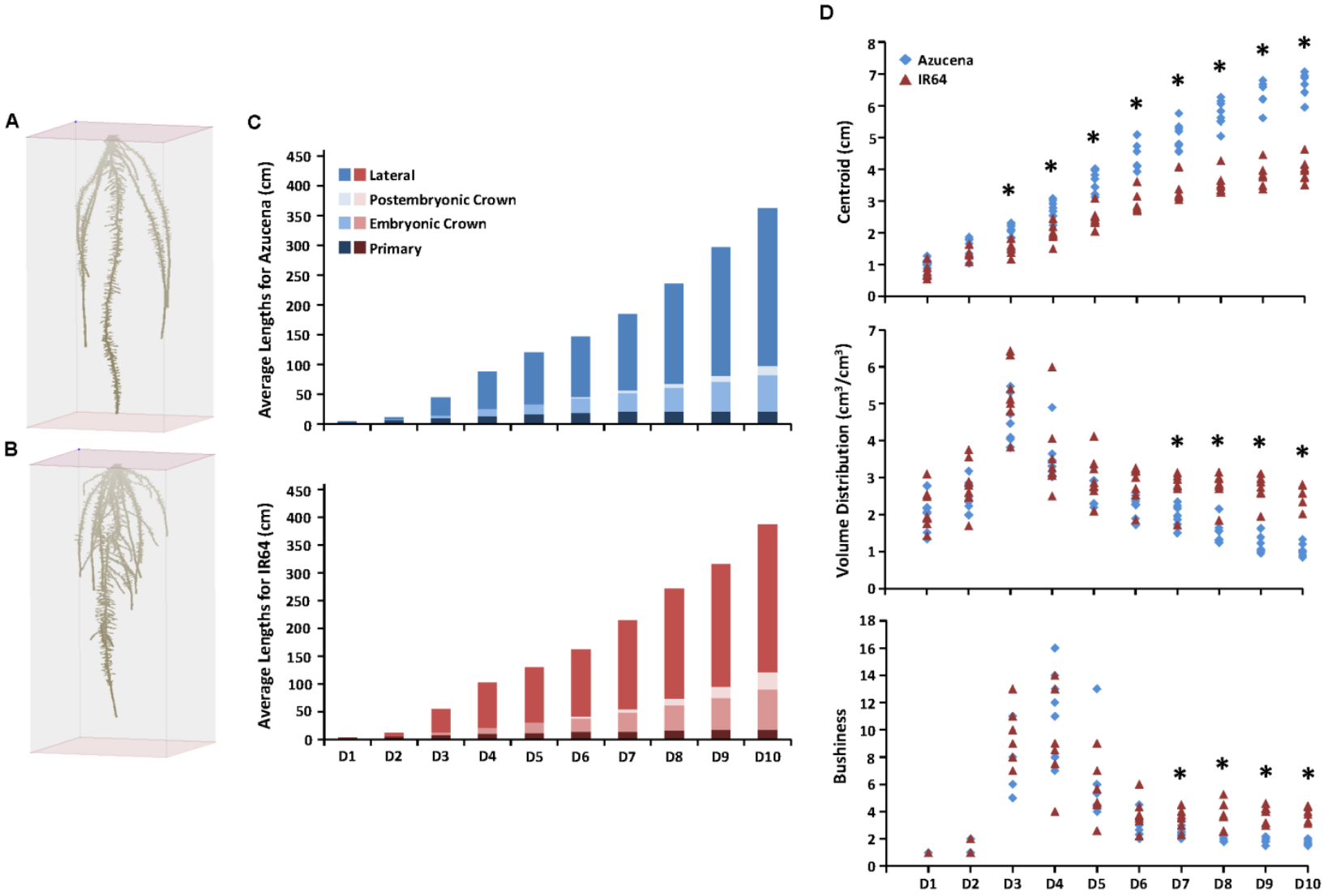
A
B
C
Lateral
Postembryonic Crown
Embryonic Crown
Primary
Average Lengths for Azucena (cm)
Average Lengths for IR64 (cm)
D1
D2
D3
D4
D5
D6
D7
D8
D9
D10
D
Azucena
IR64
Centroid (cm)
Volume Distribution (cm³/cm³)
Bushiness

Finally, bushiness, which was first described in Iyer-Pascuzzi *et al.*, 2010, is the ratio of the maximum number roots (MaxR) divided by median number of roots (MedR) and can be considered a measure of the global branching complexity of the root system. As seen in the bottom panel of Figure 3.6D, IR64 has higher bushiness values over days 7 through 10 of the growth experiment, indicating that IR64 has a more highly branched and complex root system. For a complete summary of the analyzed root traits, see Table 3.2.

Validation of 3D measurements

To validate the root system measurements made by the phenotyping platform, a set of root system traits measured from the reconstructed 3D root models were compared to 2D measurements made on the same root systems using the methods described in Famoso *et al.*, 2010. These traits included primary root length (PRL), total root system length (TRL), and maximum root system width (maxW), which were selected to examine the geometric accuracy and consistency of the 3D root reconstruction and measurements made with the RootReader3D software. All traits were found to be significantly correlated ($p<0.05$) between the 3D and 2D measurement methods (Figure 3.7), with linear fit estimates of $R^2=0.55$, slope (m) =1.10 for PRL, $R^2=0.91$, m=1.54 for TRSL, and $R^2=0.99$, m=1.05 for maxW.

Comparison of RSA traits for plants grown in gellan gum systems vs. hydroponic and sand growth systems

To evaluate if the gellan gum system had specific impacts on rice root characteristics, 2D root traits were compared between the root systems of plants grown in the gellan gum system versus those of plants grown in hydroponic or sand culture

Figure 3.7: 3D Measurements versus 2D Measurements. A) Comparison of total root system length (TRL) measurements - 3D TRL vs. 2D TRL. B) Comparison of primary root length (PRL) measurements - 3D PRL vs. 2D PRL. C) Comparison of maximum root system width(maxW) measurements - 3D maxW vs. 2D maxW.

A

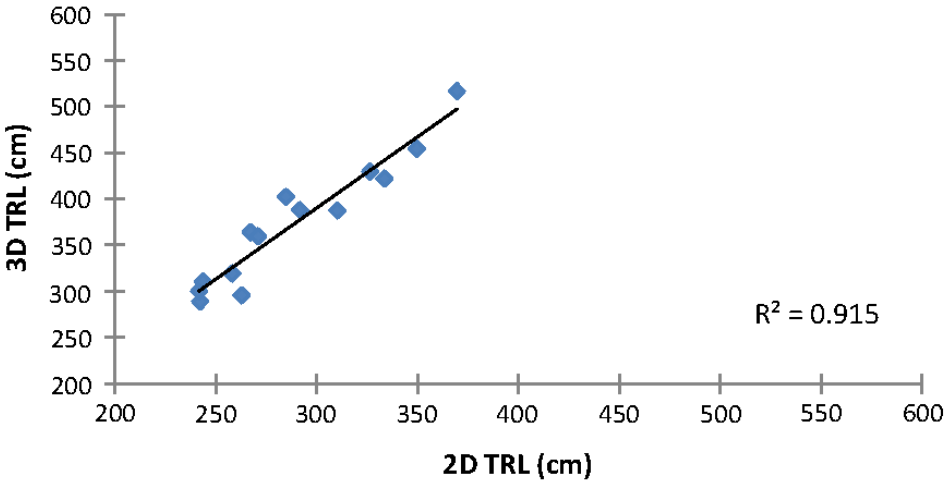
600
550
500
450
400
350
300
250
200
3D TRL (cm)
200
250
300
350
400
450
500
550
600
2D TRL (cm)
R² = 0.915

B

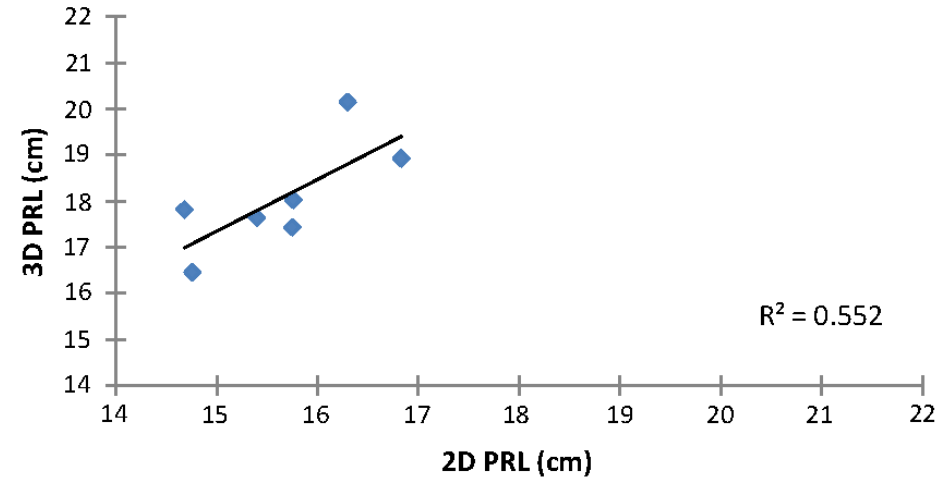
22
21
20
19
18
17
16
15
14
3D PRL (cm)
14
15
16
17
18
19
20
21
22
2D PRL (cm)
R² = 0.552

C

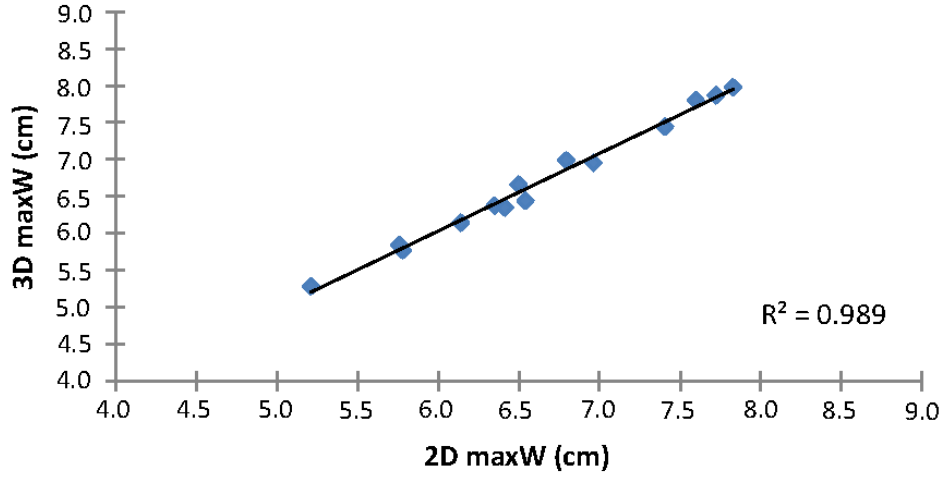
9.0
8.5
8.0
7.5
7.0
6.5
6.0
5.5
5.0
4.5
4.0
3D maxW (cm)
4.0
4.5
5.0
5.5
6.0
6.5
7.0
7.5
8.0
8.5
9.0
2D maxW (cm)
R² = 0.989

systems under aerated and non-aerated conditions with identical nutrient, lighting and temperature regimes (see Table 3.3). The set of root traits compared between the three growth systems included primary root length (PRL), total root system length (TRL), crown root number (CRN), lateral root number (LRN), average crown root length (ACRL), and average lateral root length (ALRL).

Some differences were observed between root growth in gellan gum compared to roots grown in hydroponics and sand, and there were also some genotypic-based differences in the root responses. In general, growth of the entire root system and some root types were less in gellan gum compared with the other two growth media, possibly due to slightly less oxygen availability, especially for roots growing deeper in the gellan media. Surprisingly, the biggest differences were seen between plants grown in the non-aerated sand and of the other growth systems. The greatest root growth was seen in the non-aerated sand system compared with plants grown on gellan gum, hydroponics (aerated and non-aerated) and aerated sand. For example, for Azucena seedlings, total root length (TRL) for plants grown on non-aerated sand was 42% greater than in plants grown in gellan gum, and TRL was 48%, 31% and 25% greater than in plants grown in aerated hydroponics, aerated sand, and non-aerated hydroponics, respectively. In general, root system characteristics for rice seedlings grown in gellan gum were relatively similar to the same root traits for plants grown in hydroponics and aerated sand culture, and the root systems of plants grown on all of these growth systems grew less vigorously than for plants grown on non-aerated sand.

DISCUSSION

Exploring the development of whole root systems by root types

While developing the platform to expand the throughput and phenotyping capability of 3D RSA traits analysis, it was found that many additional aspects of root systems could also be explored. One novel feature of the platform is the ability to identify and classify five different rice root types from whole root system reconstructions.

As with other monocot species, the rice root system is largely composed of a fibrous network of embryonic and postembryonic roots. In monocots, the rapid elongation and lateral root establishment of the primary and embryonic crown roots is critical for early seedling vigor, whereas postembryonic crown roots become increasingly important during further plant growth (Hochholdinger and Tuberosa, 2009). Additionally, through mutant analysis studies in rice, it has been found that these root types are controlled by distinct genetic and developmental networks (Hochholdinger et al., 2004; Rebouillat et al., 2009). The ability of this root imaging and analysis platform to separate and track the growth features of these five root types individually can help detect and further characterize the genetic and developmental changes that occur as the root system develops and the plant matures.

Using 3D information to further investigate root traits

Building upon root type classification, the 3D information provided by the root reconstructions can also be used to investigate traits that have only been studied using 2D analysis systems. Two traits that can be enhanced by utilizing root type and 3D information are root circumnutation and gravitropism. Root circumnutation describes the tendency of roots to grow downward through their growth medium along a helical

axis, and has been mainly studied by analyzing the skewing and periodic waving patterns of the primary roots of Arabidopsis (*A. thaliana*) plants grown on 2D agar plate systems. While the causes of the observed skewing and waving patterns remains under debate, at the present they have mainly been attributed to three intrinsic growth responses: circumnutation, gravitropism and negative thigmotropism (Migliaccio and Piconese, 2001; Oliva and Dunand, 2007), and are suggested to be linked with the recent discovery of oscillating gene expression cycles that also impact the periodic establishment of lateral root prebranching sites along the primary root of Arabidopsis (Moreno-Risueno et al., 2010).

Using the 3D visualization and quantification capabilities of the phenotyping platform, comprehensive investigations into root circumnutation can be extended into rice, a model monocot crop species. Circumnutation was measured on day 10 root system models with RootReader3D (Figure 3.8A), where positive values represent a right-handed rotation and negative values a left-handed rotation. Circumnutation is measured as the change in tangential angle along the root divided by the length of the measured root section, $(\rho_{fin} - \rho_{init})/L$, where ρ_{init} is 0° and ρ_{fin} may be greater than 360°. Though more detailed studies are needed, root circumnutation is present in rice, but it does not vary between Azucena and IR64 genotypes, however, it appears to vary significantly ($p<0.05$) between different root types (Figure 3.8B).

Additionally, the gravitropic response of roots to grow along the gravity vector can also be measured on the different root types. Root gravitropism describes the tendency of plant roots to detect and grow downward along the vertical vector force of

Figure 3.8: Root circumnutation. A) Top view of a 10 day Azucena root system reconstruction showing tangential angles, ρ_{init} and ρ_{fin}, and root segment length, L, used for measuring circumnutation. Yellow lines are the selected primary and crown roots. B) Average circumnutation rates for different root types for Azucena and IR64 genotypes. Root types are abbreviated as pr (primary root), ecr (embryonic crown roots), pecr (postembryonic crown roots) and llr (large lateral roots). Error bars represent standard errors for all roots of a particular genotype and type.

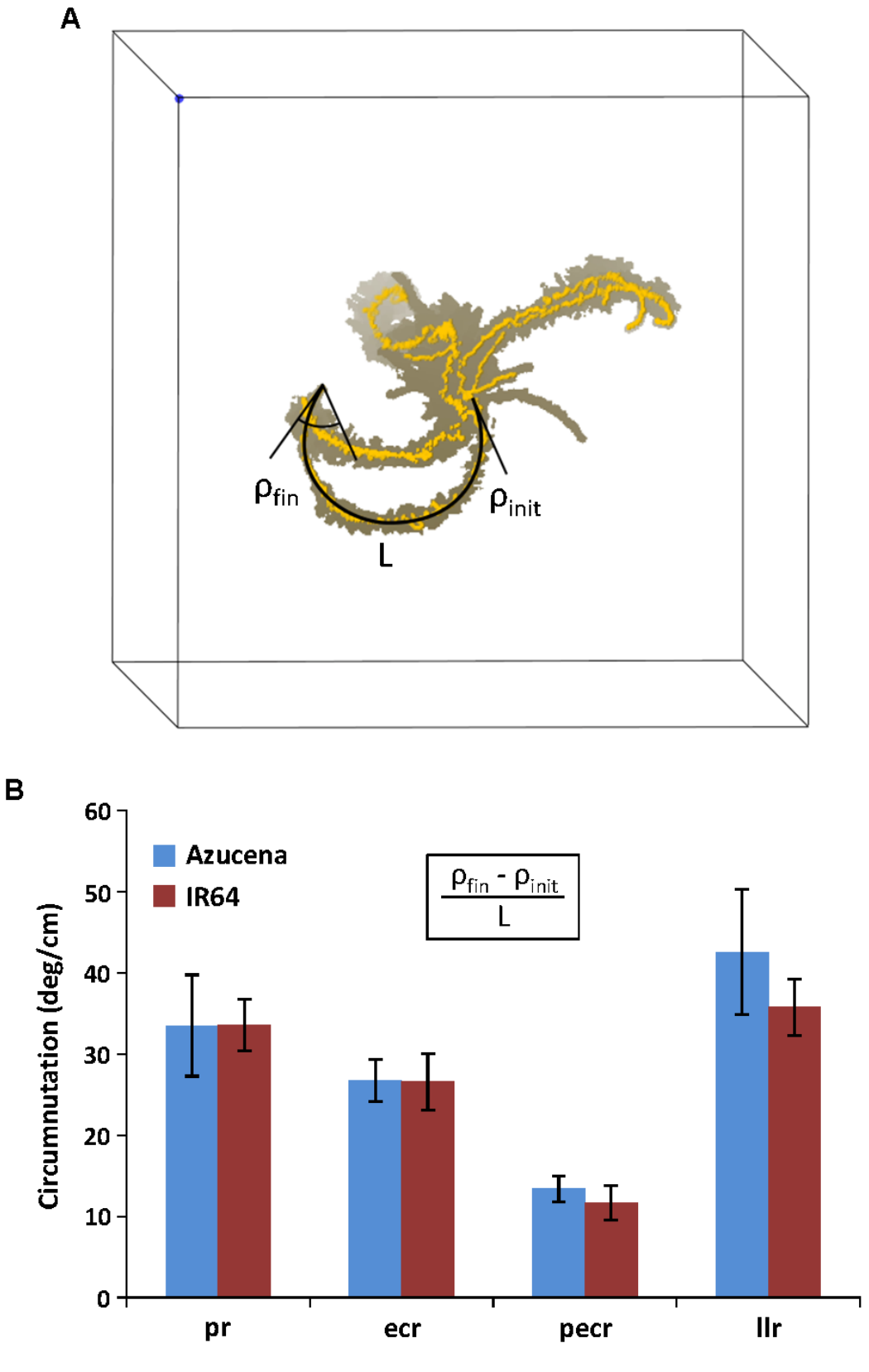
A
ρfin
ρinit
L
B
Azucena
IR64
ρfin - ρinit
L
Circumnutation (deg/cm)
60
50
40
30
20
10
0
pr
ecr
pecr
llr

gravity. In the context of RSA, the initiation angles combined with the gravitropic responses of individual roots can impact the spatial distribution of the entire root system and can ultimately influence the capability of a plant to access and acquire water and nutrient resources.

Both root initiation angle, θ_{init}, and gravitropic response were measured on day 10 root system models, where the initiation angles were measured 5mm from the basal end of the roots in relation to horizontal (or the gellan gum surface) and the gravitropic response was measured as the change in the tangential angle along the root divided by the length the measured root section, $(\theta_{fin} - \theta_{init})/L$. θ_{fin} and L were measured from the root tip or where the tangential angle to the root reached 75° (Figure 3.9A). When investigating the initiation angles of the embryonic crown, postembryonic crown and large lateral roots, it was found that root initiation angle did not vary between genotypes, however, it varied between root types. Additionally, the gravitropic responses of the embryonic crown and large lateral roots were found to be significantly higher for IR64 ($p<0.05$) (Figure 3.9B).

Environmental considerations on rice root traits

Domesticated Asian rice has a complex cultivation history and is raised under a variety of field practices and conditions, ranging from highly managed paddies to unmanaged fields (Sweeney and McCouch, 2007). The two rice varieties used in this study, Azucena and IR64, were selected to represent varieties adapted to different cultivation systems. Azucena, an upland, tropical japonica, has been adapted for growth under non-irrigated field conditions, whereas IR64, a lowland indica, has been bred for maximal yields in flooded paddy systems. The deeper rooting behavior of

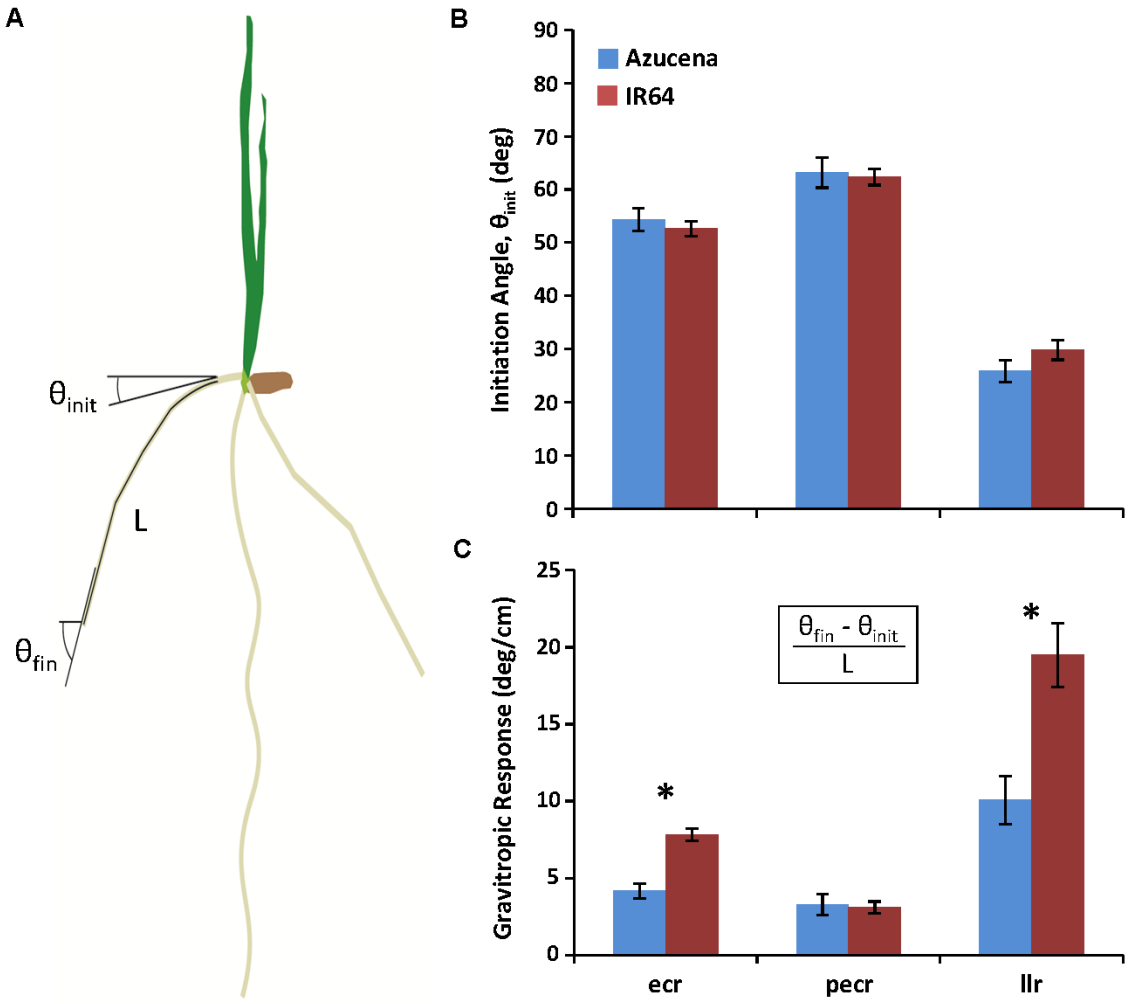

Figure 3.9: Root gravitropism. A) Depiction of a rice seedling with tangential angles, θ_{init} and θ_{fin}, and root segment length, L, used for measuring gravitropic traits. B) Average root initiation angle, θ_{init}, separated by root type. Root types are abbreviated as pr (primary root), ecr (embryonic crown roots), pecr (postembryonic crown roots) and llr (large lateral roots). C) Gravitropic responses for different root types. Error bars represent standard errors for all roots of a particular genotype and type. Asterisks indicate where significant differences were detected between Azucena and IR64 genotypes using a t-test ($p<0.05$).

Azucena compared to IR64, when grown in the gellan gum system (Figures 3.5 and 3.6), is consistent with observations made from soil studies (Yadav et al., 1997). However, as expected of varieties selected under varying cultivation practices, when either of these genotypes is subjected to different growth environments, in this case gellan gum versus aerated or non-aerated hydroponic and sand systems, changes in root traits can be dramatic and varied (Table 3.3). This variability demonstrates the complexity of rice root systems and reinforces the idea that adaptive responses to environmental change can be genotype specific (Nicotra *et al.*, 2010). Additionally, it also suggests that within a plant species there remains a certain level of plasticity in root traits that could possibly be used to further improve plant performance on diverse agricultural systems.

MATERIALS AND METHODS

Plant material and growth conditions

Rice (*Oryza sativa*) genotypes Azucena (upland, tropical japonica) and IR64 (lowland, indica) were used in this study. The hulls of the seeds were removed and the seeds were surface sterilized by soaking them in a solution of 70% ethanol for 1 minute followed by a solution of 3% sodium hypochlorite for 30 minutes. The sodium hypoclorite was removed by washing the seeds with sterile 18MΩ H_2O for a minimum of 5 rinses. Seeds were germinated in the dark at 30°C in vertically oriented, sterile petri plates with moist filter paper covering the seeds for gellan gum studies, or in moist germination paper rolls (Anchor Paper, St. Paul, MN) for hydroponic and sand culture studies.

Table 3.3: Table showing a comparison of root traits for plants grown in gellan gum, sand and hydroponics growth systems

Growth System	Condition	Genotype	PRL	TRL	CRN	LRN	ACRL	ALRL
Gellan Gum	----	Azucena	22.7	289.3	10.6	766.6	8.5	0.26
Hydroponics	Aerated	Azucena	23.5	277.2	8.5[b]	797.7	8.7	0.25
Sand	Aerated	Azucena	20.5	313.4	10.1	365.6[b]	6.4[b]	0.62[a]
Hydroponics	Non-aerated	Azucena	22	329.7	9.9	832.6	8.1	0.3
Sand	Non-aerated	Azucena	18.9[b]	410.6[a]	12.7	481.3[b]	7.1[b]	0.64[a]
Gellan Gum	----	IR64	15.6	289.6	15.3	743.7	6.1	0.26
Hydroponics	Aerated	IR64	17.3	394.7[a]	18.8[a]	1010.6[a]	5.9	0.28
Sand	Aerated	IR64	18.6[a]	259.3	15.1	367.8[b]	4.8[b]	0.46[a]
Hydroponics	Non-aerated	IR64	9.4[b]	331.4	19.2[a]	805.7	4.6[b]	0.29
Sand	Non-aerated	IR64	20.7[a]	512.8[a]	18.2	541.4[b]	5.7	0.71[a]

Primary root length (PRL), in cm; Total root length (TRL), in cm; Crown root number (CRN); Lateral root number (LRN); Average crown root length (ACRL), in cm; Average lateral root length (ALRL), in cm

[a]Significant increase from gellan gum using a t-test, $p<0.05$

[b]Significant decrease from gellan gum using a t-test, $p<0.05$

For gellan gum growth studies, when the emerging radicle had reached approximately 1 cm in length, the sterile seedlings were transplanted into glass growth cylinders (90mm ID, MicroGlass^{TM}) that contained 1.3L of modified Magnavaca's growth media (Famoso et al., 2010) at a pH of 5.5 that has been solidified with gellan gum

(Sigma-Aldrich Phytagel™, St. Louis, MO). The gellan gum growth media was prepared by dissolving and autoclaving 1.95 grams of Phytagel powder in 0.65L of 18MΩ H_2O. The sterile gellan gum solution was then combined with 0.65L of 2X modified Magnavaca's solution that had been adjusted to pH 6.0 and filter sterilized. The 2X modified Magnavaca's solution contained the following: 2.6 mM $CaCl_2$, 2.0 mM KCl, 3.0 mM NH_4NO_3, 0.4 mM $MgSO_4$, 1.0 mM $Mg(NO_3)_2$, 0.91 mM $MgCl_2$, 200 µM KH_2PO_4, 154 µM Fe-HEDTA, 18.2 µM $MnCl_2$, 50.8 µM H_3BO_3, 4.7 µM $ZnSO_4$, 1.2 µM $CuSO_4$, 1.7 µM Na_2MoO_4.

For hydroponic and sand culture studies, when the radicle had grown to 1-2 cm in length, the seedlings were transplanted into either aerated or non-aerated hydroponic or sand growth systems co**n**taining full strength modified Magnavaca's solution, pH 5.5. For hydroponics studies, the seedlings were planted into hydroponic growth systems as described in Famosa et al (2010). The aerated and non-aerated solutions were either continuously bubbled with filtered air or left stagnant. For sand culture studies, a custom ebb and flow growth system was designed where individual plants were grown in 10 cm diameter by 30 cm tall PVC columns filled with sand (Flint Silica #12, U.S. Silica Company) that had been sterilized with 70% ethanol and rinsed with pure water several times. This system involves flooding the sand cylinders up to the sand surface with Magnavaca's solution and then allowing it to drain on a 4 hour cycle for aerated plants, or continuously flooding the cylinders the for non-aerated plants.

For all three studies, seedlings were grown in a growth chamber for 10 days at 30 °C day/26 °C night, 12 h/12 h photoperiod, 550 µmol m2 s-1 photon flux.

3D imaging system and calibration

The 3D imaging system (Figure 3.1A) consists of a Nikon D300s Digital SLR Camera with a Nikon 180mm f/2.8D AF ED-IF Lens (Nikon Inc.) placed on a tripod with manual capture settings of 1/30 second shutter speed, f/22 f-stop and 200 ISO. The camera was aligned transverse to a custom developed optical correction tank that was placed 2 meters from the center of the turntable in order to minimize potential reconstruction artifacts resulting from the perspective geometry of the imaging system (Clark et al., unpublished). A rectangular optical correction tank was filled with water and incorporated into the imaging system to correct for optical refraction from the curved surface of the glass cylinder (Figure 3.10). The optical correction tank contained an internal turntable that was magnetically interfaced with an external electronic turntable (Model #: 5718, Lin Engineering). A lightbox (Model #: BL1824, Hall Productions, San Luis, CA) was placed behind the correction tank, opposite the camera, providing near-uniform backlighting. Daily image sequences were captured for each plant root system grown in gellan gum consisting of 40 silhouette images taken every 9 degrees over the entire 360 degrees of rotation and stored using LabVIEW and Nikon Camera Control Pro 2 software (Figure 3.1B,C). Individual image sequences were captured in 4 minutes, with an image resolution of 50 microns per pixel.

An axis of rotation (AOR) calibration technique was developed to determine the orientation of the AOR in relation to the camera. The AOR was determined by placing an indexed rod on the top-outside edge of the internal turntable and capturing a 2D image sequence over 360 degrees of rotation. The rotational path of each known index

Figure 3.10: Schematic of cylindrical distortion correction. By integrating the optical correction tank into the 3D imaging system, the optical refraction from the curved surface if the cylinder/gellan gum is can be almost completely corrected. Using the corrected image sequences, the root systems can be more accurately reconstructed by the silhouette-based algorithm used by the RootReader3D software.

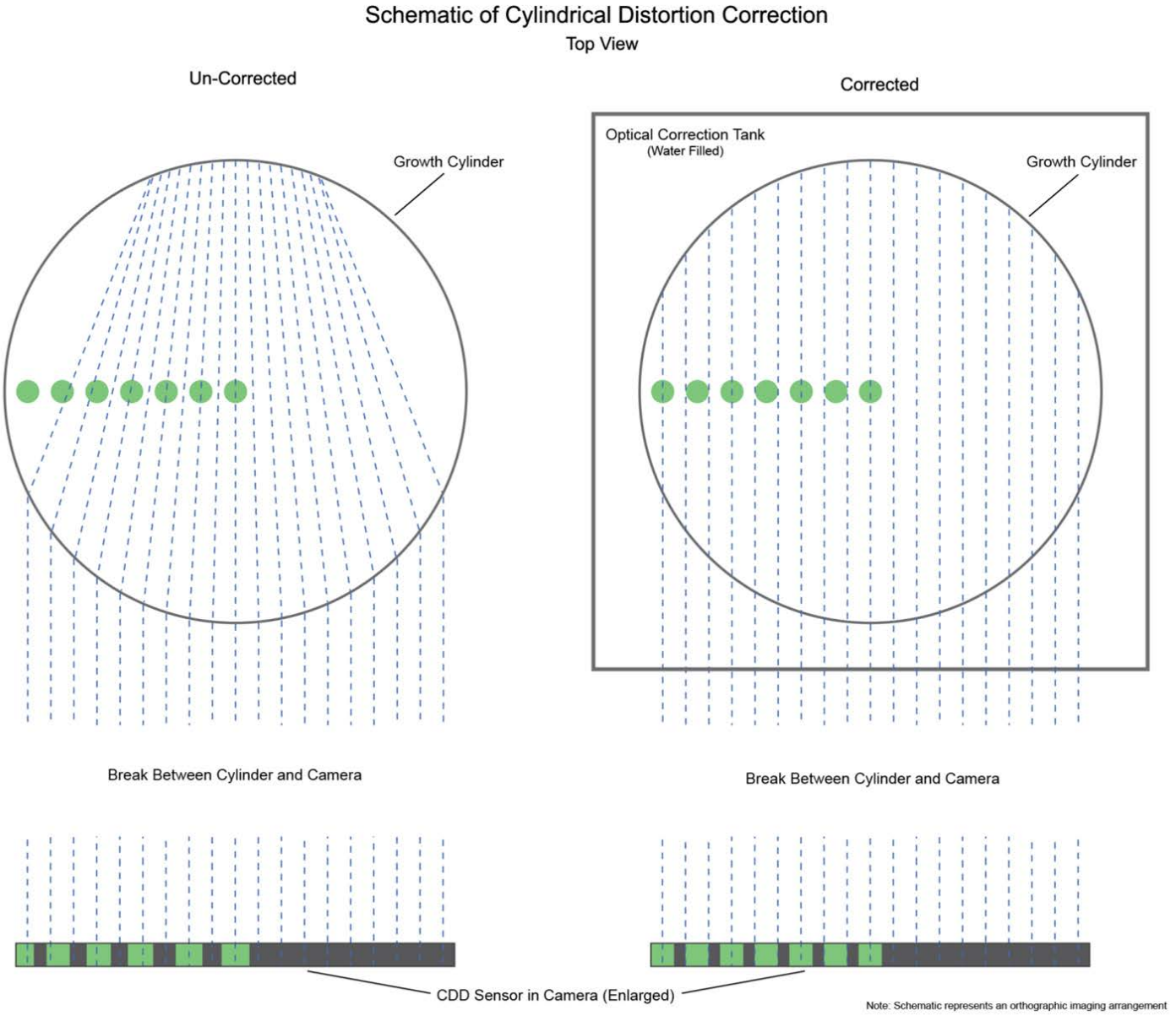
Schematic of Cylindrical Distortion Correction
Top View
Un-Corrected
Corrected
Optical Correction Tank
(Water Filled)
Growth Cylinder
Growth Cylinder
Break Between Cylinder and Camera
Break Between Cylinder and Camera
CDD Sensor in Camera (Enlarged)
Note: Schematic represents an orthographic imaging arrangement

mark was tracked and three AOR calibration parameters used during reconstruction: translation, roll and pitch, were calculated from the tracked marks (Figure 3.11). The scale of reconstruction space, in mm per voxel, was determined by measuring the pixel distance between the index marks when the rod was aligned in the imaging plane using ImageJ software (http://rsb.info.nih.gov/ij/).

Image processing and 3D reconstruction with RootReader3D

Prior to reconstruction, the 2D sequence images were identically cropped, down-sampled to a resolution of 200 microns per pixel and converted to grayscale using Adobe Photoshop (Adobe Systems Incorporated) to produce images with dark roots surrounded by a bright background. The image sequences were then thresholded, reconstructed, and analyzed using our custom RootReader3D software (www.plantmineralnutrition.net). The root system reconstructions generated with RootReader3D had the same resolution as the pre-processed image sequences.

Validation of quantification

After image sequences of the fourteen 10 day old rice seedlings (7 Azucena and 7 IR64 seedlings) were captured, the rice seedlings were removed from the gellan gum growth containers and rinsed. The root systems were excised from the shoot base, spread in the specimen/imaging tray, photographed, and measured with RootReader2D using methods described in Famoso *et al*, 2010. Primary root and total root system length measurements obtained from RootReader3D software were compared to

Figure 3.11: Axis of rotation calibration technique. A) Shown at the left is a diagram of the axis of rotation (AOR) and image plane (IP). B) Shown from left to right are depictions of the translation (T_H), roll (θ_R), and pitch (θ_P) calibration parameters. C) Sequence for the processing of calibration rod images from the original calibration rod image sequence containing forty images to a flattened image sequence used during the extraction of the calibration parameters. The flattened image (right) shows the circular paths traveled by each of the index marks (IM) on the calibration rod (CR). D) Flattened calibration rod image sequence with labels of the components used during the calculation of the calibration parameters. E) Formulae used to calculate each calibration parameter, including T_H (pixels), θ_R (degrees), θ_P (degrees) and the scale of reconstruction volume (mm/voxel).

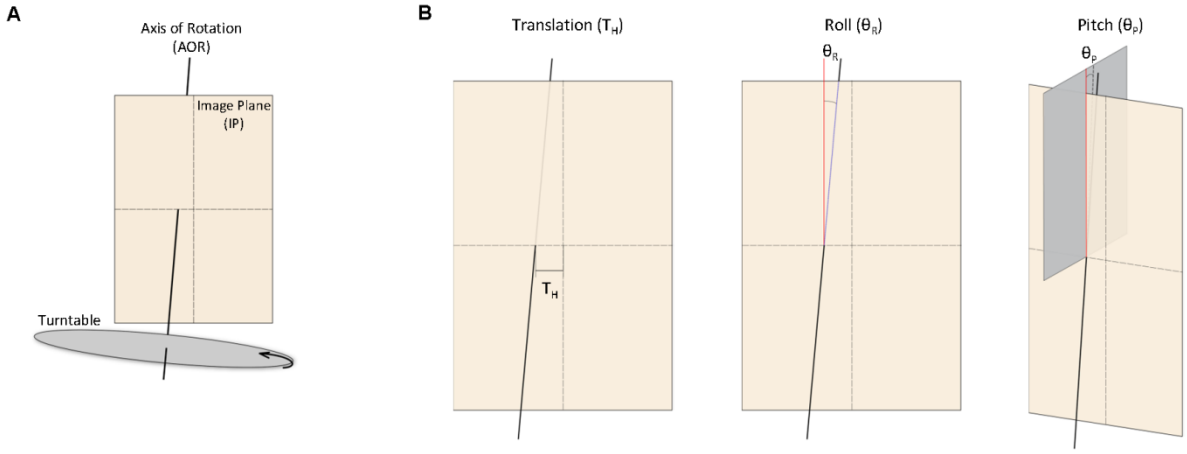

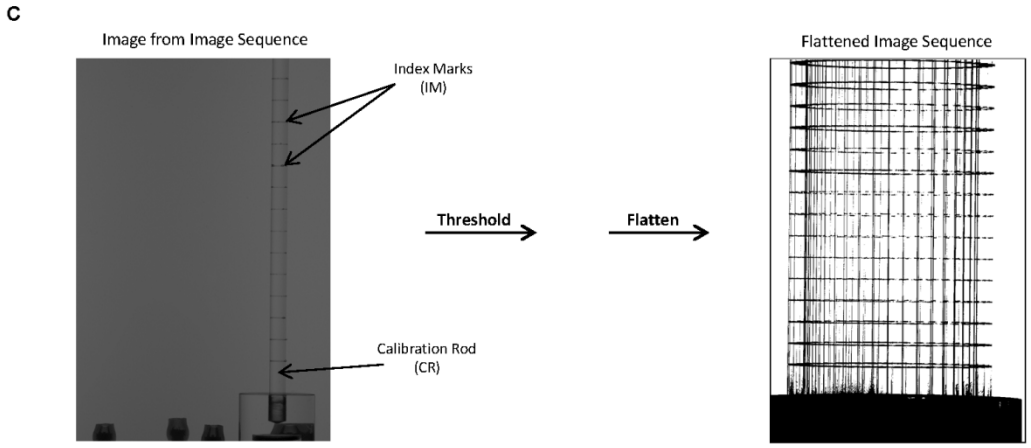

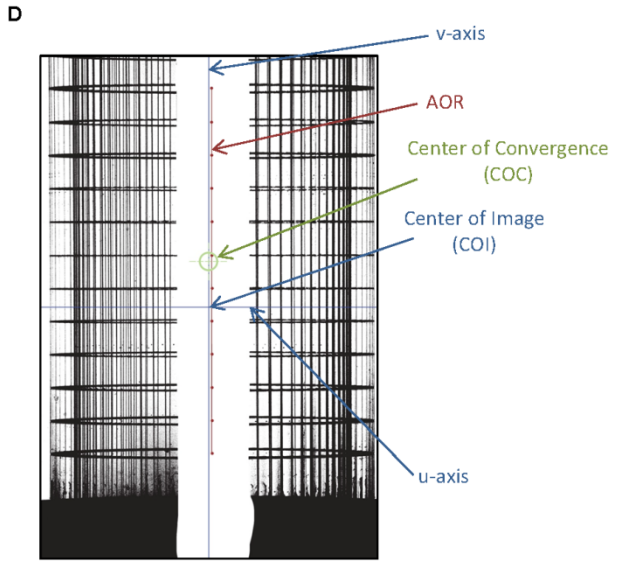

E

T_H = Distance between AOR and v-axis along u-axis

θ_R = Angle between translated AOR and v-axis

$$\theta_P = \tan^{-1}\left[\frac{\text{Distance between COI and COC along the v-axis}}{\text{Distance between the camera and the AOR}}\right]$$

$$\text{Scale} = \frac{\text{Known distance between IM on the CR}}{\text{Number of pixels between IM when the CR is aligned in the IP}}$$

RootReader2D primary root and total root system length measurements. Maximum root system widths were then determined from the original images using ImageJ and compared to RootReader3D width measurements.

CONCLUSION

The 3D imaging and RootReader3D software platform described in this chapter is a unique imaging and analysis package for investigating both static and dynamic 3D RSA characteristics of plant root systems that have been formerly difficult to measure with high throughput, accuracy and resolution. The automated and interactive features of RootReader3D also provide a flexible foundation for more extensive root trait analysis in the future. The 27 measured root traits demonstrate the platforms utility for analyzing root systems, however, many root traits and quantitative techniques, including advanced dynamic and topological analysis, have not yet been incorporated to describe and analyze the 3D root models. The presence of significant differences in basic 2D root traits between gellan gum, hydroponic and sand growth systems reinforces the fact that plant root systems are highly responsive to their growth environment and that more in-depth evaluation is needed before gellan gum root traits can be directly related to performance under field conditions. The enhanced quantification capabilities and capacity to image over one hundred root systems per day, combined with a rapidly advancing array of genetic resources, presents many opportunities for dissecting the genetic control and developmental changes of RSA, as well as opportunities to explore RSA variation within and between species grown under a range of controlled environmental conditions.

ACKNOWLEDGEMENTS

For the work presented in this chapter, I would like to thank Prof. Anthony P. Reeves for his discussions and lessons on image processing, automated analysis, and the importance of technique validation, William A. Shaben and Douglas B. Caveney for their advice and guidance throughout the system design and fabrication process, and Prof. Xiaolong Yan, Prof. Hong Liao and Dr. Suqin Fang for providing foundation and insight into 3D reconstruction and root system architecture. I would also like to thank Robert B. MacCurdy, Janelle K. Jung, Jon E. Shaff, Susan R. McCouch, Daniel J. Aneshansley and Leon V. Kochian who helped coauthor a publication with me on this work (Clark et al., 2011).

REFERENCES

Armengaud P, Zambaux K, Hills A, Sulpice S, Pattison RJ, Blatt MR, Amtmann A (2009) EZ-Rhizo: integrated software for the fast and accurate measurement of root system architecture. The Plant Journal 57: 945-956

Berntson GM (1994) Modelling Root Architecture: Are There Tradeoffs between Efficiency and Potential of Resource Acquisition? New Phytologist 127: 483-493

Clark RT, MacCurdy RB, Jung JK, Shaff JE, McCouch SR, Aneshansley DJ, Kochian LV (2011) Three-Dimensional Root Phenotyping with a Novel Imaging and Software Platform. Plant Physiology 156: 455-465

Clark RT, MacCurdy RB, Kochian LV (unpublished) 3D Model Construction of Rice Root System from 2D Image Sequences. *In* BEE Research Symposium. Cornell University, Ithaca

de Dorlodot S, Forster B, Pagès L, Price A, Tuberosa R, Draye X (2007) Root system architecture: opportunities and constraints for genetic improvement of crops. Trends in Plant Science 12: 474-481

Famoso AN, Clark RT, Shaff JE, Craft E, McCouch SR, Kochian LV (2010) Development of a Novel Aluminum Tolerance Phenotyping Platform Used for Comparisons of Cereal Aluminum Tolerance and Investigations into Rice Aluminum Tolerance Mechanisms. Plant Physiology 153: 1678-1691

Fang S, Yan X, Liao H (2009) 3D reconstruction and dynamic modeling of root architecture in situ and its application to crop phosphorus research. The Plant Journal 60: 1096-1108

Gregory PJ, Hutchison DJ, Read DB, Jenneson PM, Gilboy WB, Morton EJ (2003) Non-invasive imaging of roots with high resolution X-ray micro-tomography. Plant and Soil 255: 351-359

Ho MD, McCannon BC, Lynch JP (2004) Optimization modeling of plant root architecture for water and phosphorus acquisition. Journal of Theoretical Biology 226: 331-340

Hochholdinger F, Park WJ, Sauer M, Woll K (2004) From weeds to crops: genetic analysis of root development in cereals. Trends in Plant Science 9: 42-48

Hochholdinger F, Tuberosa R (2009) Genetic and genomic dissection of maize root development and architecture. Current Opinion in Plant Biology 12: 172-177

Iyer-Pascuzzi AS, Symonova O, Mileyko Y, Hao Y, Belcher H, Harer J, Weitz JS, Benfey PN (2010) Imaging and Analysis Platform for Automatic Phenotyping and Trait Ranking of Plant Root Systems. Plant Physiology 152: 1148-1157

Kalman P, Attila K (1999) A parallel 3D 12-subiteration thinning algorithm. Graph. Models Image Process. 61: 199-221

Liao H, Rubio G, Yan X, Cao A, Brown KM, Lynch JP (2001) Effect of phosphorus availability on basal root shallowness in common bean. Plant and Soil 232: 69-79

Liu H, Wang S, Yu X, Yu J, He X, Zhang S, Shou H, Wu P (2005) ARL1, a LOB-domain protein required for adventitious root formation in rice. The Plant Journal 43: 47-56

Lynch J (1995) Root Architecture and Plant Productivity. Plant Physiology 109: 7-13

Malamy JE (2005) Intrinsic and environmental response pathways that regulate root system architecture. Plant, Cell & Environment 28: 67-77

Migliaccio F, Piconese S (2001) Spiralizations and tropisms in Arabidopsis roots. Trends in Plant Science 6: 561-565

Moreno-Risueno MA, Van Norman JM, Moreno A, Zhang J, Ahnert SE, Benfey PN (2010) Oscillating Gene Expression Determines Competence for Periodic Arabidopsis Root Branching. Science 329: 1306-1311

Mulayim AY, Yilmaz U, Atalay V (2003) Silhouette-based 3D model reconstruction from multiple images. Systems, Man, and Cybernetics, Part B: Cybernetics, IEEE Transactions on 33: 582-591

Oliva M, Dunand C (2007) Waving and skewing: how gravity and the surface of growth media affect root development in Arabidopsis. New Phytologist 176: 37-43

Rebouillat J, Dievart A, Verdeil J, Escoute J, Giese G, Breitler J, Gantet P, Espeout S, Guiderdoni E, Périn C (2009) Molecular Genetics of Rice Root Development. Rice 2: 15-34

Ribaut J-M, Betran J, Monneveux P, Setter T (2009) Drought Tolerance in Maize. *In* JL Bennetzen, SC Hake, eds, Handbook of Maize: Its Biology. Springer New York, pp 311-344

Shaff J, Schultz B, Craft E, Clark R, Kochian L (2009) GEOCHEM-EZ: a chemical speciation program with greater power and flexibility. Plant and Soil 303: 207-214

Smit AL (2000) Root methods : a handbook. Springer, Berlin; New York

Sweeney M, McCouch S (2007) The Complex History of the Domestication of Rice. Annals of Botany 100: 951-957

Taylor HM, Upchurch DR, McMichael BL (1990) Applications and limitations of rhizotrons and minirhizotrons for root studies. Plant and Soil 129: 29-35

Trachsel S, Kaeppler S, Brown K, Lynch J (2011) Shovelomics: high throughput phenotyping of maize (Zea mays L.) root architecture in the field. Plant and Soil 341: 75-87

Tracy SR, Roberts JA, Black CR, McNeill A, Davidson R, Mooney SJ (2010) The X-factor: visualizing undisturbed root architecture in soils using X-ray computed tomography. J. Exp. Bot. 61: 311-313

Tuberosa R, Salvi S (2006) Genomics-based approaches to improve drought tolerance of crops. Trends in Plant Science 11: 405-412

Wang T, Cheng I (2008) Generation of Unit-Width Curve Skeletons Based on Valence Driven Spatial Median (VDSM). *In* Advances in Visual Computing, Vol 5358. Springer Berlin / Heidelberg, pp 1051-1060

Ward JT, Lahner B, Yakubova E, Salt DE, Raghothama KG (2008) The Effect of Iron on the Primary Root Elongation of Arabidopsis during Phosphate Deficiency. Plant

Physiol. 147: 1181-1191

Yadav R, Courtois B, Huang N, McLaren G (1997) Mapping genes controlling root morphology and root distribution in a doubled-haploid population of rice. TAG Theoretical and Applied Genetics 94: 619-632

Zhu J, Kaeppler SM, Lynch JP (2005) Topsoil foraging and phosphorus acquisition efficiency in maize (Zea mays). Functional Plant Biology 32: 749-762

Zhu T, Fang S, Li Z, Liu Y, Liao H, Yan X (2006) Quantitative analysis of 3-dimensional root architecture based on image reconstruction and its application to research on phosphorus uptake in soybean. Chinese Science Bulletin 51: 2351-2361

CHAPTER IV

GENETIC MAPPING OF ROOT SYSTEM TRAITS IN *ORYZA SATIVA* USING 3-DIMENSIONAL ROOT PHENOTYPING

ABSTRACT

The 3-dimensional (3D) root phenotyping platform that was presented in Chapter III allows root system architecture (RSA) characteristics of growing seedlings to be measured and tracked. Using this phenotyping platform in combination with publicly available germplasm and genotypic resources, thirteen core root traits were measured on days 3, 6 and 9 after planting and joint linkage-association mapping studies were performed to identify regions of the rice (*Oryza sativa*) genome that are involved in root system development. Composite interval mapping (CIM) with a recombinant inbred mapping population derived from a cross between IR64 (lowland, *indica*) and Azucena (upland, *tropical japonica*) detected 121 QTL across all 12 rice chromosomes. Genome wide association studies (GWAS) were performed using an *O. sativa* panel that captures diversity within the *aus*, *indica*, *temperate japonica* and *tropical japonica* subpopulations of domesticated rice. Eight hundred and forty-eight significant SNPs were detected in total during analyses across all accessions and within each of the four major subpopulations represented in the panel. Multi-trait analyses were performed to further narrow in on regions of the rice genome that condition global control of multiple root system traits. Significant regions from both single trait and multi-trait analyses will need to be further explored for candidate genes as well as possible functional roles in

root system adaption to optimal and suboptimal growth environments.

RESULTS

Root system architecture (RSA) in a rice diversity panel

Four hundred twenty-six diverse *Oryza sativa* accessions from the McCouch rice diversity panel (Tung et al., 2010; Zhao et al., 2011) were evaluated for root traits using the 3-dimensional root phenotyping platform described in Chapter III (Clark et al., 2011). Root system images were captured on days 3, 6, 9, and 12 after transplanting (D3, D6, D9 and D12) and 19 global root system architecture (RSA) traits (Table 4.1) were measured from the reconstructed root systems imaged on D3, D6 and D9. The RSA measurements were transformed to improve normality of the trait distributions and further reduced to 13 core RSA trait measures (Table 4.2). Markov Chain Monte Carlo (MCMC) resampling was performed to account for environmental effects and low replicate numbers during the screening experiment, and median core trait estimates were generated (Figure 4.1). To investigate the amount of phenotypic variation that was described by rice subpopulation alone, one-way ANOVA across the 4 major rice subpopulations represented in the diversity panel (*aus*, *indica*, *temperate japonica* and *tropical japonica*) was performed. It was found that rice subpopulation structure described between 5.2 and 58.5% of the observed trait variation in the panel for a single trait and time point (Table 4.3). Broad sense heritability (H^2) was estimated during the MCMC resampling process and found to range from 0.26 to 0.79 (Table 4.3). Overall, it was observed that rice subpopulation structure tended to describe more of the variation

Table 4.1: 19 Original RSA Traits

Trait	Description
Bushiness	Ratio maximum number of roots to median number of roots. Adapted from Iyer-Pascuzzi, et al (2010).
Centroid	Vertical position of the center of mass of the whole root system.
ConvexHull	Volume of the convex hull that encompasses the whole root system. The convex hull is found by summing the convex hulls of all horizontal cross-sectional slices through the root system, where the convex hull is the smallest convex set of voxels that contains all other root voxels in the slice. Adapted from Iyer-Pascuzzi, et al (2010).
MaxDepth	Maximum vertical depth of the whole root systems measured in relation to upper most slice containing a root system voxel.
MaxRoots	Number of roots at the 84th percentile of a sorted list (smallest to largest) of root counts from all horizontal cross-sections through the entire root system. Adapted from Iyer-Pascuzzi, et al (2010).
MaxWidth	Minimum horizontal width of the whole roots system measured every 0.2 degrees of rotation.
MaxWidth/MaxDepth	Ratio of maximum width to maximum depth.
MedRoots	Median number of roots from root counts taken from all horizontal cross-sectional slices through the entire root system. Adapted from Iyer-Pascuzzi, et al (2010).
MinWidth/MaxWidth	Ratio of minimum width to maximum width.
MinWidth	Minimum horizontal width of the whole roots system or root system component measured every 0.2 degrees of rotation.
Solidity	Ratio of volume to convex hull volume. Adapted from Iyer-Pascuzzi, et al (2010).
SRL	Ratio of length to volume of the whole root system. Adapted from Eissenstat (1991) and Iyer-Pascuzzi, et al (2010).
TipCount	Number of root tips in the whole root system. Measured from root system skeleton and is the number of skeleton voxels that have only one 26-connected neighbor voxel.
TRSL	Length along the skeleton of the whole root system using a polyline length estimation technique.
TRSL/TRSSA	Ratio of length to surface area.
TRSSA	Summed surface area of the whole root system voxels that are 6-connected with a background voxel.
TRSSA/TRSV	Ratio of surface area to volume.
TRSV	Volume of the whole root system.
VolumeDistribution	Ratio of the volume of root system contained above one third depth of the root system to the volume of root system contained below one third depth of the root system.

Table 4.2: 13 MCMC Resampled Traits

Trait	Description
Centroid	Vertical position of the center of mass of the whole root system.
ConvexHull	Volume of the convex hull that encompasses the whole root system. The convex hull is found by summing the convex hulls of all horizontal cross-sectional slices through the root system, where the convex hull is the smallest convex set of voxels that contains all other root voxels in the slice. Adapted from Iyer-Pascuzzi, et al (2010).
MaxDepth	Maximum vertical depth of the whole root systems measured in relation to upper most slice containing a root system voxel.
MaxRoots	Number of roots at the 84th percentile of a sorted list (smallest to largest) of root counts from all horizontal cross-sections through the entire root system. Adapted from Iyer-Pascuzzi, et al (2010).
MaxWidth	Minimum horizontal width of the whole roots system measured every 0.2 degrees of rotation.
MinWidth	Minimum horizontal width of the whole roots system or root system component measured every 0.2 degrees of rotation.
mmRtpcC	Contrast (2nd) principle component of the pairwise principle component analysis of MaxRoots and MedRoots.
Solidity	Ratio of volume to convex hull volume. Adapted from Iyer-Pascuzzi, et al (2010).
SRL	Ratio of length to volume of the whole root system. Adapted from Eissenstat (1991) and Iyer-Pascuzzi, et al (2010).
TipCount	Number of root tips in the whole root system. Measured from root system skeleton and is the number of skeleton voxels that have only one 26-connected neighbor voxel. (Note: This also effectively represents TRSL, TRSSA, and TRSV)
TRSLVpcC	Contrast (2nd) principle component of the pairwise principle component analysis of TRSL and TRSV.
TRSVSApcC	Contrast (2nd) principle component of the pairwise principle component analysis of TRSV and TRSSA.
VolumeDistribution	Ratio of the volume of root system contained above one third depth of the root system to the volume of root system contained below one third depth of the root system.

Figure 4.1: Boxplots of MCMC resampled 3D root systems RSA trait measures from the rice diversity panel on D3, D6, D9 and Davg.

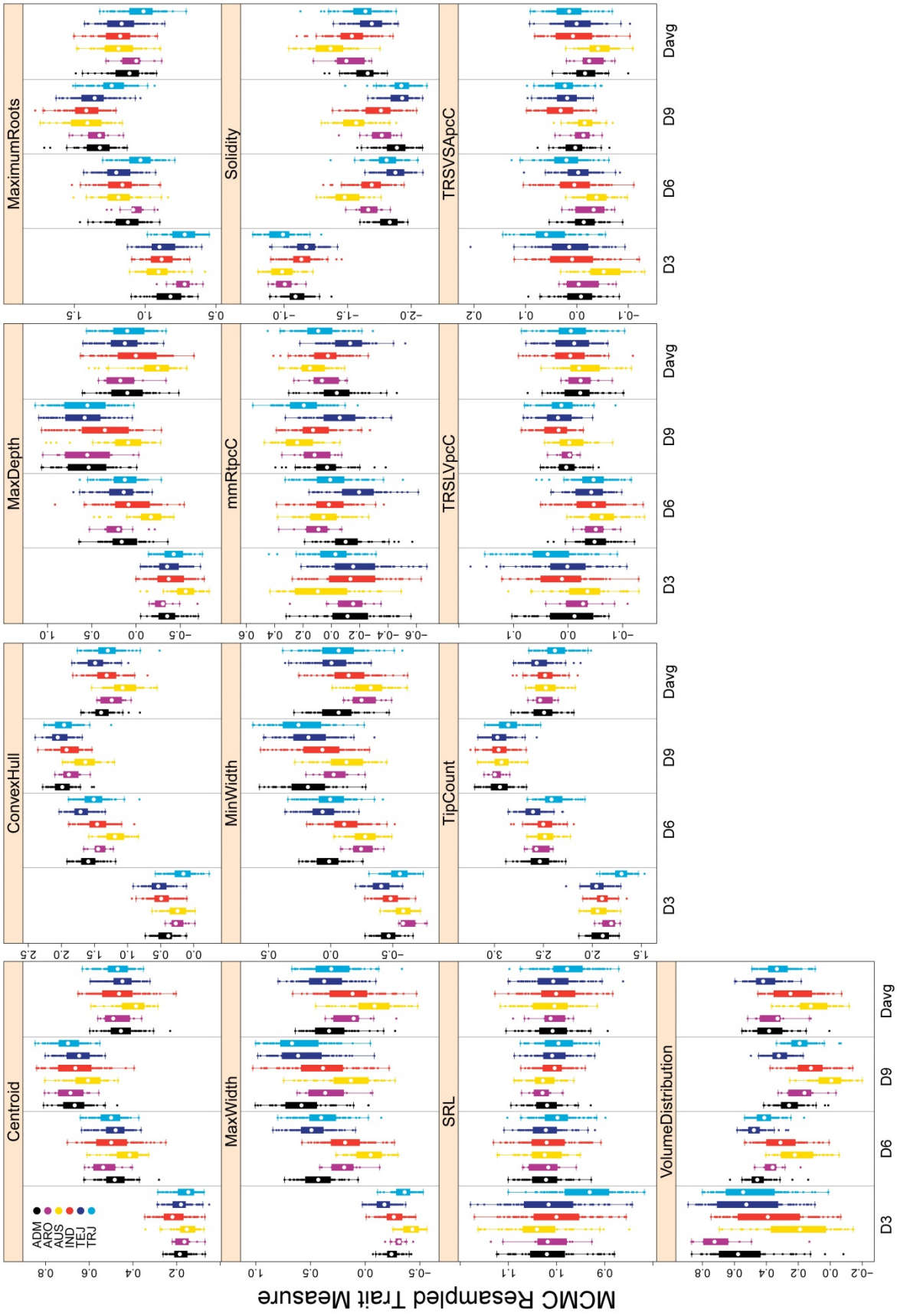
MCMC Resampled Trait Measure
Centroid
ConvexHull
MaxDepth
MaximumRoots
MaxWidth
MinWidth
mmRtpcC
Solidity
SRL
TipCount
TRSLVpcC
TRSVSApcC
VolumeDistribution
ADM
ARO
AUS
IND
TEJ
TRJ
D3
D6
D9
Davg

in traits related to root system density and compactness, whereas root depth related traits tended to have higher heritabilities.

RSA in a recombinant inbred (RI) rice population

Two hundred fifty-five recombinant inbred lines (RILs) from a population derived from a cross between IR64 (*indica*) and Azucena (*tropical japonica*) were screened for 3D RSA traits. Nineteen global root system traits (Table 4.1) were measured from root system reconstructions on D3, D6, and D9, then reduced to 13 core trait measurements (Table 4.2) and transformed to improve normality across the trait distributions (Table 4.4). The mean of the trait measurements across the RILs population fell within the parental mean measurements for all of the core traits except specific root length (SLR) on D6 and D9, VolumeDistribution on D9, and the contrast principle components. The two parent varieties of the RIL population displayed RSA traits consistent with previous root system studies of varieties from the *Indica* and *Japonica* subspecies (Iyer-Pascuzzi et al., 2010; Topp et al., 2013). IR64, the *indica* parent, had a shallow, more compact root system with longer lateral root branches, whereas Azucena, the *tropical japonica* parent, had a root system comprised predominantly of deeper primary and crown roots with shorter lateral root branches. Despite the many differences between these distinct varieties, all core traits showed transgressive variation within the derived RIL population. While some root trait distributions displayed bimodal characteristics, such as VolumeDistribution, MaxDepth and Centroid (Figure 4.2), transgressive variation was still observed among the RILs, where the population contained RILs which displayed trait values higher than that of the higher parent and lower than that of the lower parent.

Genome wide association (GWA) analysis

Using a custom genotypic dataset consisting of the 673,937 SNP markers, genome wide association (GWA) studies were performed with the MCMC core trait measurements from D3, D6, D9 and Davg. GWA analysis was performed using a linear mixed model approach (Kang et al., 2008), across all accessions (ALL) and within the *aus* (AUS), *indica* (IND), *temperate japonica* (TEJ) and *tropical japonica* (TRJ) rice subpopulations (Figure 4.3). To better define genomic regions of interest, peak SNPs of having a $-\log_{10}(p\text{-}value)$ near or higher than 4 with strong support from surrounding SNPs were manually selected from the significance results for each respective GWA analyses. SNPs that were highly significant, but were not supported by surrounding SNPs were excluded during this selection process. In total, 848 SNPs were selected from the GWA results, with 235, 182, 199, 76 and 156 from ALL, AUS, IND, TEJ and TRJ subpopulations, respectively. As shown in Figure 4.3, some of the selected SNP were significant across multiple traits, days and subpopulations, whereas others were only significant for a specific trait, day and/or subpopulation.

When factoring in linkage disequilibrium (LD), which has been estimated to range between 50kb and 500kb in rice (Mather et al., 2007; Zhao et al., 2011), based on the extensive spread of 848 selected SNPs, it appears that from these results (Figure 4.3) a large percentage of the rice genome could potentially be involved in RSA development at some point during the experimental period. These results highlight the complex nature of the root development, thus specific traits of interest and multi-trait approaches are focused on during subsequent analyses in order to narrow down and prioritize the genomic regions for further investigation.

Table 4.3: Broad sense heritability estimates (H^2) and one-way ANOVA R^2 results from analysis across the 4 major rice subpopulations represented in the rice diversity panel.

Trait	Day	Heritability (H^2)	One-way ANOVA (R^2)
Centroid	D3	0.50 (0.43, 0.57)	0.174
	D6	0.70 (0.65, 0.75)	0.123
	D9	0.74 (0.69, 0.78)	0.126
	Davg	0.65 (0.62, 0.69)	0.095
ConvexHull	D3	0.43 (0.35, 0.51)	0.475
	D6	0.53 (0.46, 0.59)	0.468
	D9	0.58 (0.51, 0.65)	0.367
	Davg	0.51 (0.47, 0.55)	0.317
MaxDepth	D3	0.64 (0.58, 0.69)	0.153
	D6	0.78 (0.74, 0.82)	0.194
	D9	0.79 (0.75, 0.83)	0.255
	Davg	0.72 (0.69, 0.75)	0.195
MaximumRoots	D3	0.54 (0.47, 0.61)	0.356
	D6	0.63 (0.57, 0.69)	0.238
	D9	0.67 (0.61, 0.72)	0.279
	Davg	0.60 (0.56, 0.64)	0.230
MaxWidth	D3	0.38 (0.30, 0.47)	0.505
	D6	0.49 (0.42, 0.56)	0.549
	D9	0.68 (0.61, 0.73)	0.307
	Davg	0.53 (0.49, 0.58)	0.346
MinWidth	D3	0.40 (0.32, 0.48)	0.438
	D6	0.48 (0.40, 0.55)	0.480
	D9	0.60 (0.52, 0.66)	0.304
	Davg	0.51 (0.46, 0.55)	0.295
mmRtpcC	D3	0.43 (0.35, 0.50)	0.162
	D6	0.41 (0.34, 0.49)	0.273
	D9	0.50 (0.43, 0.57)	0.365
	Davg	0.26 (0.22, 0.30)	0.351
Solidity	D3	0.42 (0.34, 0.51)	0.402
	D6	0.46 (0.39, 0.54)	0.585
	D9	0.59 (0.52, 0.66)	0.540
	Davg	0.46 (0.41, 0.50)	0.413
SRL	D3	0.43 (0.34, 0.50)	0.245
	D6	0.43 (0.35, 0.50)	0.063
	D9	0.38 (0.31, 0.46)	0.103
	Davg	0.37 (0.33, 0.42)	0.076
TipCount	D3	0.42 (0.33, 0.49)	0.509
	D6	0.58 (0.51, 0.64)	0.311
	D9	0.60 (0.54, 0.66)	0.137
	Davg	0.54 (0.50, 0.59)	0.201
TRSLVpcC	D3	0.46 (0.37, 0.53)	0.166
	D6	0.44 (0.36, 0.51)	0.052
	D9	0.41 (0.33, 0.48)	0.121
	Davg	0.39 (0.34, 0.43)	0.062
TRSVSApcC	D3	0.58 (0.51, 0.65)	0.359
	D6	0.56 (0.49, 0.62)	0.249
	D9	0.55 (0.48, 0.61)	0.264
	Davg	0.43 (0.39, 0.48)	0.256
VolumeDistribution	D3	0.61 (0.55, 0.67)	0.246
	D6	0.52 (0.45, 0.59)	0.502
	D9	0.57 (0.51, 0.63)	0.573
	Davg	0.34 (0.29, 0.38)	0.472

The upper and lower bounds of the 95% credibility interval shown in parenthesis following the H^2 estimates.

Table 4.4: 3D RSA trait measures from D3, D6, and D9 RIL population screening.

Trait	Day	IR64	Azucena	RILs
Centroid	D3	1.05 (0.196)	1.35 (0.331)	1.32 (0.300)*
	D6[a]	0.30 (0.053)	0.53 (0.099)	0.44 (0.093)***
	D9[a]	0.48 (0.044)	0.74 (0.113)	0.61 (0.096)***
ConvexHull	D3[b]	1.37 (0.504)	0.94 (0.183)	1.34 (0.530)**
	D6[b]	5.96 (1.851)	4.74 (1.433)	5.76 (1.820)
	D9[b]	10.95 (2.598)	8.92 (2.642)	10.21 (3.039)*
MaxDepth	D3	3.18 (0.774)	6.21 (2.146)	5.02 (2.199)***
	D6	7.14 (0.894)	14.03 (3.192)	10.97 (3.324)***
	D9[c]	0.01 (0.077)	1.14 (0.467)	0.47 (0.510)***
MaximumRoots	D3[a]	0.93 (0.138)	0.59 (0.209)	0.82 (0.224)***
	D6[a]	1.27 (0.159)	0.90 (0.144)	1.13 (0.189)***
	D9[a]	1.50 (0.164)	1.06 (0.165)	1.33 (0.193)***
MaxWidth	D3	3.03 (0.830)	2.48 (0.638)	2.90 (0.807)
	D6[d]	3361 (1627)	1579 (980)	2348 (1587)**
	D9[e]	0.90 (0.180)	0.48 (0.322)	0.63 (0.311)***
MinWidth	D3	2.07 (0.629)	1.77 (0.442)	1.96 (0.594)
	D6	4.48 (0.995)	4.00 (0.886)	4.40 (1.109)
	D9	6.13 (1.063)	4.94 (1.104)	5.66 (1.285)**
mmRtpcC	D3	0.26 (0.814)	0.24 (0.471)	0.00 (0.564)
	D6	0.22 (0.304)	0.38 (0.501)	0.00 (0.530)
	D9	-0.01 (0.385)	0.39 (0.310)	0.00 (0.406)**
Solidity	D3[a]	-1.02 (0.216)	-0.82 (0.157)	-0.96 (0.214)*
	D6[a]	-1.82 (0.216)	-1.68 (0.214)	-1.74 (0.198)
	D9[a]	-2.01 (0.124)	-1.93 (0.182)	-1.93 (0.187)
SRL	D3	165.7 (33.13)	156.0 (30.67)	164.0 (29.35)
	D6	200.0 (18.69)	199.4 (15.28)	197.1 (19.10)
	D9	204.3 (15.12)	200.4 (13.06)	195.8 (15.93)
TipCount	D3[b]	8.71 (2.024)	6.51 (1.054)	8.060 (2.141)**
	D6[b]	16.25 (3.509)	15.45 (2.403)	16.41 (3.568)
	D9[b]	28.56 (5.837)	24.35 (3.784)	26.62 (5.722)
TRSLVpcC	D3	0.04 (0.231)	0.00 (0.280)	0.00 (0.240)
	D6	0.04 (0.190)	0.04 (0.161)	0.00 (0.211)
	D9	-0.09 (0.146)	-0.06 (0.131)	0.00 (0.169)
TRSVSApcC	D3	0.19 (0.156)	-0.10 (0.161)	0.00 (0.154)***
	D6	0.11 (0.104)	-0.03 (0.122)	0.00 (0.174)**
	D9	0.10 (0.112)	-0.01 (0.099)	0.00 (0.144)*
VolumeDistribution	D3[b]	1.17 (0.274)	2.09 (0.640)	1.57 (0.635)***
	D6[b]	1.33 (0.181)	1.59 (0.286)	1.57 (0.330)*
	D9[b]	1.37 (0.208)	1.29 (0.167)	1.39 (0.231)

Transformations made to trait measures are indicated with the following symbols: a=$\log_{10}$, b=square root, c=logit (upper bound of 21), d=forth power, e=logit (upper bound of 10). The trait means are followed by their standard deviation surround in parentheses. The difference in trait measures between of the parental lines (IR64 and Azucena) were tested using a two-sided t-test and the significance values are denoted as: p≥0.5 (no mark), p<0.05 (*), p<0.01 (**), and p<0.001 (***).

QTL Analysis

Using a genotypic dataset of 1559 SNP markers (Spindel et al., 2012), composite interval mapping (CIM) was performed with the 13 core RSA trait measures from the IR64 x Azucena RIL population on D3, D6 and D9. In total, 121 QTL with LOD scores ranging from 3.1 to 13.1 and R^2 values from 0.05 to 0.23 were detected (Table 4.5). These QTL were spread across all 12 of the rice chromosomes, however most QTL localized to hotspots regions of the genome (Figure 4.4). Similar to what was observed for root systems characteristics of the RIL parents, Azucena tended to additively contribute more to QTL detected for deeper, sparser root system traits (i.e. Centroid, MaxDepth and ConvexHull) whereas IR64 additively contributed more to QTL for denser, more compact root system traits (i.e. Solidity and SLR). However, there were also a few QTL detected where the IR64 parent also contributed to increased depth. As highlighted in Figure 4.4, most hotspot regions were composed of traits related to either root system depth (hotspots on chromosomes 2, 6 and 8) or root system density (hotspots on chromosomes 1, 3, 6 and 9). Interestingly enough, there was very little overlap between QTL detected for either of the two types of roots traits (depth-related and density-related). Additionally, the hotspot regions typically persisted over multiple days, though one region related to depth (chromosome 8) and one related to density (chromosome 9) were only detected for a single time point (D3 and D6 respectively). One hotspot region related to total root system length which persisted over all three time points was also detected on chromosome 10, for which IR64 additively contributed to increased root lengths.

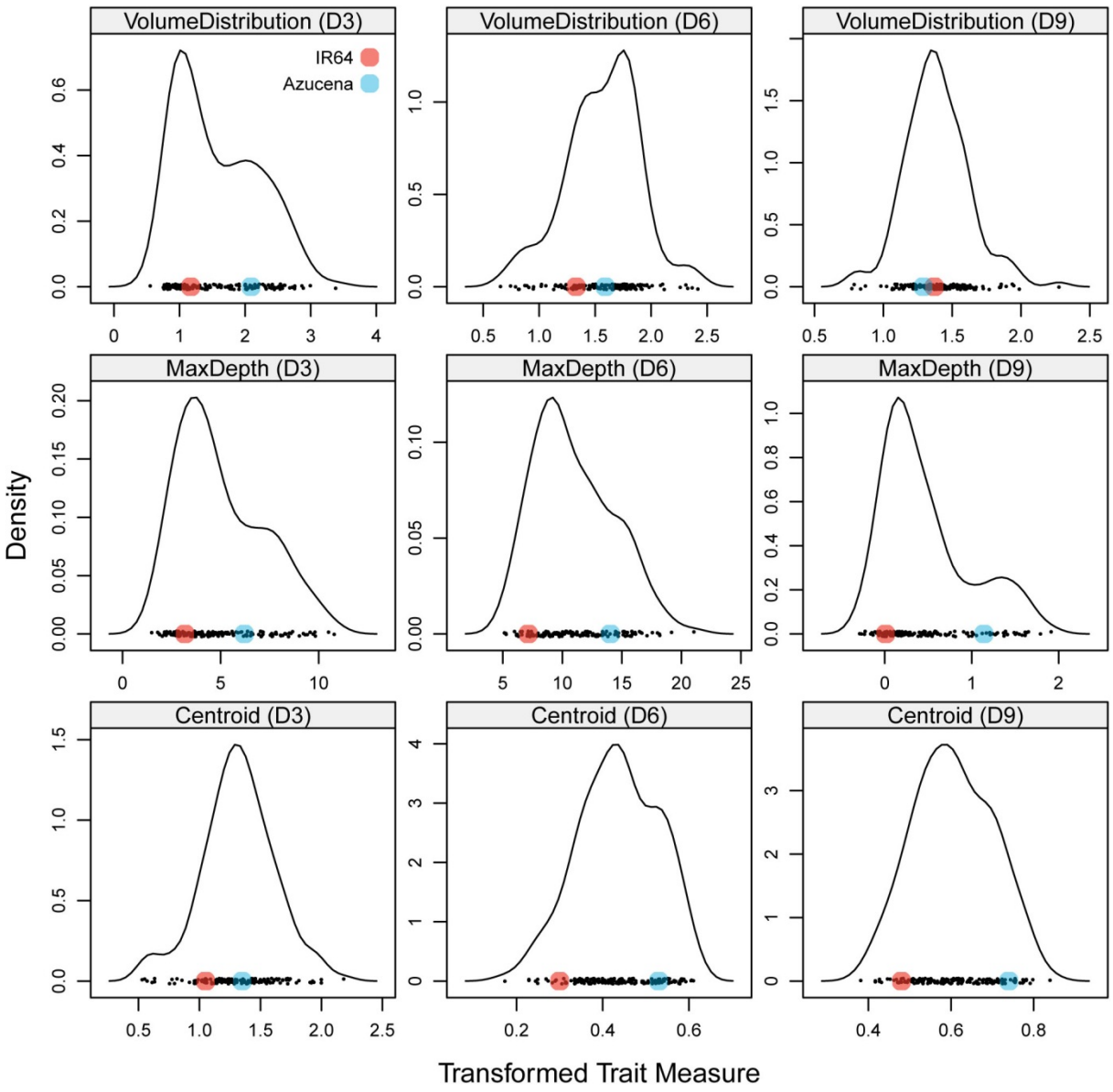

Figure 4.2: Density plots generated with the densityplot function in the R lattice package (Sarkar, 2008) for VolumeDistribution, MaxDepth, and Centroid traits measured on D3, D6 and D9 in the RIL mapping population. The mean trait values of the individual RILs are displayed on the x-axis with parental lines means highlighted with red (IR64) and blue (Azucena) circles.

Figure 4.3: Manhattan heatmap plots from genome wide association (GWA) analysis of the 13 core RSA traits measured on D3, D6, D9 and Davg. SNP significances are highlighted by color gradients from the minimum (yellow) to the maximum (blue) for each individual Manhattan plot. The genomic locations that were selected for further investigation are marked with triangles (red) along base of each Manhattan plot. Plots from analysis performed: A) across all subpopulation; B) within the *aus* (AUS) subpopulation; C) within the *indica* (IND) subpopulation; D) within the *temperate japonica* (TEJ) subpopulation; E) within the *tropical japonica* (TRJ) subpopulation.

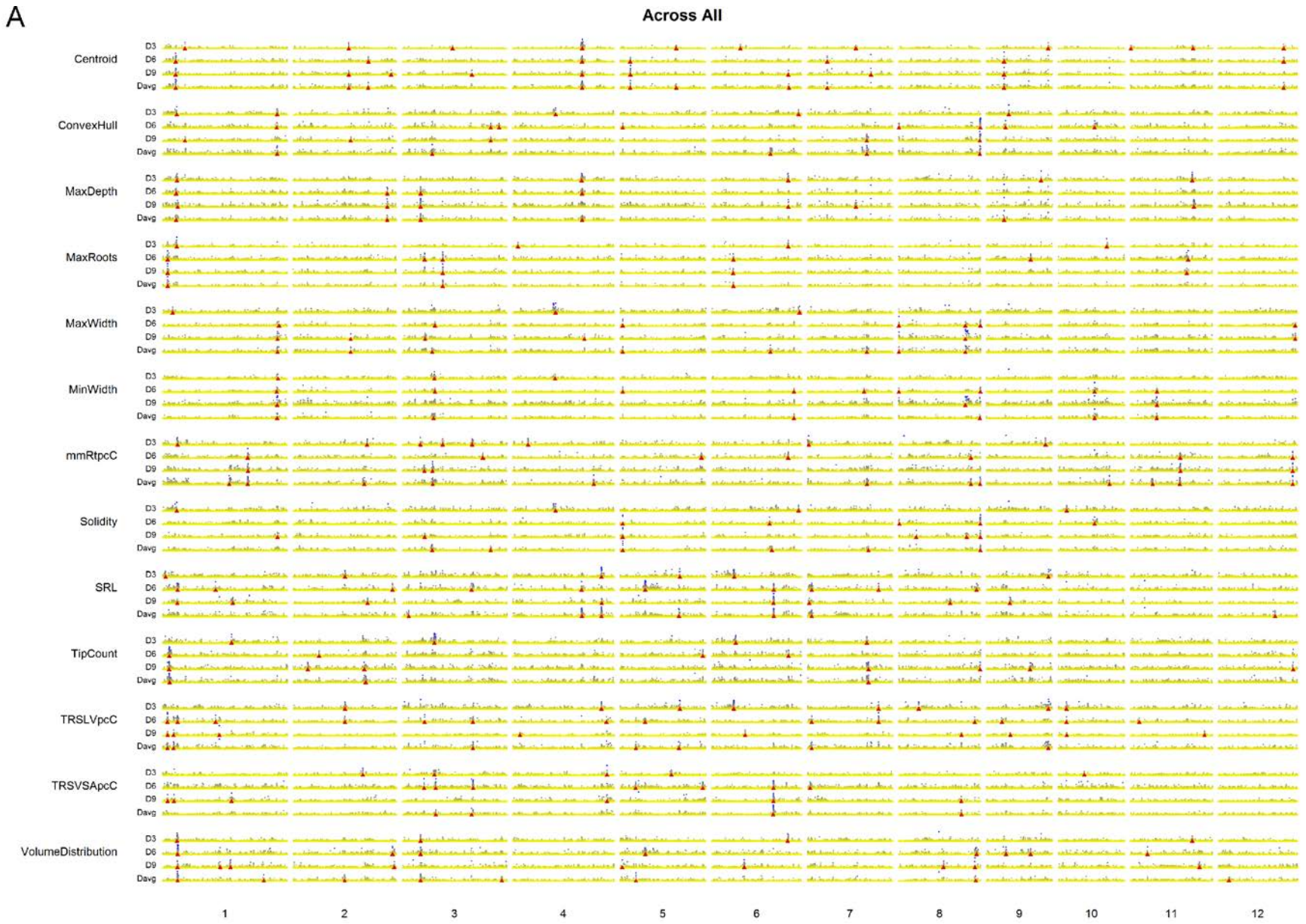
A
Across All
Centroid
ConvexHull
MaxDepth
MaxRoots
MaxWidth
MinWidth
mmRtpcC
Solidity
SRL
TipCount
TRSLVpcC
TRSVSApcC
VolumeDistribution
D3
D6
D9
Davg
1
2
3
4
5
6
7
8
9
10
11
12

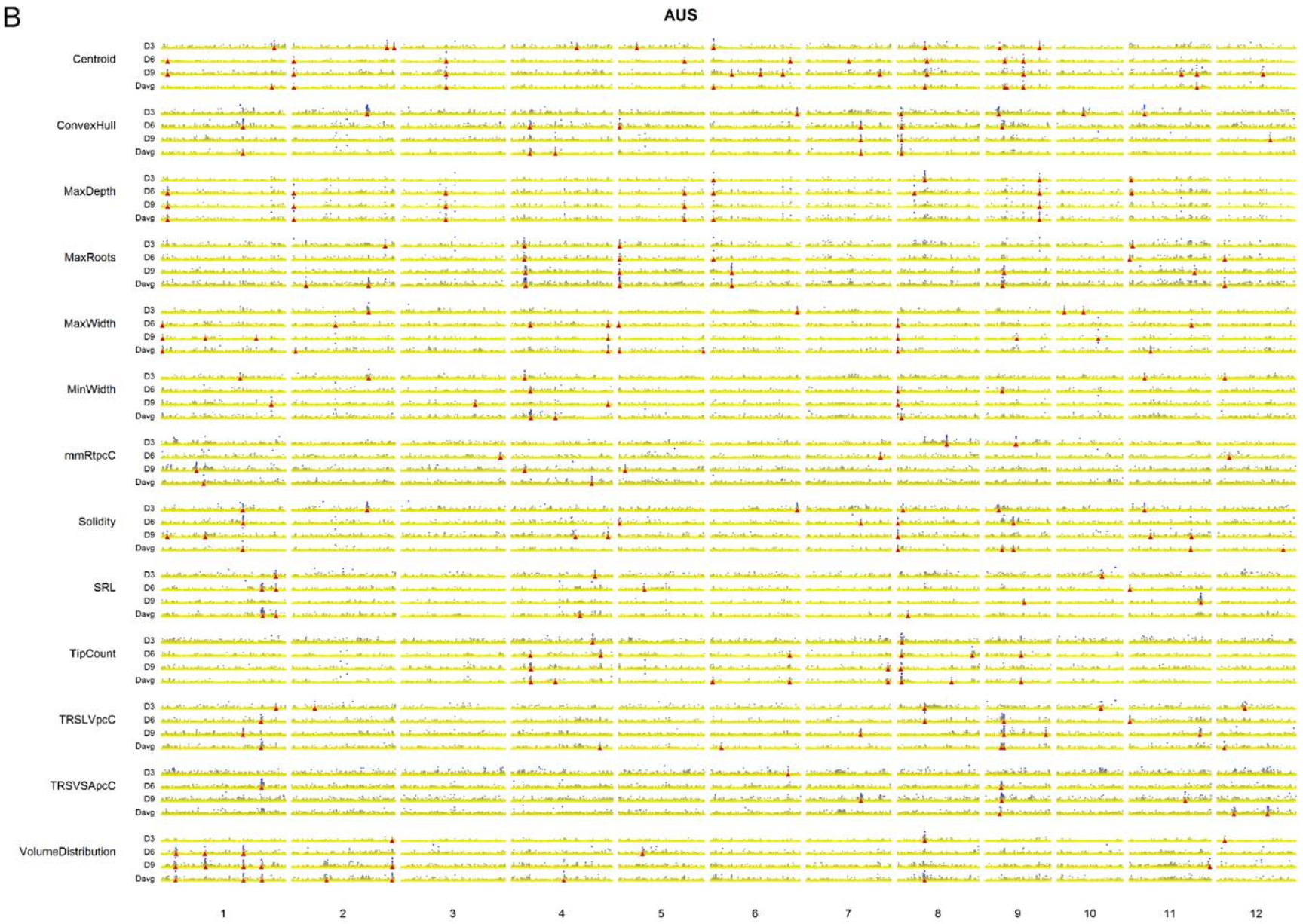
B
AUS
Centroid
ConvexHull
MaxDepth
MaxRoots
MaxWidth
MinWidth
mmRtpcC
Solidity
SRL
TipCount
TRSLVpcC
TRSVSApcC
VolumeDistribution
D3
D6
D9
Davg
1
2
3
4
5
6
7
8
9
10
11
12


C
IND
Centroid
ConvexHull
MaxDepth
MaxRoots
MaxWidth
MinWidth
mmRtpcC
Solidity
SRL
TipCount
TRSLVpcC
TRSVSApcC
VolumeDistribution
D3
D6
D9
Davg
1
2
3
4
5
6
7
8
9
10
11
12

D

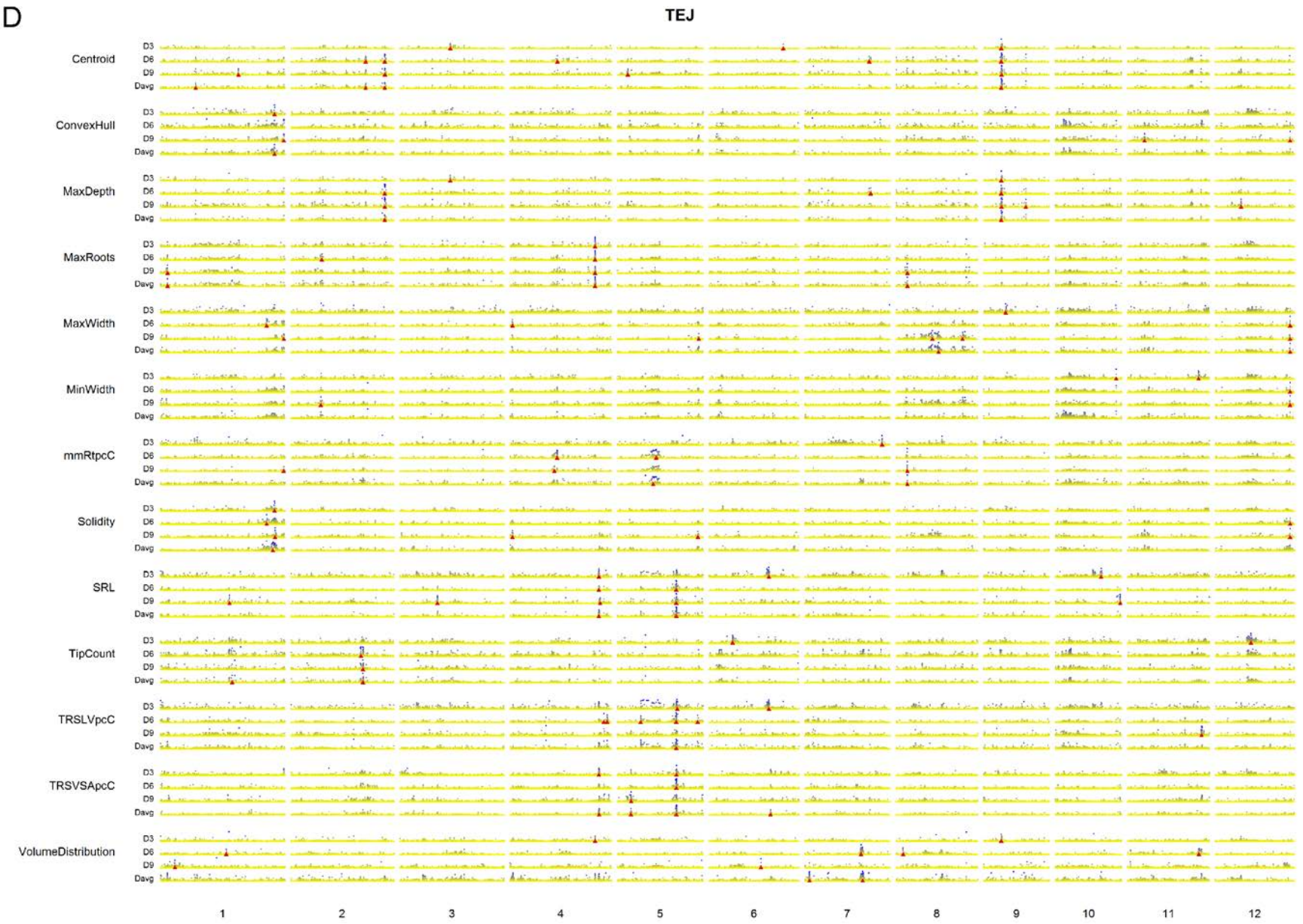
TEJ
Centroid
ConvexHull
MaxDepth
MaxRoots
MaxWidth
MinWidth
mmRtpcC
Solidity
SRL
TipCount
TRSLVpcC
TRSVSApcC
VolumeDistribution
D3
D6
D9
Davg
1
2
3
4
5
6
7
8
9
10
11
12

E

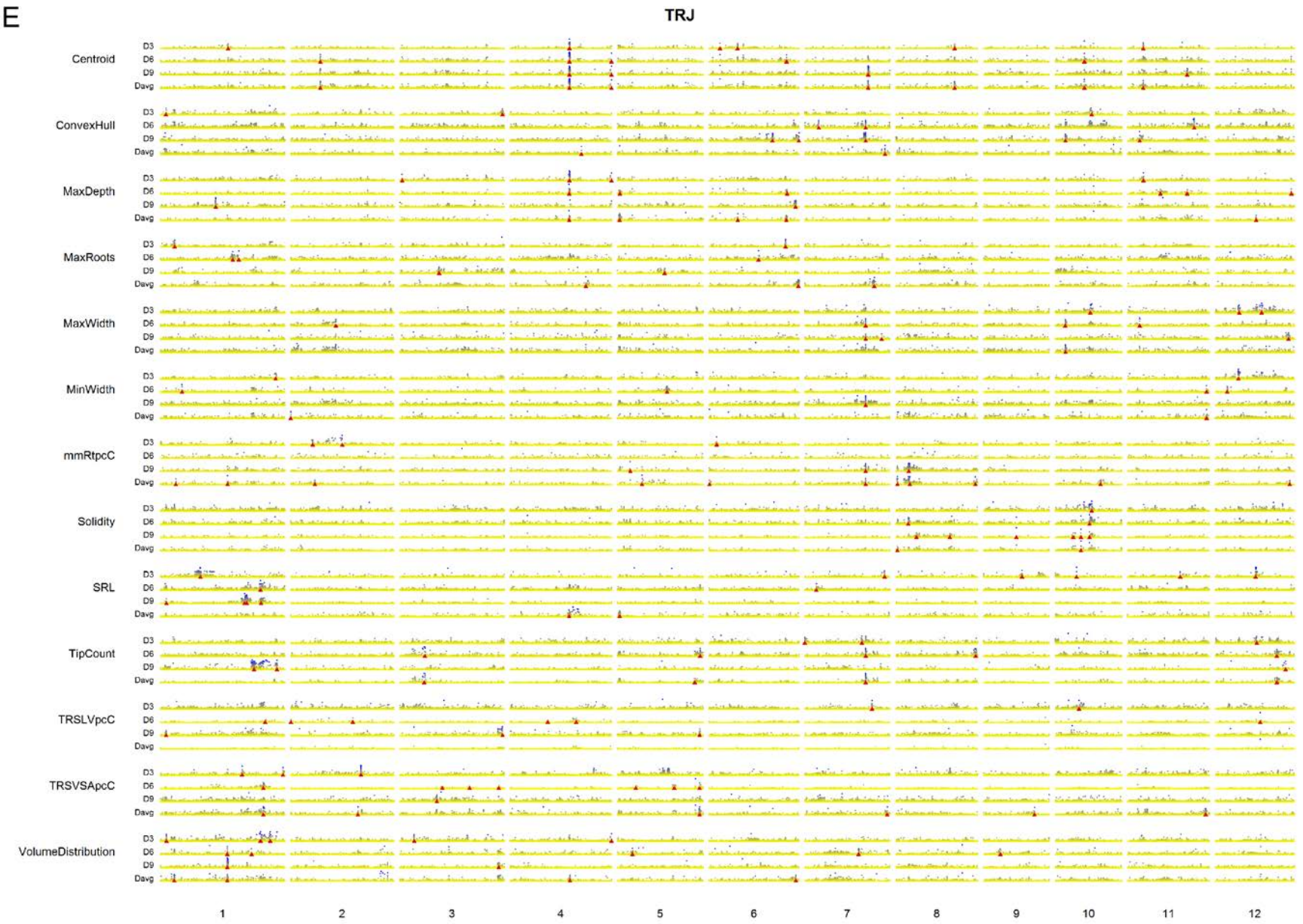
TRJ
Centroid
ConvexHull
MaxDepth
MaxRoots
MaxWidth
MinWidth
mmRtpcC
Solidity
SRL
TipCount
TRSLVpcC
TRSVSApcC
VolumeDistribution
D3
D6
D9
Davg
1
2
3
4
5
6
7
8
9
10
11
12

Table 4.5: QTL detected during composite interval mapping of RSA traits in the IR64 x Azucena RIL population.

Trait	QTL	Day	Chr	Position (Mb)	LOD1 L (Mb)	LOD1 R (Mb)	LOD	Additive Effect	R^2
Centroid	Centroid 6.2.1	D6	2	22.382	21.829	23.084	4.25	0.0254 (Azu)	0.073
	Centroid 6.2.2	D6	2	23.795	23.144	24.530	3.63	0.0244 (Azu)	0.065
	Centroid 9.2.1	D9	2	20.738	20.411	21.443	4.65	0.0278 (Azu)	0.081
	Centroid 9.2.2	D9	2	22.188	21.769	22.797	5.28	0.0288 (Azu)	0.088
	Centroid 9.2.3	D9	2	23.697	23.144	23.921	4.47	0.0272 (Azu)	0.078
	Centroid 3.6.1	D3	6	6.442	5.905	6.804	3.27	0.0799 (Azu)	0.066
	Centroid 3.6.2	D3	6	6.983	6.814	7.866	3.72	0.0888 (Azu)	0.078
	Centroid 6.6.1	D6	6	25.384	25.112	25.772	7.45	0.0354 (Azu)	0.142
	Centroid 6.6.2	D6	6	26.099	25.971	26.407	8.38	0.0374 (Azu)	0.161
	Centroid 6.6.3	D6	6	27.035	26.848	27.255	9.35	0.0394 (Azu)	0.174
	Centroid 6.6.4	D6	6	28.371	28.093	28.487	4.90	0.0305 (Azu)	0.103
	Centroid 9.6.1	D9	6	26.292	26.292	26.407	10.99	0.0439 (Azu)	0.210
	Centroid 9.6.2	D9	6	27.035	26.861	27.226	12.43	0.0461 (Azu)	0.231
	Centroid 9.6.3	D9	6	28.371	28.093	28.487	7.17	0.0376 (Azu)	0.150
	Centroid 6.7.1	D6	7	23.893	23.151	24.445	3.48	0.0228 (Azu)	0.059
	Centroid 9.7.1	D9	7	23.893	23.254	24.445	5.08	0.0279 (Azu)	0.084
ConvexHull	ConvexHull 6.1.1	D6	1	38.102	37.770	38.600	5.93	0.6046 (Azu)	0.104
	ConvexHull 9.1.1	D9	1	35.933	35.893	36.231	3.64	0.8690 (Azu)	0.070
	ConvexHull 9.1.2	D9	1	38.102	37.898	38.268	8.40	1.2238 (Azu)	0.151
	ConvexHull 9.3.1	D9	3	32.576	32.423	32.797	3.60	0.7547 (Azu)	0.060
	ConvexHull 3.6.1	D3	6	7.321	7.031	7.866	4.39	0.1729 (Azu)	0.101
	ConvexHull 6.6.1	D6	6	5.245	5.227	5.645	5.73	0.6045 (Azu)	0.110
	ConvexHull 6.6.2	D6	6	6.602	6.210	6.804	6.53	0.6561 (Azu)	0.125
	ConvexHull 6.6.3	D6	6	7.683	7.671	7.854	8.10	0.7450 (Azu)	0.156
	ConvexHull 6.6.4	D6	6	9.142	8.310	9.960	4.35	0.5723 (Azu)	0.092
	ConvexHull 9.6.1	D9	6	7.683	7.647	7.830	8.25	1.2461 (Azu)	0.157
	ConvexHull 9.6.2	D9	6	9.469	8.310	9.960	5.39	1.0567 (Azu)	0.113
	ConvexHull 6.9.1	D6	9	15.663	15.145	15.840	3.69	0.4680 (Azu)	0.064
MaxDepth	MaxDepth 6.2.1	D6	2	23.795	23.161	24.102	5.62	1.0454 (Azu)	0.093
	MaxDepth 6.2.2	D6	2	24.205	24.102	24.706	5.35	0.9950 (Azu)	0.085
	MaxDepth 9.2.1	D9	2	8.695	8.547	10.049	5.87	0.1640 (Azu)	0.100
	MaxDepth 9.4.1	D9	4	29.318	28.547	30.386	3.33	-0.1196 (IR64)	0.054
	MaxDepth 6.5.1	D6	5	19.544	19.100	19.926	3.81	0.8394 (Azu)	0.062
	MaxDepth 3.6.1	D3	6	29.789	29.563	30.474	6.17	0.7909 (Azu)	0.123
	MaxDepth 6.6.1	D6	6	26.407	26.341	26.564	13.11	1.6139 (Azu)	0.230
	MaxDepth 6.6.2	D6	6	26.861	26.634	27.255	12.61	1.6150 (Azu)	0.230
	MaxDepth 6.6.3	D6	6	28.371	28.093	28.487	7.85	1.3243 (Azu)	0.156
	MaxDepth 9.6.1	D9	6	26.407	26.325	26.493	10.92	0.2287 (Azu)	0.192
	MaxDepth 9.6.2	D9	6	27.102	26.634	27.565	9.36	0.2148 (Azu)	0.169
	MaxDepth 9.6.3	D9	6	28.477	28.093	28.584	6.56	0.1842 (Azu)	0.123
	MaxDepth 3.7.1	D3	7	21.677	20.948	22.001	4.30	0.6458 (Azu)	0.084

Table 4.5 (continued)

Trait	QTL	Day	Chr	Position (Mb)	LOD1 L (Mb)	LOD1 R (Mb)	LOD	Additive Effect	R^2
MaxDepth (continued)	MaxDepth 3.8.1	D3	8	21.785	21.515	22.047	3.27	0.5958 (Azu)	0.064
	MaxDepth 3.8.2	D3	8	23.916	23.869	24.368	6.83	-1.0510 (IR64)	0.135
	MaxDepth 3.8.3	D3	8	24.863	24.542	25.140	5.67	-0.8645 (IR64)	0.114
	MaxDepth 3.8.4	D3	8	25.460	25.358	25.799	6.00	-0.8336 (IR64)	0.120
	MaxDepth 3.8.5	D3	8	27.554	27.188	27.593	3.35	-0.6462 (IR64)	0.076
MaxRoots	MaxRoots 3.5.1	D3	5	0.596	0.201	0.962	5.28	0.0789 (Azu)	0.118
	MaxRoots 9.6.1	D9	6	29.789	28.981	30.212	5.63	-0.0700 (IR64)	0.122
MaxWidth	MaxWidth 6.1.1	D6	1	31.468	31.296	31.744	3.29	412.51 (Azu)	0.062
	MaxWidth 6.1.2	D6	1	33.965	33.801	34.024	6.14	552.92 (Azu)	0.112
	MaxWidth 6.1.3	D6	1	35.127	34.411	35.364	7.79	622.95 (Azu)	0.138
	MaxWidth 9.1.1	D9	1	32.608	32.297	32.865	3.75	0.0824 (Azu)	0.069
	MaxWidth 9.1.2	D9	1	34.591	34.189	35.512	3.77	0.0825 (Azu)	0.069
	MaxWidth 9.3.1	D9	3	32.217	31.541	32.397	3.65	0.0836 (Azu)	0.071
	MaxWidth 9.3.2	D9	3	32.576	32.397	32.797	4.29	0.0880 (Azu)	0.079
	MaxWidth 3.6.1	D3	6	9.142	8.310	9.714	5.24	0.3190 (Azu)	0.149
	MaxWidth 6.6.1	D6	6	12.997	11.629	13.247	4.45	522.76 (Azu)	0.076
	MaxWidth 6.6.2	D6	6	17.628	13.906	17.906	4.61	522.06 (Azu)	0.082
	MaxWidth 9.6.1	D9	6	6.030	5.739	6.442	6.12	0.1102 (Azu)	0.119
	MaxWidth 9.6.2	D9	6	7.166	6.959	7.928	7.05	0.1199 (Azu)	0.140
	MaxWidth 9.6.3	D9	6	9.306	8.310	9.960	5.27	0.1099 (Azu)	0.119
	MaxWidth 6.9.1	D6	9	13.968	13.820	14.485	8.73	0.0000	0.158
MinWidth	MinWidth 6.1.1	D6	1	34.189	33.837	34.364	3.67	0.2933 (Azu)	0.069
	MinWidth 6.1.2	D6	1	34.719	34.364	35.372	3.79	0.2975 (Azu)	0.071
	MinWidth 9.1.1	D9	1	32.608	32.283	33.223	3.84	0.3570 (Azu)	0.075
	MinWidth 9.1.2	D9	1	34.719	34.591	35.364	5.23	0.4094 (Azu)	0.101
	MinWidth 6.3.1	D6	3	32.576	32.303	32.941	3.65	0.2916 (Azu)	0.069
	MinWidth 9.3.1	D9	3	32.576	32.440	32.764	4.79	0.3886 (Azu)	0.092
	MinWidth 3.6.1	D3	6	7.744	6.862	8.165	3.84	0.1890 (Azu)	0.092
	MinWidth 6.6.1	D6	6	7.805	7.321	8.165	3.87	0.3236 (Azu)	0.079
	MinWidth 9.6.1	D9	6	7.744	7.050	8.186	4.41	0.3978 (Azu)	0.091
	MinWidth 9.6.2	D9	6	9.960	9.110	10.766	4.64	0.3905 (Azu)	0.087
	MinWidth 6.9.1	D6	9	14.907	13.852	14.994	4.68	0.3536 (Azu)	0.095
	MinWidth 6.9.2	D6	9	16.069	15.906	16.242	4.25	0.3204 (Azu)	0.082
	MinWidth 3.10.1	D3	10	10.074	5.711	11.376	3.32	-0.1896 (IR64)	0.074
mmRtpcC	mmRtpcC 9.6.1	D9	6	7.928	7.659	8.227	3.69	-0.1226 (IR64)	0.082
	mmRtpcC 3.10.1	D3	10	18.350	17.884	18.874	3.56	-0.1728 (IR64)	0.082
Solidity	Solidity 9.1.1	D9	1	37.535	37.249	37.770	4.30	-0.0567 (IR64)	0.084
	Solidity 9.1.2	D9	1	38.238	37.914	38.612	4.83	-0.0590 (IR64)	0.093
	Solidity 6.3.1	D6	3	31.534	30.508	31.805	3.30	-0.0467 (IR64)	0.053

Table 4.5 (continued)

Trait	QTL	Day	Chr	Position (Mb)	LOD1 L (Mb)	LOD1 R (Mb)	LOD	Additive Effect	R^2
Solidity (continued)	Solidity 6.3.2	D6	3	32.576	32.397	32.797	3.39	-0.0462 (IR64)	0.055
	Solidity 9.3.1	D9	3	30.902	30.521	31.805	5.12	-0.0617 (IR64)	0.099
	Solidity 9.3.2	D9	3	32.576	32.450	32.731	5.20	-0.0606 (IR64)	0.101
	Solidity 6.6.1	D6	6	5.432	5.385	5.645	4.44	-0.0601 (IR64)	0.093
	Solidity 6.6.2	D6	6	6.602	6.287	6.804	5.45	-0.0653 (IR64)	0.108
	Solidity 6.6.3	D6	6	7.683	6.996	7.866	6.49	-0.0725 (IR64)	0.128
	Solidity 6.6.1	D6	6	9.306	8.310	9.960	4.50	-0.0624 (IR64)	0.095
	Solidity 9.6.1	D9	6	7.321	6.898	7.866	5.45	-0.0639 (IR64)	0.106
	Solidity 9.6.2	D9	6	8.019	7.928	8.248	4.32	-0.0585 (IR64)	0.085
	Solidity 9.6.3	D9	6	8.979	8.310	9.960	3.72	-0.0557 (IR64)	0.078
	Solidity 6.9.1	D6	9	14.282	13.699	14.574	4.39	-0.0589 (IR64)	0.079
SRL	SRL 9.3.1	D9	3	21.149	17.141	22.643	3.41	-5.2213 (IR64)	0.082
	SRL 9.4.1	D9	4	26.935	25.197	27.794	3.75	-5.0823 (IR64)	0.090
	SRL 6.7.1	D6	7	27.715	27.677	27.994	4.16	-6.5745 (IR64)	0.096
	SRL 6.7.2	D6	7	28.408	28.277	28.846	6.20	-7.2882 (IR64)	0.135
	SRL 3.12.1	D3	12	4.426	3.852	4.667	3.93	-8.7750 (IR64)	0.084
TipCount	TipCount 3.6.1	D3	6	7.805	7.031	8.206	4.85	0.7728 (Azu)	0.119
	TipCount 6.6.1	D6	6	4.998	4.977	5.459	4.36	1.1250 (Azu)	0.095
	TipCount 3.10.1	D3	10	4.350	4.017	5.601	3.61	-0.6560 (IR64)	0.080
	TipCount 6.10.1	D6	10	2.931	2.703	3.935	4.99	-1.2382 (IR64)	0.103
	TipCount 9.10.1	D9	10	2.703	2.098	3.894	3.33	-1.6554 (IR64)	0.070
TRSLVpcC	TRSLVpcC 3.12.1	D3	12	4.483	4.225	4.654	4.14	-0.0738 (IR64)	0.088
TRSVSApcC	TRSVSApcC 9.1.1	D9	1	4.576	4.050	4.909	3.47	0.0459 (Azu)	0.096
	TRSVSApcC 3.3.1	D3	3	26.455	25.955	26.780	3.91	0.0474 (Azu)	0.085
	TRSVSApcC 3.4.1	D3	4	17.364	16.891	18.709	4.63	-0.0545 (IR64)	0.102
	TRSVSApcC 9.5.1	D9	5	1.257	1.129	1.481	3.12	-0.0410 (IR64)	0.076
	TRSVSApcC 6.7.1	D6	7	28.647	28.346	29.012	4.46	-0.0525 (IR64)	0.091
	TRSVSApcC 3.8.1	D3	8	0.425	0.000	0.865	3.56	-0.0434 (IR64)	0.077
	TRSVSApcC 6.8.1	D6	8	0.000	0.000	0.150	5.80	-0.0833 (IR64)	0.133
	TRSVSApcC 6.8.2	D6	8	0.633	0.282	0.767	3.35	-0.0506 (IR64)	0.079
	TRSVSApcC 6.8.3	D6	8	2.172	2.124	2.280	3.64	0.0635 (Azu)	0.078
	TRSVSApcC 6.11.1	D6	11	24.649	24.363	24.931	4.39	-0.0544 (IR64)	0.091
	TRSVSApcC 6.11.2	D6	11	25.314	25.044	26.342	3.65	-0.0509 (IR64)	0.076
VolumeDistribution	VolumeDistribution 9.5.1	D9	5	0.352	0.000	0.962	3.37	-0.0635 (IR64)	0.072
	VolumeDistribution 3.6.1	D3	6	29.789	29.578	30.272	6.08	0.2310 (Azu)	0.126
	VolumeDistribution 6.6.1	D6	6	25.112	24.974	25.772	3.58	0.0956 (Azu)	0.082
	VolumeDistribution 6.6.2	D6	6	26.407	26.242	27.115	6.62	0.1270 (Azu)	0.146
	VolumeDistribution 9.6.1	D9	6	7.805	7.640	8.059	5.64	0.0906 (Azu)	0.139
	VolumeDistribution 3.8.1	D3	8	23.916	23.869	24.534	3.49	-0.1856 (IR64)	0.072
	VolumeDistribution 3.8.2	D3	8	25.460	25.321	25.691	4.70	-0.2086 (IR64)	0.096
	VolumeDistribution 3.8.3	D3	8	25.907	25.691	26.141	4.35	-0.2005 (IR64)	0.089

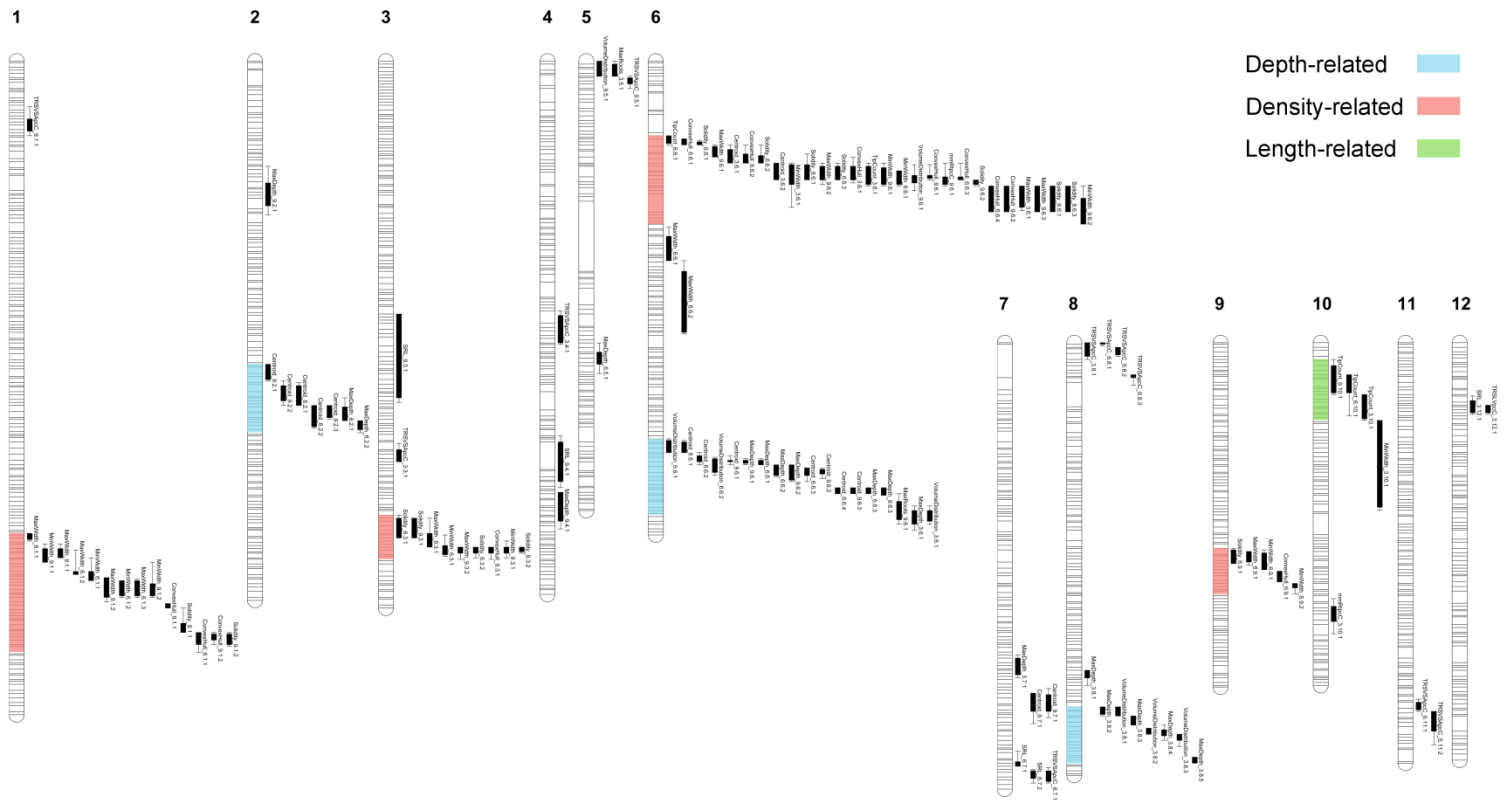

Figure 4.4: Depiction of chromosomal positions of detected QTL from mapping of RSA traits in the IR64 x Azucena RIL population. The solid regions and whiskers of the QTL boxes represent the LOD1 and LOD2 confidence regions of the QTL, respectively. Hotspot regions related to root system depth, density and total length are highlighted in color on the chromosomes (blue, red, and green, respectively). The horizontal bars along the inside of the chromosomes depict the physical positions of the 1559 SNP markers used during composite interval mapping.

DISCUSSION

How do we identify functional RSA traits?

Using 3D phenotyping tools and whole genome approaches to investigate root system architecture provides many opportunities to discover genetic factors involved in root traits. However, it also presents many challenges due to the complex nature of root systems and their development. Even when studying root systems at the early seedling stage in a highly controlled, artificial growth environment, GWA and QTL mapping studies with the detailed phenotypes obtained in this study generate an overwhelming amount of information. For instance, during the mapping of the 13 core traits across all days (D3, D6, D9 and Davg) in the *indica* subpopulation alone, approximately 93 genomic regions with strong SNP support (where LD was assumed to be 500kb) were designated during first pass selections of SNPs for further investigation. Several of these regions overlap between analyses with other subpopulations; however, many are also unique to the *indica* subpopulation and/or specific to a single trait.

One strategy to help refine this genomic search space and narrow down the dataset is to select a few traits that can be further contextualized from a functional perspective based on phenotypic observations. As mentioned before, one important area of abiotic stress research is plant adaption to limited nutrient and water resources. Although plant adaptation involves the coordination of responses across the whole plant, root systems are the main site of nutrient and water uptake in plants, so understanding the genetic components of their development may help researchers develop improved varieties with enhanced abilities to survive and thrive in suboptimal environments.

As climates shift and freshwater resources become more scarce and strained, drought tolerance and water conservation will continue to be an important area of abiotic stress research (Li et al., 2009; Gornall et al., 2010). Much of modern rice production is still optimized for irrigated paddy systems, but some upland rice breeding programs have also been focusing for decades on developing cultivars with improved growth and production under dryer and less predictable rainfed environments, where most of the high performance, deep rooting breeding cultivars have been identified from the *Japonica* subspecies (Gowda et al., 2011). Recent QTL studies in a population derived from a cross between a deeper-rooting upland *tropical japonica* cultivar (cv: Kinandang Putong) and a shallow rooted, irrigated paddy *indica* cultivar (cv: IR64) have identified a deep rooting gene, Dro1, for which the Kinandang Putong allele improves the rooting depth in the IR64 background (Uga et al., 2011). The selection of *indica* cultivars in breeding programs to improve yield under aerobic or alternate wetting and drying (AWD) cultivation has been limited possibly because *indica* cultivars are not typically evaluated for beneficial deep rooting qualities; however, some mapping studies have found that *indica* parents can contribute alleles with greater penetration ability in dry or compacted soils (Ray et al., 1996; Cairns et al., 2011).

When performing GWA analysis in the rice diversity panel, several hotspot regions related to root system depth were detected. One example of a depth-related hotspot was detected during GWA analysis on the entire set of accessions on chromosome 4 with the peak SNP located at 24.084 Mb (MSU6; SNP ID: c4p24084119). It is interesting to note that this association was not detected when GWA analysis was conducted only with the accessions within the IND subpopulation.

However, when the reconstructed root images for the IND accessions were analyzed in more detail, a strikingly significant difference in root depth traits was found between SNPs alleles at this region of chromosome 4 for the IND accessions (Figure 4.5). The absence of any detected associations around this location during GWA studies in the IND population is a bit disconcerting; however, this non-association could have arisen due to the control for kinship structure and relatedness in the mixed model GWA approach.

Since this control might have been a possible cause, introgression analysis was performed to investigate whether there might be unique introgressions in some accessions at this genomic location that resulted in the kinship structure that was corrected for during GWA analysis within the *indica* subpopulation. Using a preliminary introgression map constructed with the 700k SNP dataset (Figure 4.6), testing showed that there was a likely introgression from the *Japonica* subspecies (TEJ and TRJ subpopulations) between 23.792 and 24.162 Mb that resulted in shallower root systems with smaller Centroid (Figure 4.7), MaxDepth and VolumeDistribution trait values within an *indica* background. Although further analysis in this region needs to be performed, given the assumption that a deeper root system helps a plant to better tolerate drought conditions, and that root trait alleles conferring greater drought tolerance mainly come from *Japonica* germplasm, these findings highlight the fact that beneficial trait alleles can also be found in unlikely germplasm backgrounds (McCouch, 2012).

Exploring multi-trait approaches

To complement efforts to directly follow-up on traits and mapping results from a functional perspective, further multi-trait approaches were also performed to help

reduce and prioritize the number of genomic regions for candidate genes and their possible involvement in plant adaptation to abiotic stress. Multi-trait approaches were explored with both the MCMC resampled core trait measures (pre-mapping) and with the significance results generated during mapping analysis (post-mapping). The first approach was applied to the post-mapping results and will be referred to as weighted multi-trait averaging (WMTA) analysis. During the WMTA analysis either the single trait GWA p-values or QTL LOD scores were consolidated by multiplying the single trait p-value (and LOD score) results by the positive compliment of the trait correlation matrix in order to generate a weighted p-value (or LOD score) average that accounts for pairwise correlation between traits. This adjustment for correlation helped to reduce the core trait analysis results from a given time point and within a given subpopulation from the GWA studies down to single sets of multi-trait p-values or LOD scores (Figure 4.8). From these reduced results, regions that are highly involved in overall global RSA features and that possibly influence whole root system development could be identified and selected for further follow-up. In many cases, hotspot regions where multiple SNPs or QTL were detected from single trait analyses appeared to localize to the same regions of high significance during multi-trait analysis; however, there are also a high number of cases where hotspot regions for single traits showed only modest multi-trait significances and vice versa. These results highlight that similarity between trait measures can result in correlation that can confound insights into the ultimate global influence of hotspot regions from single trait analyses and that these correlations should be considered when drawing conclusions about those region.

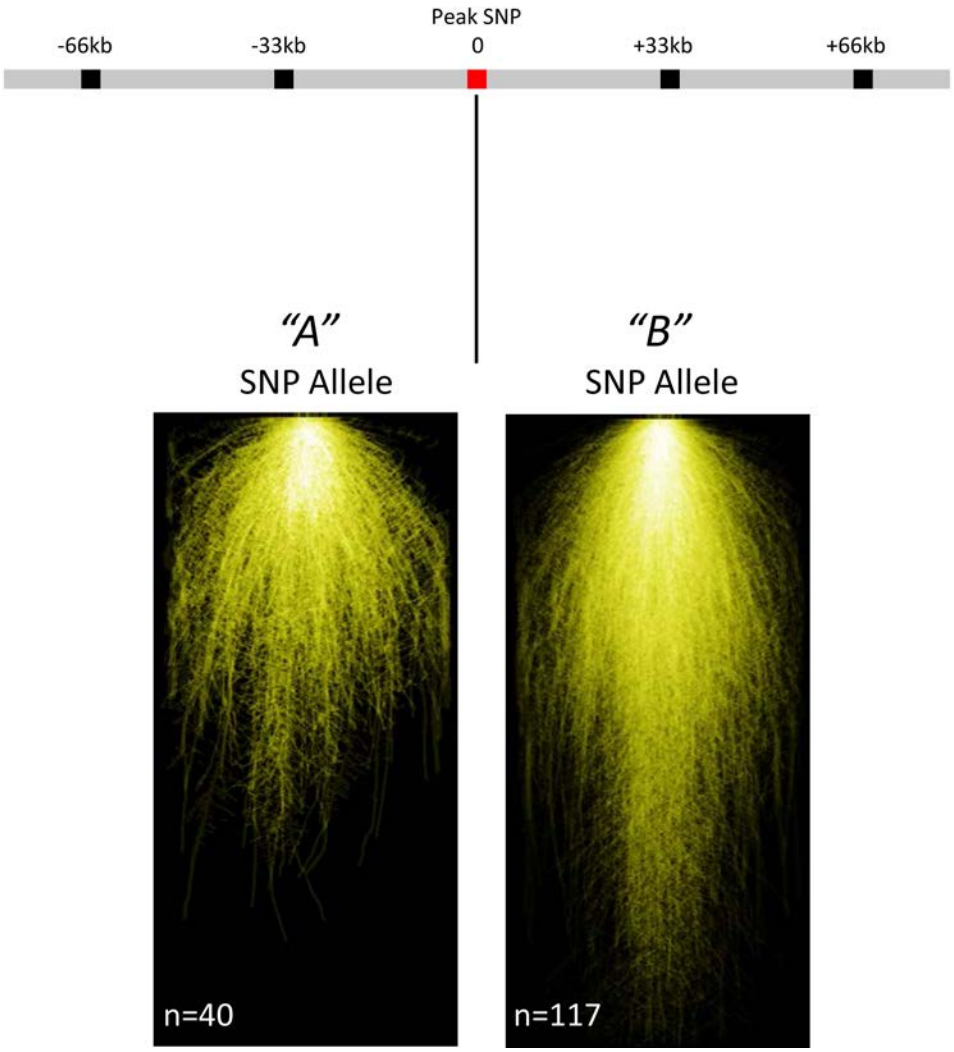

Figure 4.5: Composite images generated from day 9 reconstructions for *indica* accessions based on the peak SNP alleles at the depth related hotspot detected on chromosome 4 (SNP ID: c4p24084119). The composite images were generated by overlaying the root system reconstructions of accessions the same versions of the SNP allele and then combining them into a single image where higher intensity (brighter) regions represent areas of higher overlap.

Figure 4.6: Introgression map of the 316 rice diversity panel accessions that were previously designated as either *aromatic*, *aus*, *indica*, *temperate japonica* or *tropical japonica* accessions (Zhao et al., 2011). The accessions have been grouped into respective subpopulations and displayed in order of the relative prevalence of inter-subpopulation introgressions, such that accessions with a greater percentage of introgressed regions are displayed at the top of each grouping. The subpopulations have been color coded as *aromatic* (purple), *aus* (yellow), *indica* (red), *temperate japonica* (dark blue) and *tropical japonica* (light blue).

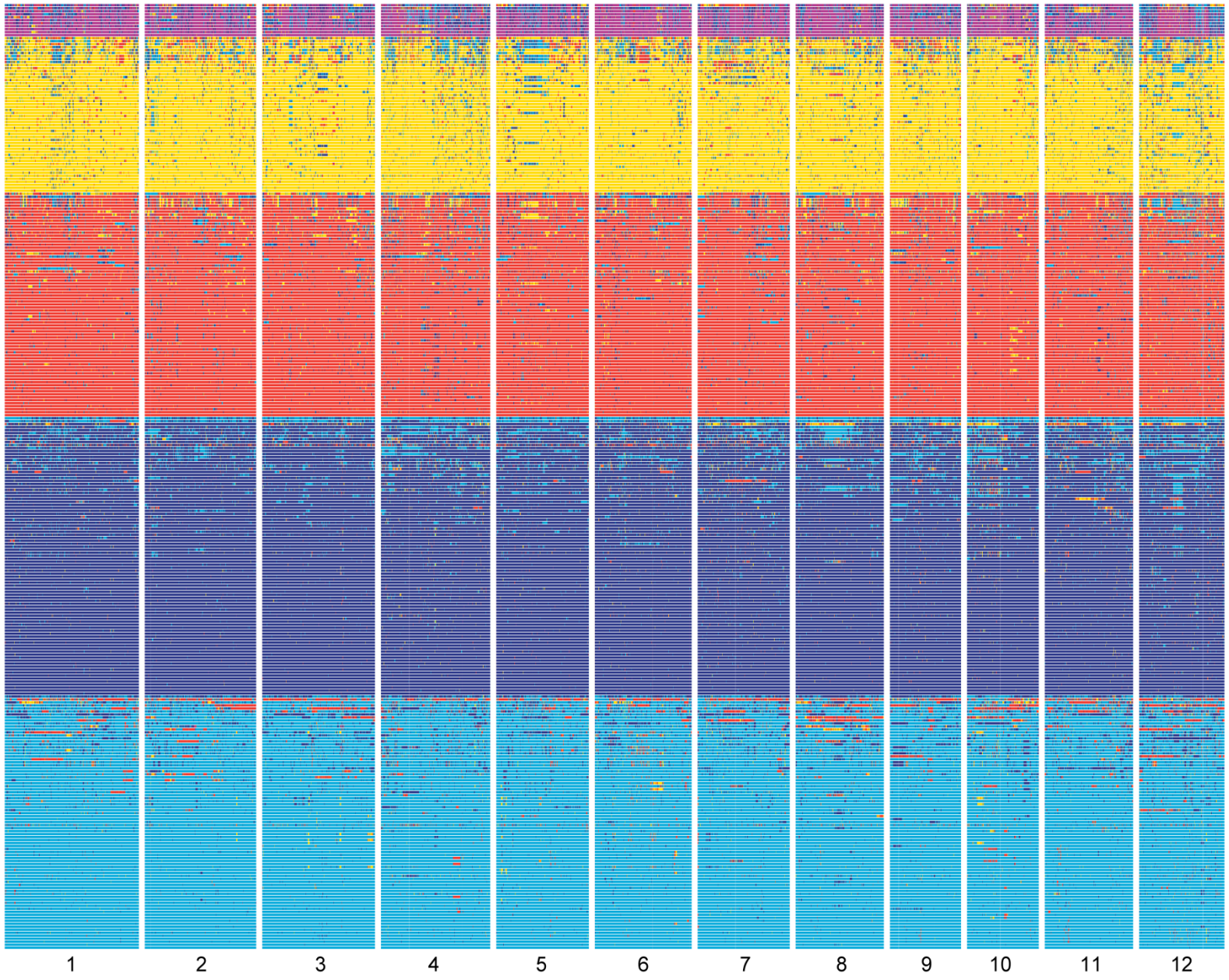
1
2
3
4
5
6
7
8
9
10
11
12

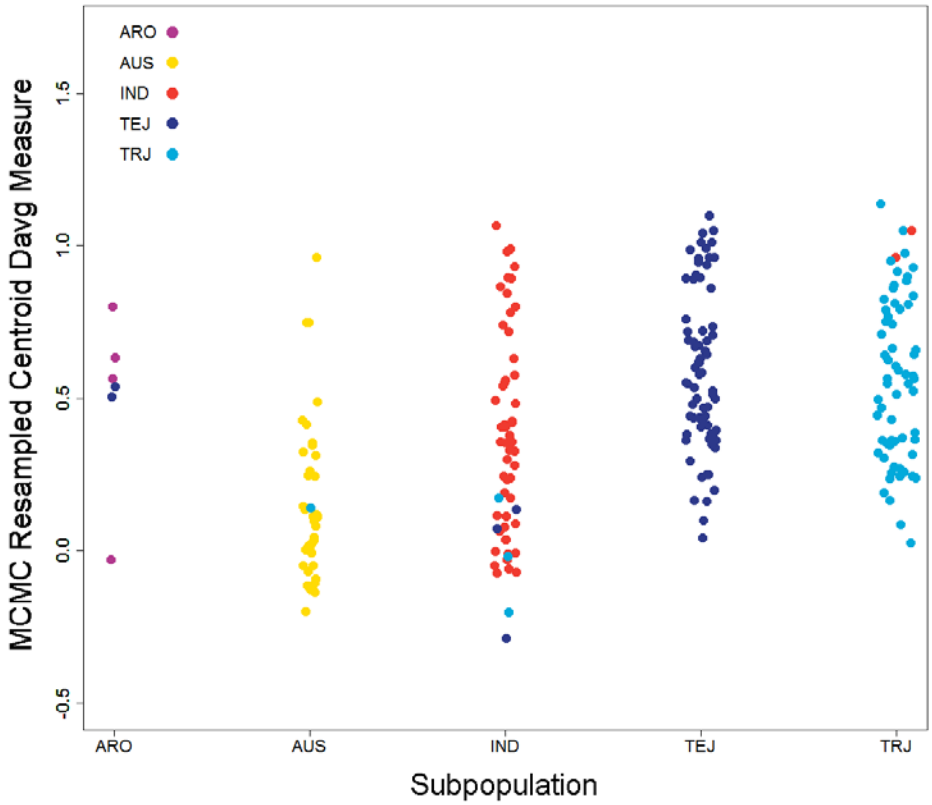

Figure 4.7: Plot depicting introgression analysis results for the Davg centroid trait measure at the peak rooting depth SNP on chromosome 4 (SNP ID: c4p24048146). The data points represent individual accessions that have been grouped along the x-axis respective to their subpopulation designation as previously characterized by Zhao et al, 2011. The color-code of the data points displays the predicted subpopulation introgression at the peak SNP when using a Hidden Markov model (HMM) to evaluate the region. The rice subpopulations are denoted as ARO (*aromatic*), AUS (*aus*), IND (*indica*), TEJ (*temperate japonica*) and TRJ (*tropical japonica*).

Figure 4.8: Manhattan and heatmap plots generate from the weight multi-trait averaging (WMTA) of the genome wide association (GWA) analysis and then subsequent composite interval mapping of the 13 RSA traits. Manhattan plot summaries for GWA studies are shown for D3, D6, D9 and Davg across all subpopulations and within the aus (AUS), indica (IND), temperate japonica (TEJ) and tropical japonica (TRJ) rice subpopulations. Heatmap plot summaries for bi-parental QTL studies are shown for D3, D6, and D9. Each plot displays the average core RSA significance p-values or LOD scores that have been adjusted based on the amount of pairwise correlation between core traits. The yellow to blue color gradient on the plots represents the adjusted significance values from the minimum (yellow) to the maximum (blue) for each respective dataset. Selected SNP summary bands appear below each set of Manhattan plots and represent overlays of the SNPs (red triangles) that were selected from the individual core trait analyses within their respective subpopulation (see Figure 4.4) where selected regions with higher overlap appear darker.

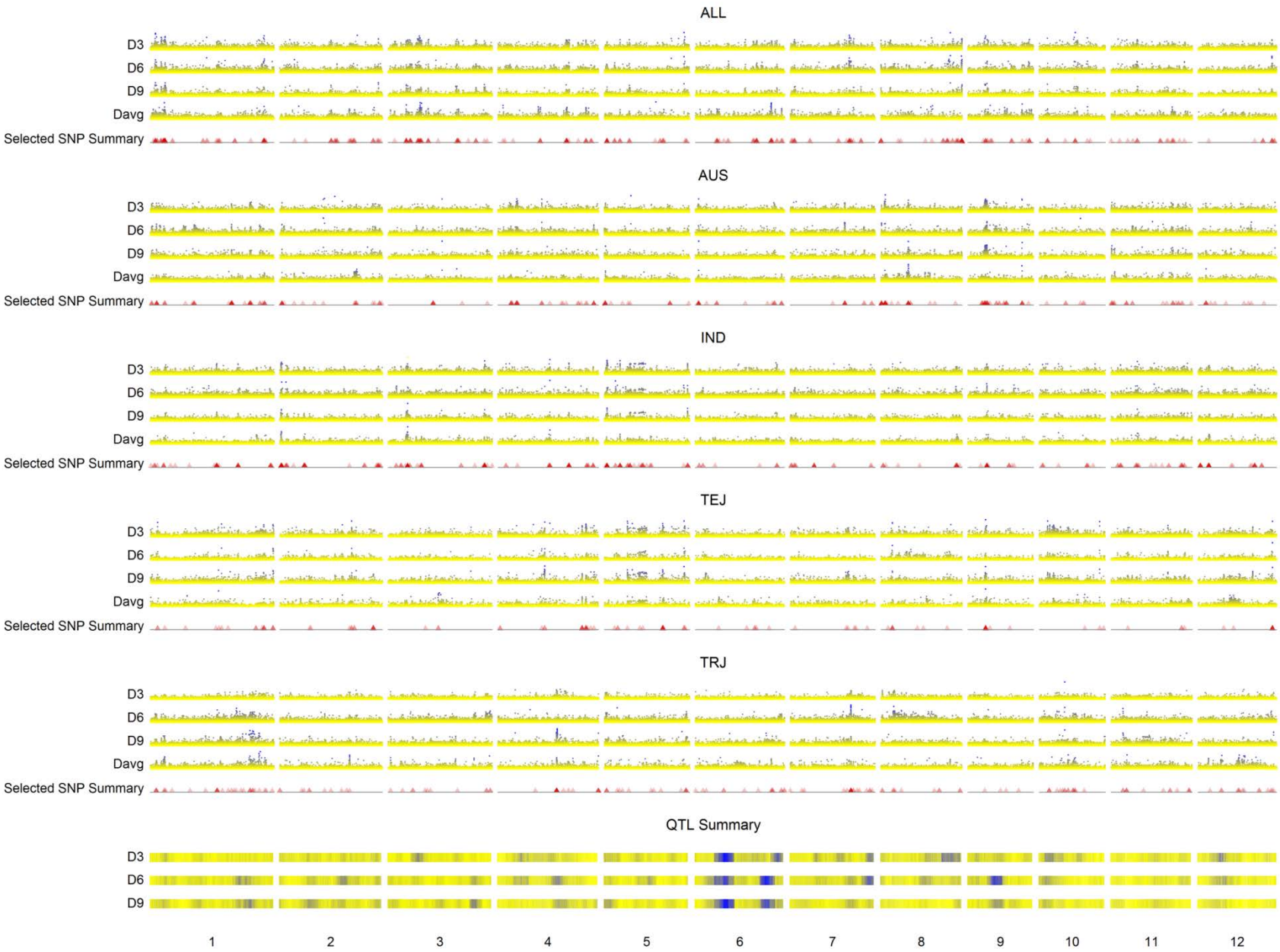
ALL
D3
D6
D9
Davg
Selected SNP Summary
AUS
D3
D6
D9
Davg
Selected SNP Summary
IND
D3
D6
D9
Davg
Selected SNP Summary
TEJ
D3
D6
D9
Davg
Selected SNP Summary
TRJ
D3
D6
D9
Davg
Selected SNP Summary
QTL Summary
D3
D6
D9
1
2
3
4
5
6
7
8
9
10
11
12

The second multi-trait approach that was investigated was a phenotypic processing and composite mapping approach that involves the clustering of accessions into discrete groups based on multiple traits and is hereby referred to as composite trait (CT) analysis. This CT approach also aims to detect genomic regions that are highly involved in overall RSA features. During CT analysis, once the accessions have been clustered into N distinct cluster groups (Rocha et al., 2009), a binomial association analysis can be performed for each SNP marker in the genotypic dataset. SNP significance p-values are determined separately for each cluster group using a binomial test where the observed allele frequency within each group is compared to the probability density function (pdf) created based on the number of accessions present in the group and the global marker allele frequency for the SNP under a binomial assumption.

Since the binomial testing is quite efficient, it is possible to perform a high number (>10,000) of permutation tests in order to control for multiple testing and determine a suitable p-value significance threshold. This scale of permutation testing is not currently possible across all SNPs with more sophisticated linear model analysis methods due to high computational demands; however, since population structure and relatedness are not accounted for during the binomial test in CT analysis, it is likely that a high number of false positive, structure-based associations will be detected. To control for population structure, the CT analysis was performed independently within each of the four subpopulations (AUS, IND, TEJ and TRJ); however, the approach should be extended in the future to account for some degree of relatedness between accessions within the subpopulations. Since the clustering method and binomial GWA

testing is still under validation, the ultimate utility of the CT approach has not been determined. Consequently, CT analysis should only be used alongside other multi-trait approaches to provide further supportive evidence for the results obtained by conventional GWA analysis using the core RSA traits.

To begin evaluating the CT approach, clustering was performed on three multi-trait selections. These clustering selections were chosen based on the possible functional implication of the traits and also as a comparison to both single trait GWA studies and the post-mapping multi-trait averaging approach. The first clustering selection combines information on root system investment with volume exploration and was composed of TipCount and ConvexHull, the second clustering combines the vertical placement of the entire root system within the growth volume with its maximum horizontal and vertical exploration and was composed of Centroid, MaxDepth and MaxWidth and the third was composed of all 13 core traits. The clustering and following binomial GWA testing was performed on data across all days (AllDays), for each day (D3, D6, D9 and Davg) and within each of the highly represented subpopulations (AUS, IND, TEJ and TRJ) separately (Figure 4.9). During the respective analyses, the number of groups in each clustering was constrained between 2 and 6 groups corresponding to maximum scale parameters of 0.08 to 0.15 during the clustering approach. Once the cluster groups were formed, binomial GWA analysis was performed. The resulting p-values for each of the three multi-trait selections were plotted using heatmap Manhattan plots in Figure 4.9. From these plots, it is apparent that some significant CT analysis regions appear to co-localize with hotspots from the initial single trait GWA studies. These regions are potential candidate regions for further investigation.

Figure 4.9: Manhattan and heatmap plots from binomial GWA testing during composite trait (CT) analysis for D3, D6, D9 and Davg across all subpopulations and within the *aus* (AUS), *indica* (IND), *temperate japonica* (TEJ) and *tropical japonica* (TRJ) rice subpopulations. The yellow to blue color gradient on the plots represents the adjusted significance values from the minimum (yellow) to the maximum (blue) for each respective dataset. Selected SNP summary bands appear below each set of Manhattan plots and represent overlays of the SNPs that were selected from the individual core trait analyses within their respective subpopulation (see Figure 4.4) where higher regions overlap appear with darker triangles (red). A) Composite trait (CT) plots from analysis with the ConvexHull and TipCount traits; B) CT plots from analysis with the Centroid, MaxDepth and MaxWidth traits; C) CT plots from analysis with all 13 core traits.

A

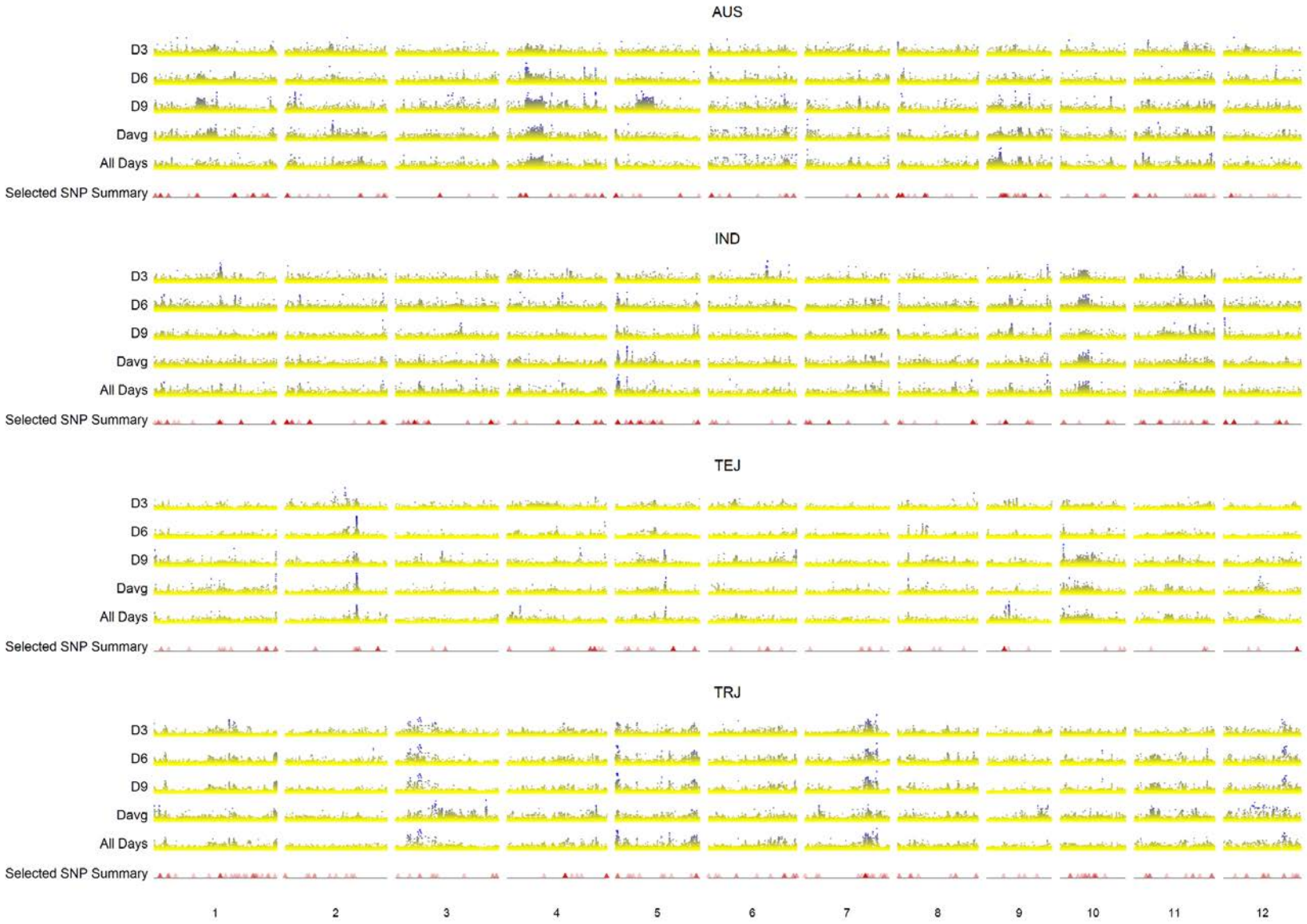
AUS
D3
D6
D9
Davg
All Days
Selected SNP Summary
IND
D3
D6
D9
Davg
All Days
Selected SNP Summary
TEJ
D3
D6
D9
Davg
All Days
Selected SNP Summary
TRJ
D3
D6
D9
Davg
All Days
Selected SNP Summary
1
2
3
4
5
6
7
8
9
10
11
12

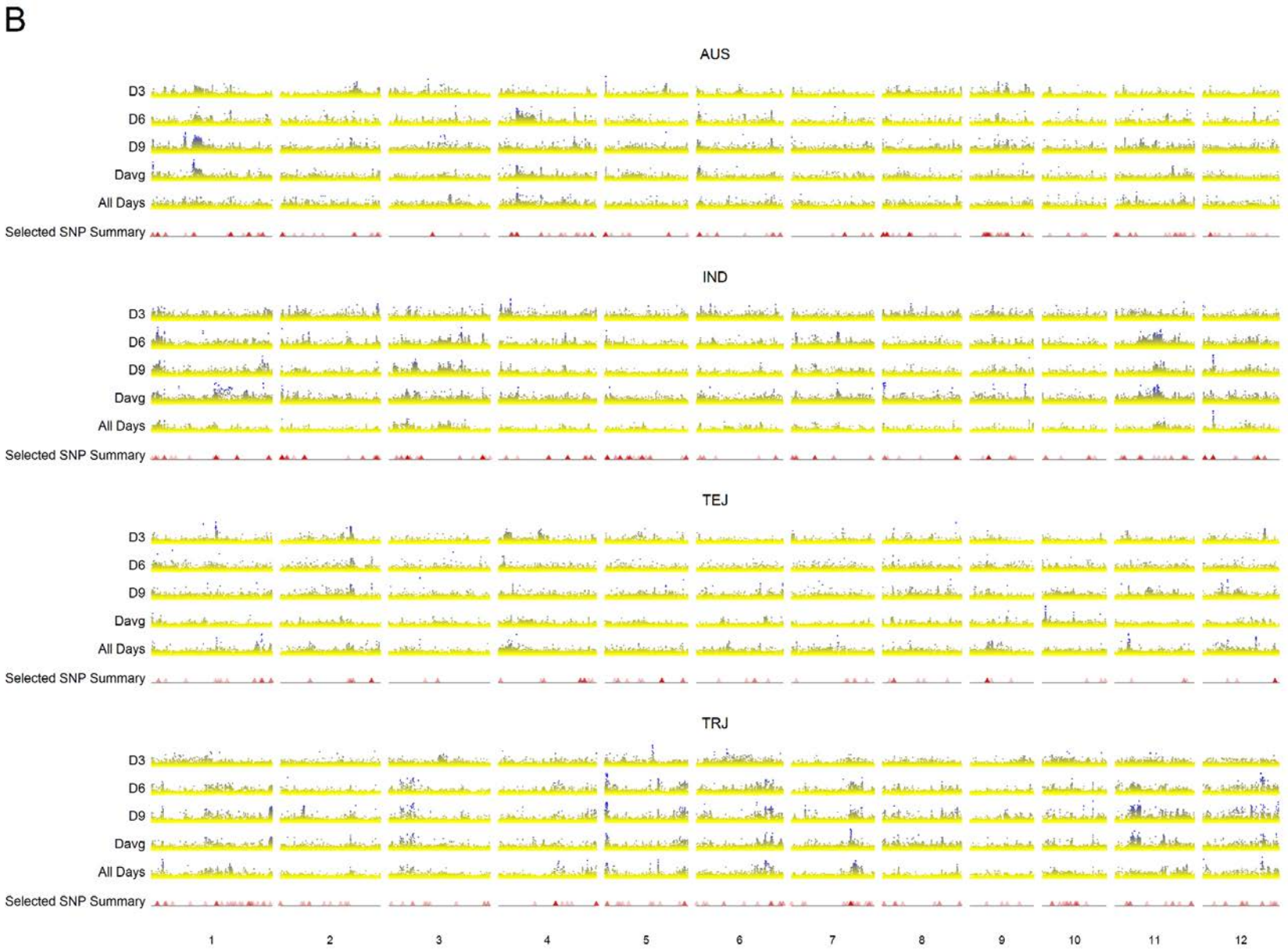
B
AUS
D3
D6
D9
Davg
All Days
Selected SNP Summary
IND
D3
D6
D9
Davg
All Days
Selected SNP Summary
TEJ
D3
D6
D9
Davg
All Days
Selected SNP Summary
TRJ
D3
D6
D9
Davg
All Days
Selected SNP Summary
1
2
3
4
5
6
7
8
9
10
11
12

C

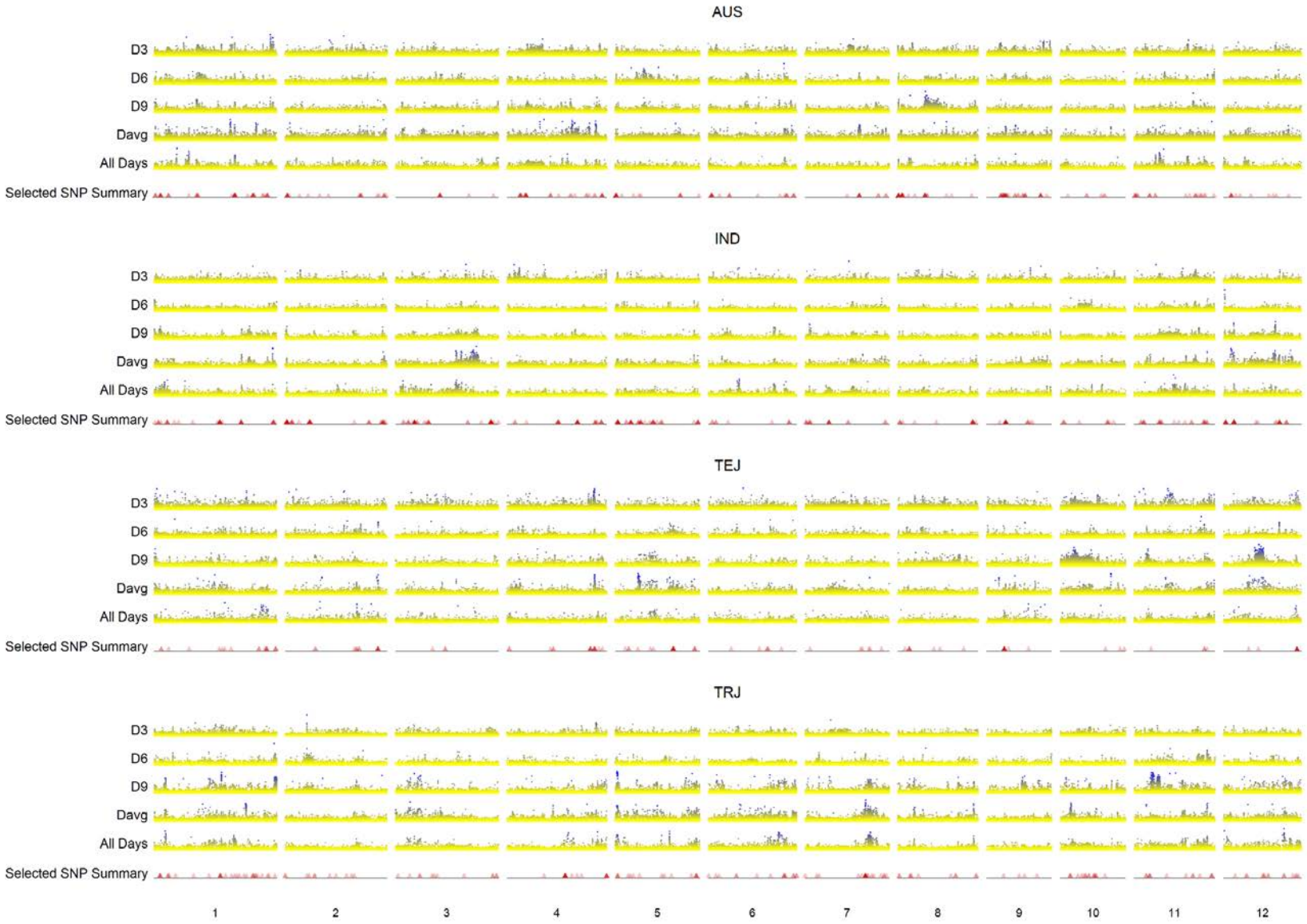
AUS
D3
D6
D9
Davg
All Days
Selected SNP Summary
IND
D3
D6
D9
Davg
All Days
Selected SNP Summary
TEJ
D3
D6
D9
Davg
All Days
Selected SNP Summary
TRJ
D3
D6
D9
Davg
All Days
Selected SNP Summary
1
2
3
4
5
6
7
8
9
10
11
12

Identifying significant genomic regions

Multi-trait approaches were explored to help condense the trait information in order to narrow down specific regions of the rice genome that are involved in root development for follow up investigations. Similar to methods used to prioritize the single trait GWA analysis results, the highly significant regions from the multi-trait analyses must be selected and prioritized for further studies aimed at discovering underlying genes involved in RSA formation. From the weighted multi-trait averaging (WMTA) analysis, 91 significant SNPs (Figure 4.10) were selected from the subpopulation analyses corresponding to 68 unique regions of the genome when using a fixed LD estimate of 250kb. From the composite trait (CT) analysis, 136 SNPs corresponding to 103 unique regions were selected (Figure 4.10). From these significant multi-trait SNPs, 10 pairs of co-localizing regions of the genome were found when using a fixed LD estimate of 250kb. The intersecting regions of overlap fell on chromosomes 1, 2, 4, 5, 7 and 8 and are highlighted in Figure 4.10. These 10 regions represent key locations in the rice genome that are likely involved in the higher level control of global root system growth and development.

FUTURE WORK

The research presented in this chapter and throughout this dissertation describes the development and use of phenotyping systems in order to capture and perform mapping studies on root traits related to rice root system architecture (RSA). When coupled with genotypic and germplasm resources, phenotyping tools are enabling researchers to explore root system development in much greater detail and are

Figure 4.10: Summary of the selected SNPs from the two multi-trait analyses. The chromosome plots display a combined summary of the selected SNPs from all of the single trait GWA studies (across all subpopulations and within the *aus*, *indica*, *temperate japonica* and *tropical japonica* rice subpopulations) where the physical Mb positions are labeled to the left of each chromosome. The yellow to blue color gradient on the chromosome plots represent the number of overlapping SNPs from 0 (yellow) to a maximum of 23 (blue) SNPs when using a fixed LD estimate of 250kb. The selected peak SNPs from the multi-trait analyses are depicted as + (blue) and x (red) symbols for the weighted multi-trait averaging (WMTA) and composite trait (CT) analyses, respectively. The 10 shaded regions (gray) surrounding the multi-trait symbols represent co-localizing regions that were detected during both multi-trait analyses when an LD estimate of 250kb was used.

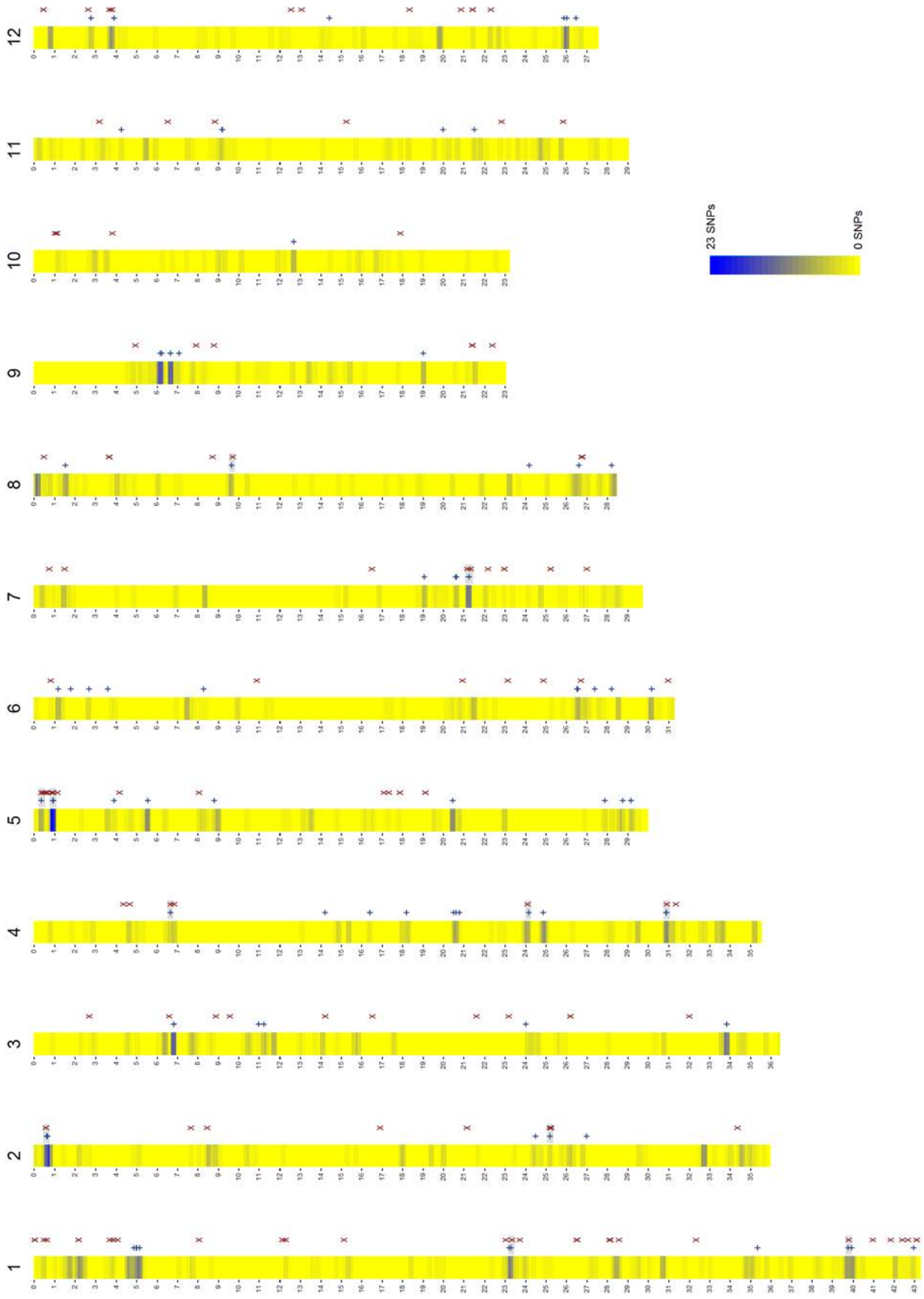
12
11
10
9
8
7
6
5
4
3
2
1
23 SNPs
0 SNPs

facilitating discovery of important genetic factors involved in natural variation and adaptive root responses at both a single plant and species level.

From both a biological and technical standpoint, much of this work only touches the surface of what can be done when measurement and analysis tools are combined with collections of genetically characterized germplasm. Additional investment and development of phenotyping tools and infrastructure, as well as genetic and germplasm resources will be necessary to fully realize the potential of phenotyping techniques during larger and more comprehensive studies of rice (*Oryza sativa*) and other plant species. Phenotyping improvements will not only require modifications to the current platforms, but will also rely on the application and integration of various phenotyping and analysis techniques with better defined data collection, management and summary practices. The scope of work being done on image-based phenotypic data management and sharing goes beyond the capabilities of a single research lab and is a current challenge for the scientific community at large. Additionally, further analysis of the current mapping results will also be necessary to elucidate underlying genes involved in root development. Any loci that are discovered will need to be validated for their functional effects on root development, RSA traits and plastic responses. Gaining a better understanding of the linkage between specific (or multiple) traits and loci to nutrient and water acquisition will also require the integration with field evaluations to determine their ultimate relevance to crop improvement programs.

To directly follow-up on the research that was presented in this dissertation, two areas that require additional research are the extension and improvement of the phenotyping platforms and further genetic and physiological analysis and growth

studies. Although the best areas and strategies for directing future work is an open-ended question that requires a greater deal of thought and consideration, some possible directions are discussed in Table 4.6.

MATERIALS AND METHODS

Growth experiments

Four hundred twenty-five *Oryza sativa* accessions from the McCouch rice diversity panel - RDP1 (Tung et al., 2010; Zhao et al., 2011), and 155 recombinant inbred lines (RILs) from a population derived from a cross between IR64 (lowland, *indica*) and Azucena (upland, *tropical japonica*) were screened for 3D root system traits. The rice seedlings were grown and imaged on days 3, 6, 9 and 12 following transplanting (D3, D6, D9, and D12) using the 3D root system phenotyping platform described in Chapter III (Clark et al., 2011). Using a staggered experimental design, the rice seedlings were planted in batches of 30 cylinders with one plant per cylinder. For each batch, 2 or 4 cylinders were planted with recurring witness accessions (NSFTV 639, NSFTV 644, IR64 and Azucena) and the remaining cylinders were planted with unique accessions or lines. The planting order of the accessions/lines was first randomized prior to each replicate through diversity panel or RIL population and each replicate through the populations was completed in consecutive batches before beginning the next replicate. During the screening experiments, each accession/line was replicated a minimum of 2 times; however, due to poor germination and a high incidence of bacterial or fungal contamination, two high-quality replicates of the each

Table 4.6: Possible areas for future research.

Phenotyping Platforms	
2D and 3D Phenotyping	Extending the flexibility of the root analysis platforms to facilitate nutritional studies and better accommodate more mature plants from a wider range of crop species is needed. Hydroponic-based 3D imaging will be a valuable approach to accomplish these tasks. Additionally, a variety of root phenotyping platforms have been developed by research groups around the world for a range of applications. Direct use or extension of those techniques will help address some limitations in order to investigate specific research questions (such as growth under phosphorus (P) limitation using growth pouches and 2D imaging) or to validate the observed root traits and assess their possible agronomic value (such as growth during pot-based studies in soil or potting mixes using x-ray or MRI imaging). The simultaneous capture of shoot traits will also help to discover links between root traits and whole plant growth, development and performance.
Data Management	While every research program has unique needs, the proper documentation and storage of experimental information (germplasm, experimental design and execution protocols, location and climate data, raw experimental data, and data processing and analysis routines) is necessary in the era high-throughput phenotyping where large datasets are often shared (somewhat blindly) amongst several individuals or lab groups. Implementing interim solutions that can be transitioned into well planned data management and tracking strategies is currently needed.
Genetic Analysis and Growth Studies	
Multivariate Analysis	Two multi-trait analyses were presented in this dissertation however these approaches were not rigorously validated and will need further extension and testing. Multivariate techniques can not only be used to reduce the dimensionality of the datasets, but can also help discover non-obvious relationships amongst captured features. These techniques will require further application and investigation. In addition to statistical-based multivariate techniques, other techniques such as mechanistic modeling will also help to integrate datasets and validate important relationships during candidate gene analysis, functional studies and whole plant performance.

Table 4.6 (continued)

Genetic Analysis and Growth Studies (continued)	
Candidate Gene Analysis	Several regions of the rice genome were found to be highly influential on the root system traits observed during these phenotyping studies, however it is still difficult to confidently define which regions to follow-up on based on the mapping and multi-trait results alone. Further investigation into candidate genes that colocalize to regions of higher priority is needed. Candidate gene include genes that have already been annotated for their involvement in rice root system development, as well as other likely genes based sequence homology to other species, putative biological function and network-based relationships from expression studies.
Functional Studies	While these phenotyping studies have helped identify genomic regions involved in root system development, the ultimate functional importance of the detected regions with regards to adaptive responses to various agricultural environments has not been determined. Taking advantage of genomic information and the theoretical importance of the certain root system architecture (RSA) traits, further follow-up studies will need to be designed and performed. In addition to lab and greenhouse-based evaluations, controlled field studies should also be integrated to better understand the direct relevance of the genes and traits to agricultural performance under both optimal and suboptimal cultivation environments.

accession/line were typically selected for further analysis.

In order to synchronize the seedling sizes for transplanting, germination studies were performed prior to beginning screening experiments to determine the proper germination period of each accession/line. During seed preparation and germination of each accession/line replicate, 5 seeds were dehulled by hand and surface sterilized by soaking with a solution of 70% ethanol for 1 minute followed by a solution of 3% sodium hypochlorite for 30 minutes. The sodium hypochlorite was removed by soaking the seeds with sterile 18MΩ H_2O for 5 minutes for a minimum of three rinses. The seeds were then covered with moist filter paper and germinated in a lighted growth chamber for 1 to 3 days in 100x100mm square, vertically-oriented petri plates under sterile conditions. When the emerging radicles had grown to approximately 1 cm in length, the most vigorous seedling of each accession was transplanted into glass growth cylinders (90mm ID, MicroGlass™) containing approximately 1.3L of modified Magnavaca's growth media (Famoso et al., 2010; Clark et al., 2011) at a pH of 5.5 that had been solidified with gellan gum (Sigma-Aldrich Phytagel™, St. Louis, MO). The modified Magnavaca's growth media contained the following: 1.3 mM $CaCl_2$, 1.0 mM KCl, 1.5 mM NH_4NO_3, 0.2 mM $MgSO_4$, 0.5 mM $Mg(NO_3)_2$, 0.455 mM $MgCl_2$, 100 µM KH_2PO_4, 77 µM Fe-HEDTA, 8.1 µM $MnCl_2$, 25.4 µM H_3BO_3, 2.35 µM $ZnSO_4$, 0.6 µM $CuSO_4$, 0.85 µM Na_2MoO_4 and 0.15% gellan gum. During transplanting, the seedlings were planted into the center of the each cylinder at a depth such that the coleoptile base was completely submerged in the growth media with the radicles oriented perpendicular to the media surface.

After transplanting, each cylinder was covered with a sterile black cap (with a

19mm diameter hole on center covered with autoclavable tape), sealed with 3M™ Micropore™ tape, and the sides were wrapped with opaque plastic (Griffolyn® t-55, Reef Industries, Inc) to prevent light penetration. After imaging on D3, the autoclavable tape was removed from the hole in each cap, allowing for the shoots to grow up through the holes. The plants were germinated and grown in a walk-in growth chamber with a small air purifier (IAP-10-100, Idylis) at 30°C day/26°C night, 12 h/12 h day-neutral photoperiod, 550 µmol m^2 s^{-1} photon flux for the duration of the experiments.

Media preparation

For each batch of 30 cylinders, 48 liters of sterile modified Magnavaca's growth media was prepared using a custom aspiration system. This aspiration system was constructed using two autoclavable carboys with 20L and 50L capacities, Teflon® (PTFE) tubing, and autoclavable connectors and fittings. The 20L of carboy was vacuum rated for use during the filter sterilization process of the nutrient solution. As with previous studies (Clark et al., 2011), the sterile, full-strength modified Magnavaca's growth media was prepared using a two-part process. First, 24L of 2X modified Magnavaca's nutrient solution was adjusted to pH 6.0 and filter sterilized into the 20L carboy of the sterile aspiration system then transferred to the second larger carboy. Next, 24L of 2X gellan gum solution was prepared by dissolving and autoclaving 72 grams of gellan gum powder in 24L of 18MΩ H_2O using twelve 2 liter autoclave bottles (6g of gellan gum per 2 liter bottle). After autoclaving, the 2X gellan gum solution was directly aspirated from each bottle into the larger carboy within a laminar flow hood. After the 2X solutions had been completely combined, the full strength gellan gum media was allowed to gently shake for 1 hour to completely homogenize the media prior

to dispensing into sterile glass growth cylinders for cooling and solidification. Media in the cylinders was cooled at room temperature in the dark for 6-8 hours prior to seedling transplantation.

Genome wide association (GWA) analysis

Using a beta version of a rice genotypic dataset consisting of 673,937 SNPs markers (nsftv.700K_genotypes.ALCHEMY.v0.20111225), genome-wide association (GWA) analysis was performed across and within *aus*, *indica*, *temperate japonica*, and *tropical japonica* subpopulations for the core RSA trait measures from the 425 of the rice accessions from the *Oryza sativa* accessions in the McCouch rice diversity panel (RDP1). To account for different degrees of population structure and relatedness between the accessions, a linear mixed model approach used that was implemented in the R package EMMA (Yu et al., 2006; Zhao et al., 2007; Kang et al., 2008). The model can be written in matrix form as: $y = X\beta + C\gamma + Z\mu + e$ where β and X correspond to the SNP coefficient and SNP vectors, γ and C correspond to the subpopulation coefficient and subpopulation PC (principle component) vectors, μ corresponds to the random effects vector that accounts for population structures and relatedness, Z corresponds to the design matrices, and e is the random error term. SNPs having a minor allele frequency less than 5% (MAF<0.05) across and within subpopulations were excluded from the respective analyses.

Quantitative trait loci (QTL) analysis

QTL mapping studies were performed on the normalized core trait measures collected from the 155 derived RILs on D3, D6 and D9 using a subset of the 1559 markers from larger SNP dataset containing 30,894 markers (Spindel et al., 2012).

Using Windows QTL Cartographer Version 2.5_011 (Wang et al., 2012), composite interval mapping (CIM) was performed using Model 6 with default settings of 1cM walk speed, 5 control markers, 10cM window size and the backward regression method where the genetic map was estimated prior to the CIM analysis with R/qtl (Broman et al., 2003). The global LOD significance thresholds for each trait were determined using 1000 permutations with a significance level of 0.05.

Clustering during composite trait (CT) analysis

To find composite traits based on *n* selected traits, each accession *s* of a given *O. sativa* subpopulation *S* is represented by a feature vector $\mathbf{x_s} = (x_1,x_2,...,x_n)$ where $x_1,x_2,...,x_n$ indicate the normalized MCMC resampled measures for each of the *n* traits for a given accession *s*. This essentially defines an *n*-dimensional feature space $\mathbf{R}^n$ in which each accession *s* in *S* is mapped to a point $\mathbf{x_s}$ in $\mathbf{R}^n$. Clusters of accessions are defined based on their similarities according to the measures in $\mathbf{x_s}$. The similarity between two accessions *s* and *t* is estimated by finding the Euclidean distance $d(s,t) = || \boldsymbol{x_s} - \boldsymbol{x_t} ||$ between their corresponding feature vectors (points) in the feature space $\mathbf{R}^n$. The closer two points are the more similar are their corresponding accessions.

The grouping method adopted here was proposed by Rocha et al (2009) and has also been applied to brain tissue classification in magnetic resonance image analysis (Cappabianco et al., 2012). This approach exploits the distribution of accessions in the feature space as measured by their probability density function (pdf). The domes of the pdf represent the clusters of accessions that are similar in their multi-dimensional phenotype. Therefore, the clusters are identified by estimating a suitable pdf and separating the individuals that fall in different domes. The applied algorithm detects the

maxima of the pdf as representative accessions of each group, assigns a group label to each maximum, and propagates each label to the other accessions in the same dome by following the decreasing order of pdf values such that this label propagation process ends at the valleys of the pdf.

The success of this clustering technique relies on the pdf estimation and adopts a discrete approach in which each accession *s* is connected to its *k* closest neighbors (accessions) in the feature space $\mathbf{R}^n$. The pdf value estimated for each accession *s* is:

$$\rho(s) = \frac{1}{\sqrt{2\pi\sigma^2|A(s)|}} \sum_{t\epsilon A(s)} exp\left(\frac{-d^2(s,t)}{2\sigma^2}\right)$$

where *A(s)* contains the *k* closest neighbors of accession *s* (*i.e.* $|A(s)|$ is *k*) and

$$\sigma = \max_{\forall(s,t)\in A}\left\{\frac{d(s,t)}{3}\right\}$$

is a global parameter that considers the maximum distance computed from all pairs of *k* closest neighbors divided by 3. This constraint prevents the consideration of outliers among the *k* closest neighbors the calculation of ρ(*s*).

The above equation assigns higher values to accessions *s* which have closer *k* nearest neighbors, such that higher concentrations of accessions in $\mathbf{R}^n$ will represent the domes of the pdf. The parameter *k*, however, is quite application-dependent. It represents the distance scale at which the distribution of the accessions is observed from a reference point in the feature space $\mathbf{R}^n$. Higher values of *k* represent longer distances from which all points will appear as a single cluster (group). As the value of *k* decreases, one can observe higher number of clusters being formed in the feature space. Therefore, for a given application, one needs to find the best value of *k* (scale) within range of all possible *k* values, 1 to k_{max}, such that the total number of individuals

in *S* is the maximum possible value for k_{max}.

CONCLUSION

Root development and architecture are complex traits that are under both intrinsic and extrinsic control. Gaining a clearer understanding of the genetics involved in root growth will help researchers and breeders to develop rice cultivars (and other crops) with improved root system characteristics for nutrient and water acquisition. The research in this chapter describes the screening and preliminary genetic analysis of 3-dimesional root system architecture traits in rice and present methods that have helped narrow down and prioritize genomic regions that appear to be highly involved in root development and architectural traits. Further follow-up studies will require a diverse set of skills and knowledge spanning the plant biology, agronomy, genetics and breeding, statistics, and engineering disciplines.

ACKNOWLEDGEMENTS

For the work presented in this chapter, I would especially like to thank the members of the RSA Team who include: Janelle Jung who helped take the lead during all phases of this work from the initially conception through the writing of this chapter and James Jones-Rounds whose continuous devotion and endless brainstorming helped make the screening experiments possible. I am also grateful to and would like to thank the following people: Robert MacCurdy, Bill Shaben, Doug Caveney and Jon Shaff for their assistance during the development of the 3D growth and imaging platform; Anthony Greenberg for his expertise and efforts during the root trait

resampling; Pavel Korniliev for performing the GWA analysis; Teresa Hancock, Georgia Eizenga and Sandra Harrington for maintaining and providing the purified seed stocks of the rice diversity panel; Genevieve DeClerck, Francisco Agosto-Perez, Mark Wright and Chih Wei Tung for generating and providing access to the SNP marker data on rice diversity panel; Alexandre Falcao for working to develop and refine the composite trait analysis methods; Brigitte Courtois and Nour Ahmadi (CIRAD-France) for granting access to the IR64/Azucena RIL mapping population; and Jen Spindel and Josh Cobb for providing the GBS marker data for the RIL mapping population and giving insights into QTL analysis.

REFERENCES

Broman KW, Wu H, Sen Ś, Churchill GA (2003) R/qtl: QTL mapping in experimental crosses. Bioinformatics 19: 889-890

Cairns JE, Impa SM, O'Toole JC, Jagadish SVK, Price AH (2011) Influence of the soil physical environment on rice (Oryza sativa L.) response to drought stress and its implications for drought research. Field Crops Research 121: 303-310

Cappabianco FAM, Falcão AX, Yasuda CL, Udupa JK (2012) Brain tissue MR-image segmentation via optimum-path forest clustering. Computer Vision and Image Understanding 116: 1047-1059

Clark RT, MacCurdy RB, Jung JK, Shaff JE, McCouch SR, Aneshansley DJ, Kochian LV (2011) Three-Dimensional Root Phenotyping with a Novel Imaging and Software Platform. Plant Physiology 156: 455-465

Eissenstat DM (1991) On the Relationship between Specific Root Length and the Rate

of Root Proliferation: A Field Study Using Citrus Rootstocks. New Phytologist 118: 63-68

Famoso AN, Clark RT, Shaff JE, Craft E, McCouch SR, Kochian LV (2010) Development of a Novel Aluminum Tolerance Phenotyping Platform Used for Comparisons of Cereal Aluminum Tolerance and Investigations into Rice Aluminum Tolerance Mechanisms. Plant Physiol. 153: 1678-1691

Gornall J, Betts R, Burke E, Clark R, Camp J, Willett K, Wiltshire A (2010) Implications of climate change for agricultural productivity in the early twenty-first century. Philosophical Transactions of the Royal Society B: Biological Sciences 365: 2973-2989

Gowda VRP, Henry A, Yamauchi A, Shashidhar HE, Serraj R (2011) Root biology and genetic improvement for drought avoidance in rice. Field Crops Research 122: 1-13

Iyer-Pascuzzi AS, Symonova O, Mileyko Y, Hao Y, Belcher H, Harer J, Weitz JS, Benfey PN (2010) Imaging and Analysis Platform for Automatic Phenotyping and Trait Ranking of Plant Root Systems. Plant Physiology 152: 1148-1157

Kang HM, Zaitlen NA, Wade CM, Kirby A, Heckerman D, Daly MJ, Eskin E (2008) Efficient Control of Population Structure in Model Organism Association Mapping. Genetics 178: 1709-1723

Li Y, Ye W, Wang M, Yan X (2009) Climate change and drought: a risk assessment of crop-yield impacts. Climate Research 39: 31-46

Mather KA, Caicedo AL, Polato NR, Olsen KM, McCouch S, Purugganan MD (2007) The Extent of Linkage Disequilibrium in Rice (Oryza sativa L.). Genetics 177:

2223-2232

McCouch SR (2012) *Personal communication*.

Ray JD, Yu L, McCouch SR, Champoux MC, Wang G, Nguyen HT (1996) Mapping quantitative trait loci associated with root penetration ability in rice (Oryza sativa L.). Theoretical and Applied Genetics 92: 627-636

Rocha LM, Cappabianco FAM, Falcão AX (2009) Data clustering as an optimum-path forest problem with applications in image analysis. International Journal of Imaging Systems and Technology 19: 50-68

Sarkar D (2008) Lattice multivariate data visualization with R. Springer Science+Business Media, New York; London

Spindel J, Wright M, Chen C, Cobb J, Gage J, Harrington S, Ahmadi N, McCouch S (2012) Map construction as error correction for Genotyping-by-Sequencing (GBS). Submitted Manuscript

Topp CN, Iyer-Pascuzzi AS, Anderson JT, Lee C-R, Zurek PR, Symonova O, Zheng Y, Bucksch A, Mileyko Y, Galkovskyi T, Moore BT, Harer J, Edelsbrunner H, Mitchell-Olds T, Weitz JS, Benfey PN (2013) 3D phenotyping and quantitative trait locus mapping identify core regions of the rice genome controlling root architecture. Proceedings of the National Academy of Sciences

Tung C-W, Zhao K, Wright M, Ali M, Jung J, Kimball J, Tyagi W, Thomson M, McNally K, Leung H, Kim H, Ahn S-N, Reynolds A, Scheffler B, Eizenga G, McClung A, Bustamante C, McCouch S (2010) Development of a Research Platform for Dissecting Phenotype–Genotype Associations in Rice (*Oryza* spp.). Rice 3: 205-217

Uga Y, Okuno K, Yano M (2011) Dro1, a major QTL involved in deep rooting of rice under upland field conditions. Journal of Experimental Botany 62: 2485-2494

Wang S, Basten CJ, Zeng ZB (2012) Windows QTL Cartographer 2.5. *In*, Department of Statistics, North Carolina State University, Raleigh, NC. (http://statgen.ncsu.edu/qtlcart/WQTLCart.htm)

Yu J, Pressoir G, Briggs WH, Vroh Bi I, Yamasaki M, Doebley JF, McMullen MD, Gaut BS, Nielsen DM, Holland JB, Kresovich S, Buckler ES (2006) A unified mixed-model method for association mapping that accounts for multiple levels of relatedness. Nat. Genet. 38: 203-208

Zhao K, Aranzana MJ, Kim S, Lister C, Shindo C, Tang C, Toomajian C, Zheng H, Dean C, Marjoram P, Nordborg M (2007) An arabidopsis example of association mapping in structured samples. PLoS Genet 3: e4

Zhao K, Tung C-W, Eizenga GC, Wright MH, Ali ML, Price AH, Norton GJ, Islam MR, Reynolds A, Mezey J, McClung AM, Bustamante CD, McCouch SR (2011) Genome-wide association mapping reveals a rich genetic architecture of complex traits in Oryza sativa. Nature Communications 2: 467